DEVELOPING PRINT® DRY POWDERS FOR PULMONARY PROTEIN DELIVERY

Erin Michelle Wilson

A dissertation submitted to the faculty at the University of North Carolina at Chapel Hill in partial fulfillment of the requirements for the degree of Doctor of Philosophy in the Division of Pharmacoengineering and Molecular Pharmaceutics in the Eshelman School of Pharmacy.

Chapel Hill
2017

Approved by:

Joseph DeSimone

Philip Smith

David Henke

J. Christopher Luft

Michael Jay

Michael Miley

ABSTRACT

Erin Michelle Wilson: Developing PRINT® Dry Powders for Pulmonary Protein Delivery
(Under the direction of Joseph DeSimone)

Pulmonary delivery is an attractive route of administration that can be used for the local delivery of therapeutics for respiratory conditions or to non-invasively deliver sufficiently low molecular weight therapeutics to systemic circulation. There is a particular interest in protein delivery, however, many respirable formulations are inefficient at delivering therapeutics to the desired region of the lungs, which precludes the development of costly biologics for inhalation. Particle engineering, a strategy that aims to rationally and precisely control particle size, shape, density, and composition, has been utilized to design high-performance dry powder aerosols that deposit efficiently and precisely in the desired area of the lungs. However, current fabrication methods offer limited control of particle geometry and impose unfavorable stresses on proteins during manufacturing.

The overall goals of this dissertation were to fabricate and characterize protein-based microparticles with Particle Replication In Non-wetting Templates (PRINT) technology and engineer these particles into high-performance protein dry powder aerosols. We hypothesized that the precise control of particle geometry afforded by PRINT along with the low physical stress imparted by the process would allow for the stable incorporation of proteins into precisely engineered particles, resulting in high-performance protein dry powder aerosols.

A generalizable formulation strategy to micromold a variety of proteins into precisely engineered PRINT particles was developed, and the incorporated proteins were found to retain

their native structure and function. Following lyophilization into dry powders, these formulations were found to fluidize, aerosolize, and deposit with high efficiency and precision. We then expanded the formulation strategy to fabricate multiple PRINT particle shapes, which were used to explore the impact of particle shape on dry powder performance in an effort to inform and improve particle engineering strategies. Informed by the formulation development and particle shape studies, dry powder formulations of two therapeutic proteins were developed and the delivery of one formulation was demonstrated *in vivo*. Overall, we have demonstrated the utility of PRINT as a platform to manufacture high-performance protein dry powders and we have furthered understanding of the impact of particle shape on aerosol performance, both of which contribute to the advancement of particle engineering strategies for inhalable formulations.

ACKNOWLEDGEMENTS

I would like to thank my advisor, Joseph DeSimone, for the opportunity to work in a transformative environment, where he continuously inspired and encouraged the application of our research to real-world problems. He changed the way I both view and approach research, and for that I will be forever grateful. I would also like to thank Chris Luft for his direction and support, constant accessibility, and his inherent ability to be a motivator. I would like to thank my committee members, Philip Smith, David Henke, Michael Jay, and Michael Miley for their time, advice, and guidance that aided in both the progression and quality of my research. Thank you to all of the DPMP faculty, staff, and students who have been invaluable in my growth as both a scientist and a person throughout graduate school.

I would also like to acknowledge the outstanding core facilities at UNC and their even more outstanding staff – Amar Kumbhar and Wallace Ambrose at CHANL, Bob Bagnell, Victoria Madden, and Kristen White at the MSL, Ashutosh Tripathy at the Mac-in-Fac, and Charlene Santos, Mark Ross, and Alain Valdivia at the Animal Studies Core Facility.

Thank you to all of the DeSimone lab members I had the pleasure of working with throughout graduate school. I would particularly like to thank the DTRA team – Ashley, Cassie, Katie, and Tojan – for their friendship, support, and constant willingness to help. In addition, I'd like to thank Jason, Jillian, Chintan, Tammy, Cathy, Cameron for their help with experimental design and instrument training.

Finally, I would like to thank my family for their unwavering support in everything I do. I couldn't have done it without you!

TABLE OF CONTENTS

LIST OF TABLES xi

LIST OF FIGURES xi

LIST OF ABBREVIATIONS AND SYMBOLS xiv

CHAPTER 1: INTRODUCTION TO PULMONARY DRUG DELIVERY 1

1.1 Overview of Drug Delivery 1

1.2 Structure and Function of the Human Respiratory Tract 2

1.2.1 Structure and Function of the Airway Epithelium 4

1.3 Aerosol Delivery to the Lungs 5

1.3.1 Target of Aerosol Deposition 5

1.3.2 Aerodynamic Diameter 6

1.3.3 Aerosol Deposition in the Lungs 6

1.3.4 Devices for Inhaled Aerosol Delivery 9

1.3.5 Aerosol Characterization of Dry Powder Inhalers 11

1.4 Particle Fabrication Techniques for Dry Powder Inhalers 13

1.4.1 Spray Drying 13

1.4.2 Spray Freeze Drying 15

1.5 Particle Replication in Non-wetting Templates 16

1.6 Overview of Dissertation 17

References 18

CHAPTER 2: HIGH-PERFORMANCE PRINT DRY POWDER AEROSOLS FOR PULMONARY PROTEIN DELIVERY 23

2.1 Introduction 23

2.2 Materials and Methods 26

2.2.1 Materials 26

2.2.2 Methods 26

2.3 Results 31

2.3.1 Fabrication of Respirable PRINT Protein Particles 31

2.3.2 Characterization of Protein Stability 34

2.3.3 *In Vitro* Aerosol Characterization 38

2.4 Discussion 41

2.5 Conclusions 47

References 49

CHAPTER 3: THE ROLE OF PARTICLE SHAPE IN FLOWABILITY, AEROSOLIZATION, AND DEPOSITION OF DRY POWDER FORMULATIONS 53

3.1 Introduction 53

3.2 Materials and Methods 54

3.2.1 Materials 54

3.2.2 Methods 55

3.3 Results 59

3.3.1 Fabrication and Characterization of Lysozyme Particle Shapes 59

3.3.2 Characterization of Bulk Powder Properties 63

3.3.3 Aerosol Characterization of Lysozyme Particle Shapes 64

3.3.4 Powder and Aerosol Properties as a Function of Particle Morphology 65

3.4 Discussion 69
3.5 Conclusions 75
References 77
CHAPTER 4: THERAPEUTIC APPLICATIONS OF PRINT DRY POWDERS 80
4.1 Introduction 80
4.2 Materials and Methods 82
4.2.1 Materials 82
4.2.2 Methods 83
4.3 Results 86
4.3.1 Fabrication and Characterization of DNase 1 μm Cylinders 86
4.3.2 Characterization of DNase Stability 88
4.3.3 *In Vitro* Aerosol Characterization of DNase 1 μm Cylinders 90
4.3.4 Fabrication and Characterization of PRINT BuChE Particles 91
4.3.5 In Vitro Aerosol Characterization of BuChE 1 μm Cylinders 93
4.3.6 Insufflation of BuChE 1 μm Cylinders 94
4.4 Discussion 97
4.5 Conclusions 104
References 106
CHAPTER 5: SUMMARY AND FUTURE DIRECTIONS 109
5.1 Summary 109
5.2 Impact and Future Directions 110
5.2.1 PRINT as a Platform for Pulmonary Protein Delivery 110
5.2.2 Role of Particle Shape in Respirable Dry Powders 112

5.2.3 Therapeutic Applications of PRINT Protein Dry Powders..... 116

5.3 Outlook 118

References..... 119

LIST OF TABLES

Table 2.1 DOE for roll-to-roll BSA 1 μm cylinders 34

Table 2.2 Aerosol parameters of lyophilized BSA and lysozyme 1 μm cylinders from an insufflator 39

Table 2.3 Aerosol parameters of lyophilized BSA and lysozyme 1 μm cylinders from an inhaler 41

Table 3.1 Particle dimensions 61

Table 3.2 Surface area and volume of particle shapes 61

Table 3.3 Shape descriptor values 61

Table 3.4 Angle of repose of lysozyme particle shapes 63

Table 3.5 Density and compressibility of lysozyme particle shapes 64

Table 3.6 Aerosol parameters of lysozyme particle shapes 65

Table 4.1 Aerosol parameters of DNase 1 μm cylinders 91

Table 4.2 Aerosol parameters of BuChE 1 μm cylinders 94

Table 5.1 ELF glutathione 118

LIST OF FIGURES

Figure 1.1 Diagram of generations of bifurcating airways 3

Figure 1.2 Diagram of progression of respiratory epithelium structure 4

Figure 1.3 Diagram of airway flow velocity by generation 7

Figure 1.4 Region of particle deposition 8

Figure 1.5 Classes of inhaled devices 9

Figure 1.6 Particle pathway through cascade impactor 12

Figure 1.7 Spray dryer diagram 14

Figure 1.8 Particle engineering with spray drying 14

Figure 1.9 Methods of droplet freezing 15

Figure 1.10 PRINT schematic 16

Figure 2.1 Formulation optimization of lysozyme 1 μm cylinders 31

Figure 2.2 SEM of dry powders of BSA and lysozyme 1 μm cylinders 32

Figure 2.3 SEM of lyophilized BSA and lysozyme 1 μm cylinders 32

Figure 2.4 SEM of BSA 80x320 nm rods 32

Figure 2.5 Composition of lyophilized BSA and lysozyme 1 μm cylinders 33

Figure 2.6 Composition of lyophilized BSA and lysozyme 1 μm cylinders 33

Figure 2.7 SEM of roll-to-roll BSA 1 μm cylinders 34

Figure 2.8 SDS-PAGE of lyophilized BSA and lysozyme 1 μm cylinders 35

Figure 2.9 Circular dichroism of lyophilized BSA and lysozyme 1 μm cylinders 36

Figure 2.10 Secondary structure of lyophilized BSA and lysozyme 1 μm cylinders 36

Figure 2.11 Intrinsic fluorescence of lyophilized BSA and lysozyme 1 μm cylinders 37

Figure 2.12 Enzymatic activity of lyophilized lysozyme 1 μm cylinders 37

Figure 2.13 SDS-PAGE of lyophilized BSA and lysozyme 1 μm cylinders 38

Figure 2.14 Cascade impaction of lyophilized BSA and lysozyme 1 μm cylinders from an insufflator 39

Figure 2.15 Cascade impaction of lyophilized BSA and lysozyme 1 μm cylinders from an inhaler 40

Figure 3.1 Models of lysozyme particle shapes 55

Figure 3.2 Image analysis process 56

Figure 3.3 Formulation optimization of lysozyme particle shapes 59

Figure 3.4 SEM of lysozyme particle shapes 60

Figure 3.5 Particle dimensions 60

Figure 3.6 Composition of lyophilized lysozyme particle shapes 62

Figure 3.7 Enzymatic activity of lysozyme particle shapes 62

Figure 3.8 Powder cones for angle of repose 63

Figure 3.9 Cascade impaction of lysozyme particle shapes 65

Figure 3.10 Powder parameters as a function of Feret max 66

Figure 3.11 Powder parameters as a function of MMAD 66

Figure 3.12 Powder parameters as a function of AR 67

Figure 3.13 Powder parameters as a function of SA/V 67

Figure 3.14 Powder parameters as a function of circularity 68

Figure 3.15 Powder parameters as a function of SVMD 68

Figure 4.1 SEM of DNase 1 μm cylinders 87

Figure 4.2 Composition of DNase 1 μm cylinders 87

Figure 4.3 SDS-PAGE of DNase 1 μm cylinders 88
Figure 4.4 Circular dichroism of DNase 1 μm cylinders 89
Figure 4.5 Secondary structure of DNase 1 μm cylinders 89
Figure 4.6 Intrinsic fluorescence of DNase 1 μm cylinders 90
Figure 4.7 Cascade impaction of DNase 1 μm cylinders 91
Figure 4.8 SEM of BuChE 1 μm cylinders 92
Figure 4.9 Composition of BuChE 1 μm cylinders 92
Figure 4.10 Enzymatic activity of BuChE 1 μm cylinders 93
Figure 4.11 SEM of BuChE nanoparticles 93
Figure 4.12 Cascade impaction of BuChE 1 μm cylinders 94
Figure 4.13 BuChE assay development 95
Figure 4.14 IVIS of BuChE 1 μm cylinders 96
Figure 4.15 Residence time of BuChE 1 μm cylinders 97
Figure 5.1 Examples of PRINT particle shapes 111
Figure 5.2 Levels of lung targeting 115

LIST OF ABBREVIATIONS AND SYMBOLS

2D	Two-dimensional
3D	Three-dimensional
A	Projected area
ACI	Andersen cascade impactor
AFM	Atomic force microscopy
ANOVA	Analysis of variance
AR	Aspect ratio
BAL	Bronchoalveolar lavage
BALF	Bronchoalveolar lavage fluid
BD	Biodistribution
BSA	Bovine serum albumin
BuChE	Butyrylcholinesterase
CD	Circular dichroism
CE	Capillary electrophoresis
CF	Cystic fibrosis
CI	Compressibility index
cm	Centimeter
COPD	Chronic obstructive pulmonary disorder
DDS	Drug delivery systems
DNase	Deoxyribonucleasae I
DOE	Design of experiments
DPI	Dry powder inhaler

DSC	Differential scanning calorimetry
ED	Emitted dose
ELF	Epithelial lining fluid
ELSD	Evaporative light scattering detector
FDKP	fumaryl diketopiperazine
FEV	Forced expiratory volume
FPF	Fine particle fraction
GSD	Geometric standard deviation
GSH	Glutathione (reduced)
GSSG	Glutathione (oxidized)
HDODA	Hexanediol diacrylate
HPLC	High-performance liquid chromatography
HPMC	Hydroxypropyl methylcellulose
IACUC	Institution of Animal Care and Use Committee
IVIS	In vivo imaging system
kDa	Kilodalton
kPa	Kilopascals
L	Liter
LC	Liquid chromatography
MES	2-(N-morpholino)ethanesulfonic acid
mg	Milligram
min	Minute
mL	Milliliter

mm	Millimeter
MMAD	Mass median aerodynamic diameter
MWCO	Molecular weight cutoff
NHS	N-hydroxysuccinimide
nm	Nanometer
P	Perimeter
PAGE	Polyacrylamide gel electrophoresis
PBS	Phosphate buffered saline
PEG	Polyethylene glycol
PET	Poly(ethylene terephthalate)
PFPE	Perfluoropolyether
PK	Pharmacokinetics
pMDI	Pressurized metered dose inhaler
PPS	Pre-particle solution
PRINT	Particle replication in non-wetting templates
psi	Pounds per square inch
PVPVA	Poly(1-vinylpyrrolidone-co-vinyl acetate)
RF	Respirable fraction
SA	Surface area
SD	Spray drying
SDS	Sodium dodecyl sulfate
SEC	Size exclusion chromatography
SEM	Scanning electron microscopy

SFD	Spray freeze drying
SVMD	Surface volume mean diameter
tan	Tangent
T_g	Glass transition temperature
TGA	Thermogravimetric analysis
Trp	Tryptophan
V	Volume
V_0	Initial volume
V_f	Final volume
wt%	Weight percent
$x_{F,max}$	Maximum Feret diameter
$x_{F,min}$	Minimum Feret diameter
%	Percent
°	Degrees
°C	Degrees Celsius
ρ_{bulk}	Bulk density
ρ_{tap}	Tapped density
α	Angle of repose
λ_{max}	Wavelength of maximum signal
µL	Microliter
µm	Micrometer
π	Pi

CHAPTER 1: INTRODUCTION TO PULMONARY DRUG DELIVERY

1.1 Overview of Drug Delivery

Conventional oral and parenteral formulations allow therapeutics to diffuse and distribute throughout the body upon entering systemic circulation.[1,2] These formulations offer little control over drug distribution, resulting in inefficient drug accumulation at the desired therapeutic site of action and undesirable side effects due to drug accumulation at off-target sites.[1–3] Modern drug delivery systems (DDS) aim to alter the biodistribution (BD) and/or pharmacokinetics (PK) of incorporated drugs to improve drug efficacy and minimize side effects.[1,2] Advances in nanotechnology in the last two decades have resulted in the development of several nano- and microfabrication methods.[4–7] These fabrication methods have been used to manufacture precisely engineered nano- and microparticle DDS which have the potential to revolutionize medicine.[8–10]

One popular application of microfabricated particles in drug delivery is pulmonary administration, which can be used for both local and systemic drug delivery.[11–15] Direct administration of therapeutics to the lungs for respiratory conditions localizes drug to the desired site of therapeutic effect, thereby minimizing the required drug dose and systemic exposure to the drug.[14,16] Systemic delivery of inhaled therapeutics is possible due to the large alveolar surface area of the lungs, which provides an abundance of capillaries and a direct route of drug absorption into systemic circulation.[17] The pulmonary route is particularly promising for protein delivery, as it can be used to locally deliver adequately high doses of protein drugs and to deliver low molecular weight proteins to systemic circulation in a non-invasive manner.[12,15,18] Despite the opportunities available with pulmonary delivery, the development of inhaled formulations

remains limited by poor delivery efficiency and dose consistency.[16,19,20] Precisely engineered microfabricated particles provide an excellent opportunity to rationally design respirable formulations and improve the delivery efficiency and deposition precision of inhaled aerosols, which could decrease the costs, dose variability, and side effects associated with current inhaled medicines.[14,21]

The work presented in this dissertation represents our efforts to develop high-performance aerosols of precisely engineered microfabricated particles. The content of this chapter provides an overview of the structure of the respiratory system, important concepts in pulmonary delivery, and particle fabrication methods. A basic understanding of these concepts is required to develop an improved respirable formulation comprised of engineered particles.

1.2 Structure and Function of the Human Respiratory Tract

Thorough knowledge of the structure and function of the respiratory tract are critical to understanding the impact that airway architecture and transport has on respiratory drug delivery.[18,22] The architecture of the respiratory tract is characterized by extensive bifurcating airways that serve as pathways for gas transport, as shown in **Figure 1.1**.[20,23] These bifurcating airways are divided into two regions based on their functions: the conducting zone and the respiratory zone.[17,22] The conducting zone is the upper portion of the respiratory tract and is responsible for transporting gas to and from the respiratory zone.[18,20,22] The conducting zone begins in the oral and nasal cavities, progresses through the larynx and trachea, enters the lungs through the bronchi, then continues to the bronchioles and concludes in the terminal bronchioles.[22,23] From the trachea to the terminal bronchioles, the airways in the conducting zone bifurcate approximately 17 times, which progressively increases the surface area of the airways and decreases the velocity of air flow.[20,22]

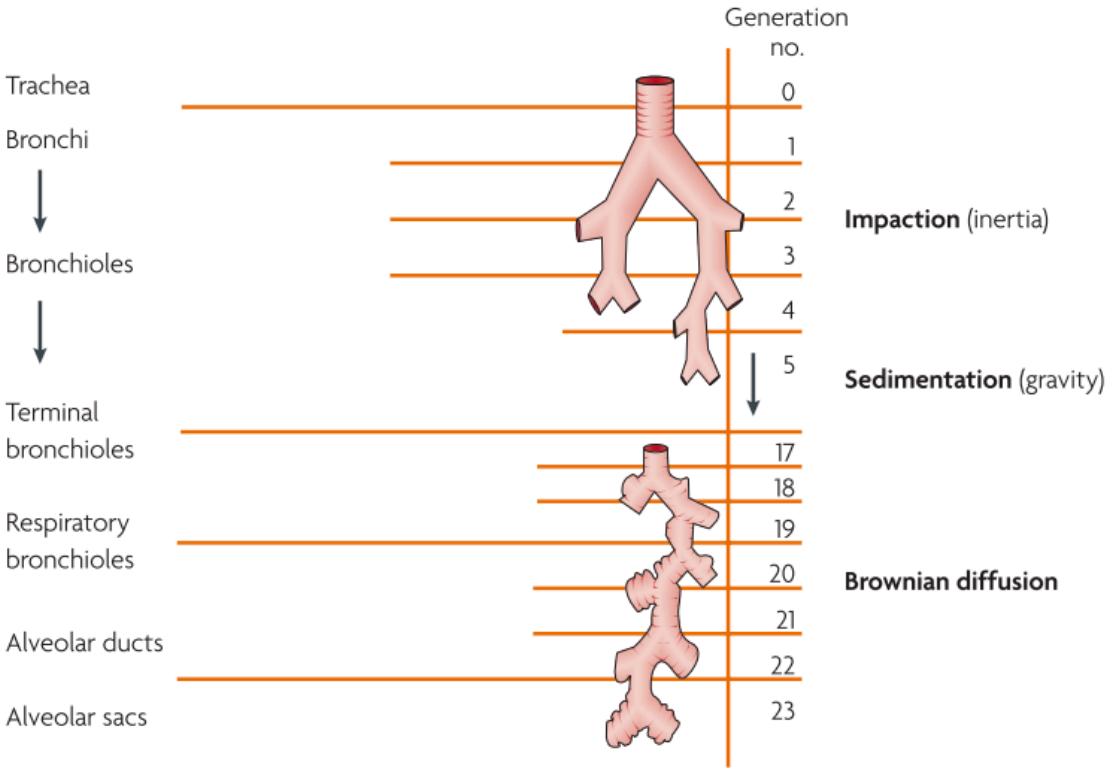

Figure 1.1 Diagram of generations of bifurcating airways. Diagram of the generations of bifurcating airways within the human respiratory system from the trachea to the alveolar sacs. Reproduced from Patton and Byron[18] with permission.

The respiratory zone, comprised of all airways distal to the terminal bronchioles, bifurcates 6 additional times to form the respiratory bronchioles, alveolar ducts, and alveolar sacs.[17,20,22] The respiratory zone is where diffusion of oxygen from the alveoli into the blood and diffusion of carbon dioxide from the blood into the alveoli occurs.[18,23] The surface area of the respiratory zone is more than 100 square meters.[18] Air is transported in and out of the lungs upon contraction and relaxation of the diaphragm, which changes the volume of the lungs.[23] Upon contraction of the diaphragm, the lung volume increases, resulting in new air being drawn into the lungs.[22,23] The new air provides the partial pressure gradient necessary to allow gas exchange.[22] Gas exchange is facilitated by both the large surface area and submicron thickness of the alveolar epithelium in the respiratory zone.[22,23] Blood re-oxygenated from contact with the respiratory zone then circulates throughout the body.[23]

1.2.1 Structure and Function of the Airway Epithelium

In addition to the functional difference between the conducting and respiratory zones, there are major differences in the epithelium structure in the two zones.[18] The airway epithelium serves as the final barrier between the contents of the airways and the bloodstream.[18,24] Generally, traveling from the bronchi to the alveolar sacs, the thickness of both the epithelium and the epithelial lining fluid (ELF) decreases.[18,22] A diagram of the changes in both the structure of the epithelium and the thickness of the ELF are presented in **Figure 1.2**.

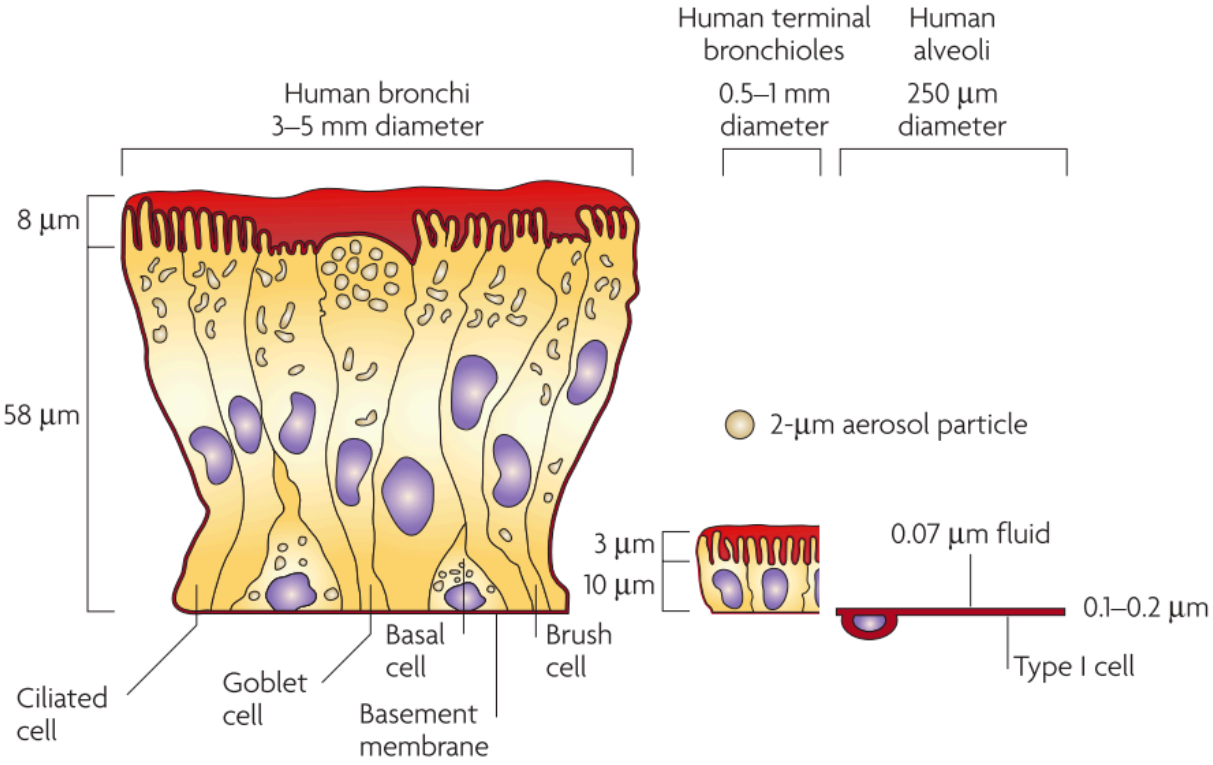

Figure 1.2 Diagram of progression of respiratory epithelium structure. Diagram of the airway epithelium structure of the human respiratory system, including the bronchi, terminal bronchioles, and alveoli. Reproduced from Patton and Byron[18] with permission.

From the bronchi until the terminal bronchioles, a ciliated pseudostratified columnar epithelium is present, which is comprised primarily of ciliated cells, goblet cells, and basal cells.[18,24,25] The goblet cells produce mucus that is moved upwards by ciliated cells resulting in a clearance mechanism known as the mucociliary escalator.[18,24] The mucociliary escalator is the

primary route of clearance for insoluble particles deposited in the conducting zone, while soluble particles are generally cleared from the conducting zone by absorptive mechanisms.[24]

Distal to the terminal bronchioles, the columnar epithelial cells of the conducting zone are absent and are replaced by type 1 cells of submicron thickness.[18] Along with the submicron epithelium, the thickness of the layer of ELF is only 70 nm in the respiratory zone, resulting in an extremely thin path for gas diffusion and exchange.[22] The thin epithelium in the respiratory zone is protected by several alveolar macrophages for each alveolar sac.[17,18,24] The alveolar macrophages are the primary clearance mechanism for insoluble particles in the respiratory region.[24] Soluble particles, which largely avoid internalization by macrophages, are primarily removed from the alveolar sacs by absorption to systemic circulation, either intact or following metabolism.[18,24] Although some proteins undergo degradation in the alveoli, it is not a major clearance mechanism for the majority of proteins.[24,26,27] Both the structure of the airway epithelium and the resulting predominate clearance mechanism must be considered to rationally design efficacious inhaled formulations.

1.3 Aerosol Delivery to the Lungs

1.3.1 Target of Aerosol Deposition

The complicated architecture of the airways, epithelium structure, lung clearance mechanisms, and the desired site of therapeutic action must all be carefully considered when determining the optimal region of deposition for a respirable formulation.[24] The low surface area, long diffusion path, and rapid mucociliary clearance present from the trachea to the terminal bronchioles make the conducting zone a poor target for drug deposition and efficient drug absorption.[22,25] Although many common respiratory diseases exert their pathological effect on the conducting airways, the poor absorption potential in the conducting zone precludes efficient

delivery directly to the site of therapeutic need.[22,25] Therefore, the ideal deposition target for the majority of therapeutics for both local and systemic delivery is the alveolar region of the respiratory zone.[22,24,25] The large surface area and short diffusion path present in alveoli provides the best opportunity for the absorption of both small molecule and biologic formulations.[18] While the alveoli provide an excellent pathway for drug absorption, they also contain alveolar macrophages, which internalize insoluble drug particles and reduce the bioavailability of drug delivered to the alveoli.[18,24,25] Internalization of therapeutics by alveolar macrophages can be avoided by delivering rapidly soluble particles[24], particles larger than 5 μm in diameter[28,29], or particles with a stealth coating.[30,31] Soluble particles deposited in the alveoli can be absorbed into systemic circulation.[24]

1.3.2 Aerodynamic Diameter

The behavior of a particle as an aerosol is dependent on particle diameter, density, and shape.[11] As such, the size of aerosol particles is described as aerodynamic diameter, which is the diameter of a sphere of unit density that has the same settling velocity as the given particle.[11] The aerodynamic diameter is frequently used to estimate the site of particle deposition within the respiratory tract.[22]

1.3.3 Aerosol Deposition in the Lungs

The alveolar region is the ideal target of aerosol deposition for many local and systemic therapies. In order to engineer particulate aerosols that efficiently deposit in the alveolar region, a basic understanding of the mechanisms driving particle deposition is needed. The three mechanisms by which particle deposition occurs in the respiratory system are impaction, sedimentation, and diffusion.[22,32,33] One major factor, along with aerodynamic diameter, driving particle deposition in the numerous bifurcating airways in the lungs is the rate of air flow through

the airways.[33] Generally, air flow decreases in velocity as airways progressively become smaller in diameter at each bifurcation, as modeled in **Figure 1.3**.[24,32,34] Deposition by impaction generally occurs with particles larger than 2 μm in aerodynamic diameter in the upper airways, where the air flow velocity gives the particles sufficient inertia to exit the air stream and deposit in the airways.[22,33] Particles between 0.5 and 2 μm in aerodynamic diameter typically deposit by sedimentation in the respiratory zone, which has a low air flow velocity.[22] Sedimentation occurs as a result of the gravitational forces on particles, and particle deposition by sedimentation with particle diameter, particle density, and time available for sedimentation.[33] The low flow rate of the respiratory region results in sufficient residence time for particles to deposit by sedimentation.[33] The final mechanism for particle deposition is diffusion, which is dependent on the Brownian motion of particles less than 0.5 μm in aerodynamic diameter in a low flow region.[22] In practice, diffusion is not an efficient mechanism for the deposition of particles in the respiratory region.[18]

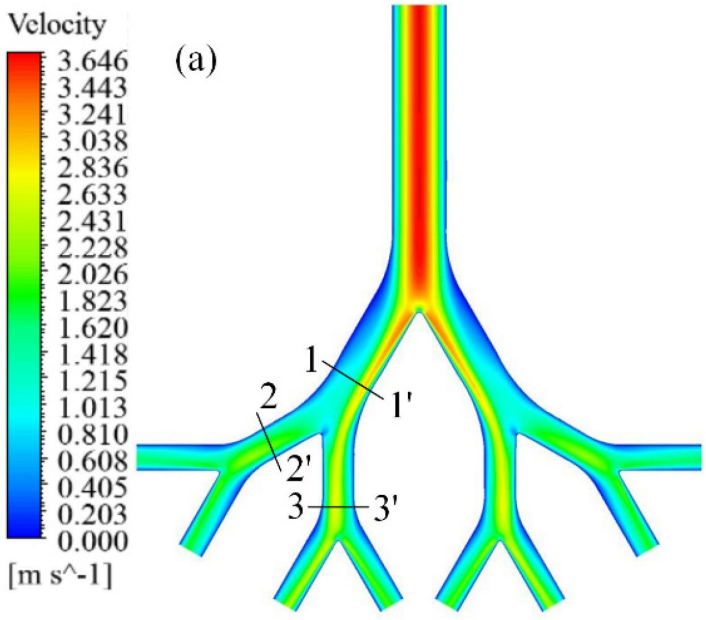

Figure 1.3 Diagram of airway flow velocity by generation. Diagram of the progressively decreasing velocity of air flow that occurs in the human respiratory tract as a result of airway bifurcation and narrowing. Reproduced from Augusto et al.[35] with permission.

The approximate deposition profile expected for particles from 0 to 15 μm in aerodynamic diameter is presented in **Figure 1.4**. As previously stated, particles less than 0.5 μm are expected to deposit by diffusion, particles between 0.5 and 2 μm are expected to deposit by sedimentation, and particles larger than 2 μm are expected to deposit by impaction. Particles between 0.1 and 0.5 μm in aerodynamic diameter are not well-suited for efficient alveolar delivery, as they are largely exhaled.[14,20,36] Particles larger than 5 μm in diameter also fail to efficiently accumulate in the alveolar region as a result of extensive mouth and throat impaction, with deposition shifting higher in the respiratory tract with increasing particle aerodynamic diameter.[18,20]

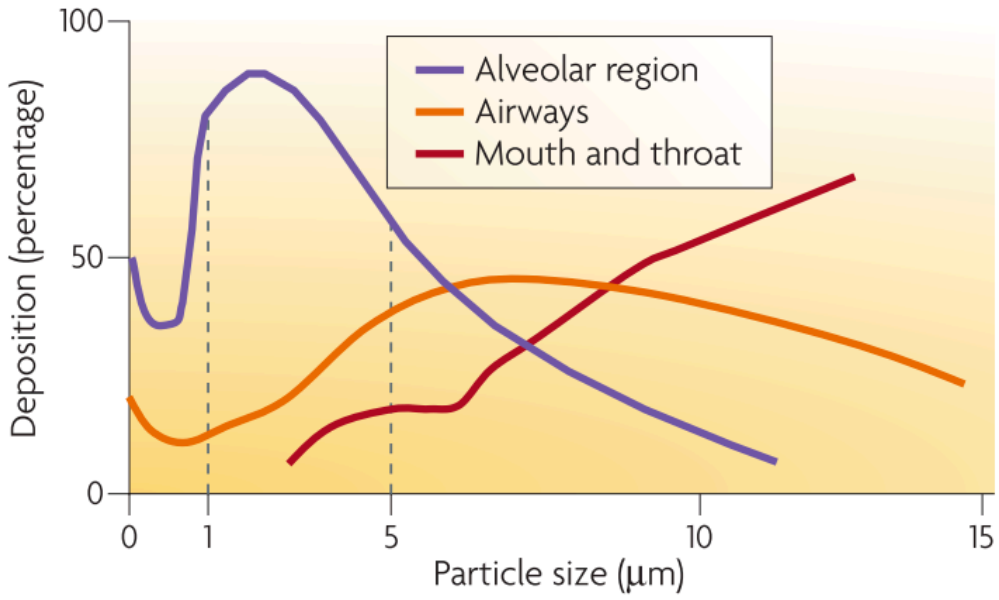

Figure 1.4 Region of particle deposition. Diagram of the region of deposition for particles from 0 to 15 μm in aerodynamic diameter. Reproduced from Patton and Byron[18] with permission.

Optimal deposition in the alveolar region is achieved for aerosols of particles with aerodynamic diameters between 1 and 5 μm.[18] Given that the ideal site of deposition for most therapeutics is in the alveolar region, engineered particle formulations should be developed to yield a specific aerodynamic diameter between 1 and 5 μm.[22]

1.3.4 Devices for Inhaled Aerosol Delivery

Though the history of inhaled aerosol delivery dates back more than 3000 years ago, the development of modern inhaled technologies with strict regulatory requirements began in the past 50 years.[22,37] There are three primary classes of these inhaled technologies, including nebulizers, pressurized metered dose inhalers (pMDIs), and dry powder inhalers (DPIs), each of which operate based on unique principles.[15,22,38,39] A diagram representative of each device class is presented in **Figure 1.5**. A fundamental knowledge of each type of aerosol device along with an extensive understanding of the therapeutic to be delivered is required to choose the appropriate device for aerosol delivery.

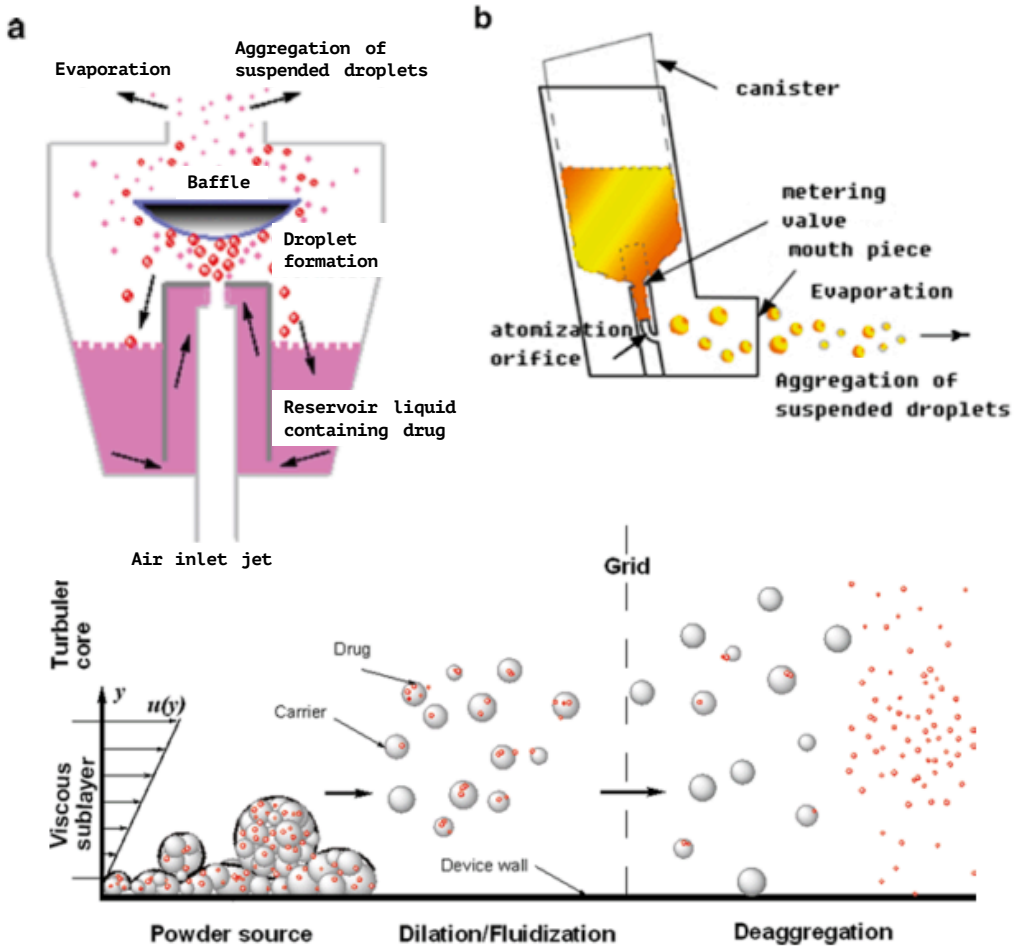

Figure 1.5 Classes of inhaled devices. Devices for pulmonary aerosol delivery, including (a) nebulizers, (b) pMDIs, and (c) DPIs. Figure adapted from Smyth and Hickey[22] with permission.

The oldest device is the nebulizer, which uses an external energy source to generate an aerosol from a liquid formulation.[38,39] Nebulizers can be used for most liquid formulations and for nearly any patient, as they require minimal patient coordination or skill.[38] Nebulizers are also useful for the delivery of therapeutics with a high dose by mass.[39] Therapeutic delivery via nebulizers is a burden to the patient, as these devices require treatments that typically last 10-20 minutes, not including the additional time required to disassemble and sanitize the nebulize after each use.[22,38] Nebulizers are generally recognized as inefficient in delivering drugs to the lungs, though modern nebulizers have been able to deliver between 30 and 75 % of the emitted dose to the lungs.[38,40] Due to the limitations of nebulizers, formulations are typically developed for delivery by nebulizers only if both pMDIs and DPIs are deemed inappropriate for the desired application.[39]

The development of pMDIs was revolutionary for pulmonary drug delivery, as it was the first highly portable device produced for inhalation.[38] pMDIs consist of a solution or suspension of drug in liquid hydrofluorocarbon propellant contained within a pressurized canister.[14,22,38] The canister has a metering valve that, upon actuation, releases a controlled volume of liquid propellant that rapidly equilibrates with the pressure of the atmosphere and forms drug-containing droplets.[22] Though pMDIs are convenient for most patients, the high velocity of aerosol emission and the requirement for coordination between device actuation and inhalation results in 50 – 80 % of the emitted dose depositing in the mouth and throat.[38,41] Despite the poor delivery efficiency, pMDIs remain common delivery devices that are frequently prescribed due to their portability, low cost, and ability to contain more than 100 doses.[38,42] The ability to overlook poor delivery efficiency is likely due to the low dose of drugs commonly delivered by pMDIs, including bronchodilators and corticosteroids, which require only microgram quantities

for therapeutic efficacy.[24]

The final class of delivery devices is DPIs, which provide an alternative to pMDIs while remaining small and portable.[38] DPIs utilize patient inhalation to generate an aerosol from a powder formulation contained within the delivery device.[21,39] Because patient inhalation produces the aerosol, the need for coordination between device actuation and inhalation required with pMDIs is eliminated.[21] Additionally, DPIs can be used to deliver milligram quantities of drug as opposed to the microgram quantities possible with pMDIs.[38,39] DPIs are particularly compatible with protein formulation, as dried protein formulations are less susceptible to degradation than liquid formulations.[15,43] However, the dry powder formulation in DPIs is susceptible to environmental humidity, which causes particles to flow poorly and deagglomerate inefficiently under air flow.[38] Inefficient deagglomeration results in premature particle deposition in the mouth and throat.[21] Proper packing of DPI formulations is required to minimize the effects of ambient humidity on moisture-sensitive formulations.[21]

As summarized above, each class of devices for pulmonary delivery has unique strengths and weaknesses which must be carefully considered to determine the ideal device for each new inhaled therapy. The dry powder formulation and increased deliverable doses of DPIs make them an ideal device for pulmonary protein delivery. As this dissertation is focused on the formulation of proteins into dry powders for pulmonary delivery, the remainder of the introduction will focus on the formulation and characterization of dry powder aerosols.

1.3.5 Aerosol Characterization of Dry Powder Inhalers

The fate of inhaled aerosols within the respiratory system can be reasonably predicted by the aerodynamic diameter of particles within the aerosol.[22] Aerosol particles with an aerodynamic diameter between 1 and 5 μm are optimal for efficient deposition in the alveoli of

the respiratory zone.[18] *In vitro* aerosol characterization must be performed as a step in the development of engineered dry powders to ensure the particles have an aerodynamic diameter between 1 and 5 μm, and thus can be expected to deposit in the alveoli.

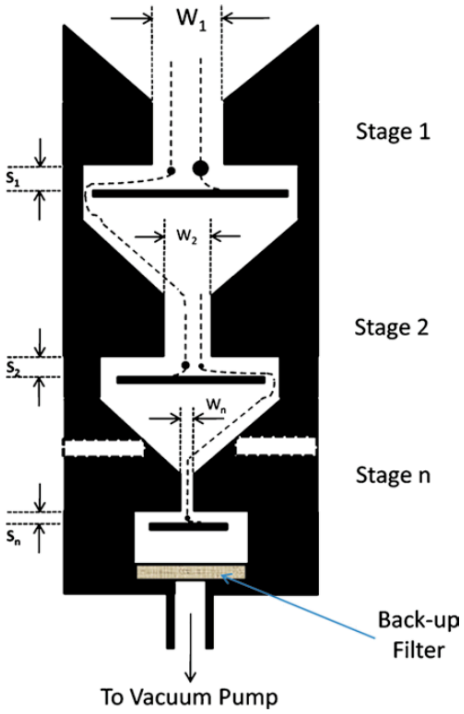

Figure 1.6 Particle pathway through cascade impactor. Diagram of the path of particle flow through an Andersen Cascade Impactor. Reproduced from Smyth and Hickey[22] with permission.

Cascade impaction is a widely-used technique to determine the aerodynamic diameter of inhaled aerosols.[44,45] Cascade impaction directly measures aerodynamic diameter by separating particles on a series of stages based on particle inertia.[45] An Andersen Cascade Impactor (ACI) contains eight vertically-stacked stages, each of which consists of a plate with holes of a specified diameter and arrangement and a collection plate for impacted particles.[45] The size and area of the holes decrease with progression through the ACI. The aerosol sample is drawn through the ACI under air flow, and, as the size of the holes progressively decreases, the velocity of air flow increases.[45] A diagram of particle flow through an ACI is presented in **Figure 1.6**. The increasing air velocity at each stage results in the collection of increasingly smaller particles

that achieve sufficient inertia to deposit by impaction. The result is a separation of particles by aerodynamic diameter on each of the eight stages.

1.4 Particle Fabrication Techniques for Dry Powder Inhalers

Particle engineering is a general strategy of manufacturing particles of optimal physical features, including size, shape, porosity, and density, to improve formulation performance. The application of particle engineering to dry powder formulations aims to decrease particle size polydispersity, improve fluidization and deagglomeration, and optimize drug bioavailability, among other goals.[11,46] In this section, two primary methods to produce engineered particles for high-performance dry powder aerosols, spray drying and spray freeze drying, are discussed. Alternative methods to manufacture engineered respirable particles are detailed in Chapter 2.

1.4.1 Spray Drying

Spray drying involves the atomization of a liquid formulation containing drug and excipient into micron-sized droplets followed by rapid drying in a heated gas stream to produce dry particles.[11,46] A diagram of the spray drying process is in **Figure 1.7**. While spray drying can be used to manufacture particles between 1 and 5 μm in aerodynamic diameter, particles this small are pushing the lower limits of spray drying, and thus require extensive particle engineering for successful production.[11] Many different process parameters can be altered to produce optimal particles, such as atomization pressure, feed flow rate and temperature, and drying chamber air flow and temperature.[46] For more information on particle engineering in spray drying, readers are referred to two excellent and comprehensive reviews by Reinhard Vehring, which discuss particle formation mechanisms in great detail.[46,47] A summary of process conditions used to fabricate engineered particles of differing morphologies in **Figure 1.8** highlights the flexibility of the spray drying process.

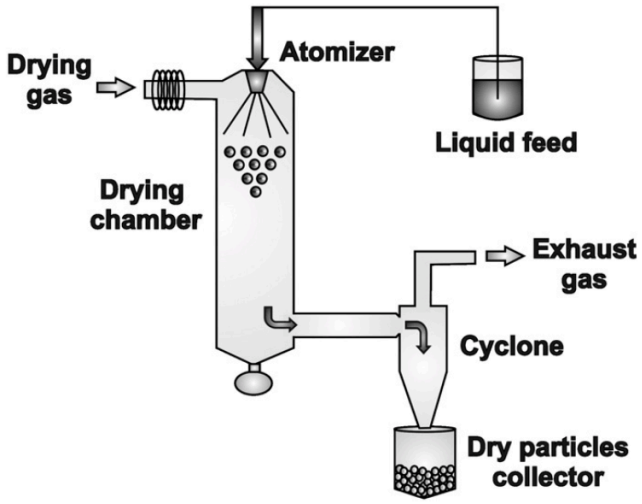

Figure 1.7 Spray dryer diagram. Process diagram of the equipment and process of a standard spray drying apparatus. Reproduced from Sosnik and Seremeta[48] with permission.

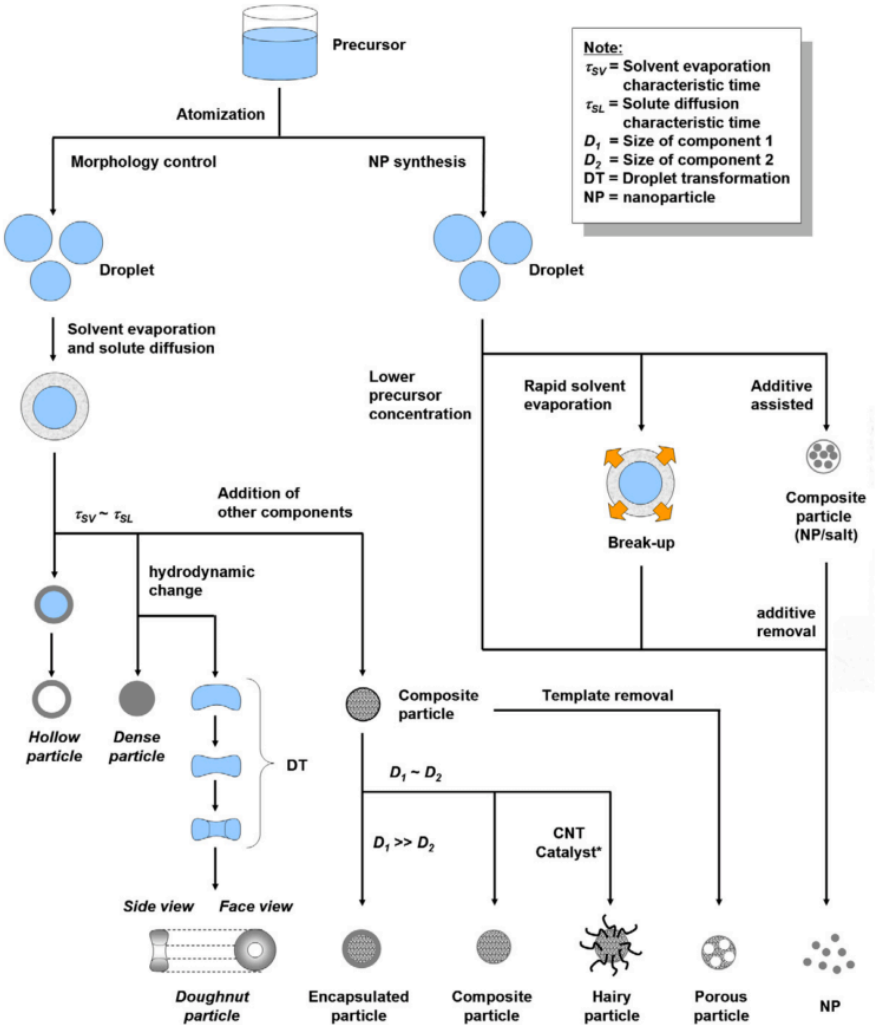

Figure 1.8 Particle engineering with spray drying. Preparation of multiple particle morphologies by spray drying. Reproduced from Nandiyanto and Okuyama with permission.

While spray drying has some control of particle size, shape, and density, control is limited to spherical particle morphologies. In addition, spray drying produces a range of particle sizes, which limits the ability of these particles to achieve efficient and precise lung deposition.[49]

1.4.2 Spray Freeze Drying

Spray freeze drying involves the atomization of a liquid formulation containing drug and excipient to form micron-sized droplets that are collected in cryogen, rather than in a cyclone as with spray drying. Droplets are frozen in either the vapor of a liquid cryogen or directly in a liquid cryogen as depicted in **Figure 1.9**. Frozen particles are then lyophilized to produce a dry powder.[11] Particles produced by spray freeze drying can be engineered into respirable particles in the range of 1 to 5 μm in aerodynamic diameter.[11,50] While processing parameters can be tuned to alter particle size and density, particle engineering strategies for spray freeze drying are not as developed as spray drying.[11] As with spray drying, spray freeze drying has limited control of particle morphology and produces a distribution of particle sizes, which limits the ability of these particles to efficiently and specifically deposit in the desired region of the lung.[50]

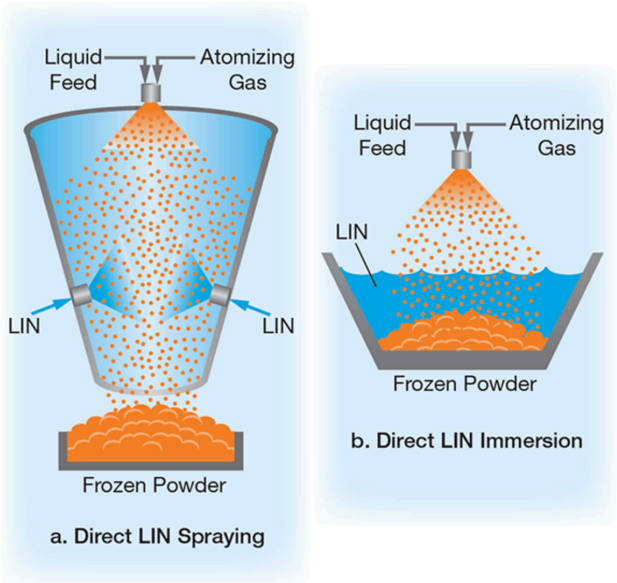

Figure 1.9 Methods of droplet freezing. Methods of droplet freezing in cryogen following atomization in spray freeze drying. Reproduced from Beteta and Ivanova[51] with permission.

1.5 Particle Replication in Non-wetting Templates

Particle replication in Non-wetting Templates (PRINT®) is a top-down nanofabrication technique that uses soft lithography to produce monodisperse nano- and microparticles with complete and independent control of particle size, shape, and composition **(Figure 1.10)**.[52–54] PRINT begins with fabrication of a silicon master by photolithography, in which the silicon is selectively etched to create an array of the desired particle geometry.[52] The master is then used to make a perfluoropolyether (PFPE) mold, which results in a mold patterned with replicates of the geometry etched into the master. The PFPE mold cavities are then filled with the desired particle composition by capillary forces, while spaces between cavities do not wet, resulting in discretely molded particles. Following particle solidification, particles are transferred from the mold to an adhesive polymer layer. The adhesive layer is then dissolved in a non-solvent to the particles, which yields a solution of monodisperse particles. The particle solution can then be lyophilized to generate a dry powder. The mild fabrication conditions of PRINT have allowed for the fabrication of particles containing therapeutic small molecules, proteins, and nucleic acids.[12,53–56]

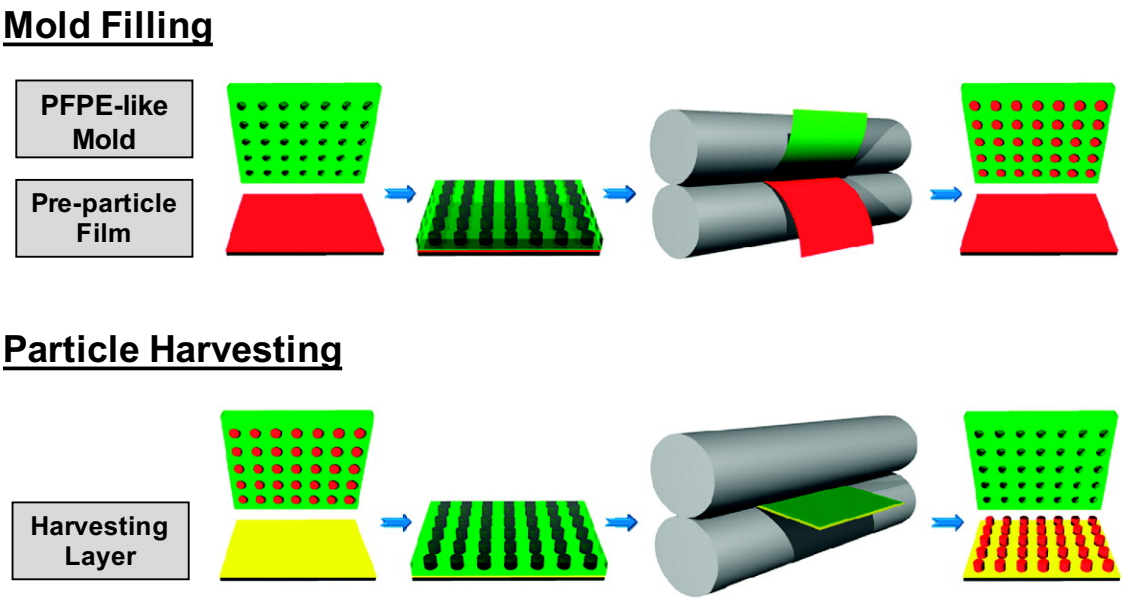

Figure 1.10 PRINT schematic. Schematic illustration of the PRINT process separated into the mold filling and particle harvesting steps. Adapted from Enlow et al.[57] with permission.

1.6 Overview of Dissertation

We hypothesized that the precise control of particle size, shape, and composition, along with the mild processing conditions afforded by PRINT, could be used to manufacture dry powder aerosols of protein particles. The overall goal of this work was to fabricate PRINT protein particles, characterize protein stability within PRINT particles, and evaluate the aerosol performance of PRINT dry powders to develop a high-performance protein dry powder formulation platform.

In Chapter 2, a formulation strategy for PRINT protein particles is optimized and a systematic approach to characterizing protein stability and dry powder aerosol parameters is established. Chapter 3 details the selection of the optimal particle shape for PRINT dry powders and probes the mechanism of particle shape in fluidization, aerosolization, and deposition. In Chapter 4, the formulation development and characterization strategies established in Chapter 2 and the optimized particle shape established in Chapter 3 are used to rapidly develop dry powder formulations of two therapeutic proteins. The delivery of a PRINT dry powder was also investigated *in vivo*. Chapter 5 contains a summary and recommendations for future work.

REFERENCES

1. Allen, T. M. & Cullis, P. R. Drug Delivery Systems: Entering the Mainstream. *Science.* **303,** 1818–1822 (2004).

2. Blanco, E., Shen, H. & Ferrari, M. Principles of nanoparticle design for overcoming biological barriers to drug delivery. *Nat. Biotechnol.* **33,** 941–951 (2015).

3. Farokhzad, O. C. & Langer, R. Impact of Nanotechnology on Drug Delivery. *ACS Nano* **3,** 16–20 (2009).

4. Park, K. Nanotechnology: What it can do for drug delivery. *J. Control. Release* **120,** 1–3 (2007).

5. Betancourt, T. & Brannon-Peppas, L. Micro-and nanofabrication methods in nanotechnological medical and pharmaceutical devices. *Int. J. Nanomedicine* **1,** 483–495 (2006).

6. Tao, S. L. & Desai, T. A. Microfabricated drug delivery systems: From particles to pores. *Adv. Drug Deliv. Rev.* **55,** 315–328 (2003).

7. Sant, S. *et al.* Microfabrication technologies for oral drug delivery. *Adv. Drug Deliv. Rev.* **64,** 496–507 (2012).

8. Tao, S. L. & Desai, T. A. Micromachined devices: The impact of controlled geometry from cell-targeting to bioavailability. *J. Control. Release* **109,** 127–138 (2005).

9. Guan, J., Ferrell, N., James Lee, L. & Hansford, D. J. Fabrication of polymeric microparticles for drug delivery by soft lithography. *Biomaterials* **27,** 4034–4041 (2006).

10. Rolland, J. & Maynor, B. Direct fabrication and harvesting of monodisperse, shape-specific nanobiomaterials. *J. Am. Chem. Soc.* 10096–10100 (2005).

11. Chow, A. H. L., Tong, H. H. Y., Chattopadhyay, P. & Shekunov, B. Y. Particle engineering for pulmonary drug delivery. *Pharm. Res.* **24,** 411–437 (2007).

12. Garcia, A. *et al.* Microfabricated Engineered Particle Systems for Respiratory Drug Delivery and Other Pharmaceutical Applications. *J. Drug Deliv.* **2012,** 1–10 (2012).

13. Mack, P., Horvath, K., Tully, J. & Maynor, B. Particle engineering for inhalation formulation and delivery of biotherapeutics. *Inhalation* **6,** 16–20 (2012).

14. Bäckman, P., Adelmann, H., Petersson, G. & Jones, C. B. Advances in inhaled technologies: understanding the therapeutic challenge, predicting clinical performance, and designing the optimal inhaled product. *Clin. Pharmacol. Ther.* **95,** 509–520 (2014).

15. Hoe, S., Boraey, M. A., Ivey, J. W., Finlay, W. H. & Vehring, R. Manufacturing and Device Options for the Delivery of Biotherapeutics. *J. Aerosol Med. Pulm. Drug Deliv.* **27,** 1–14 (2014).

16. Weers, J. G. & Miller, D. P. Formulation Design of Dry Powders for Inhalation. *J. Pharm. Sci.* **104,** 3259–3288 (2015).

17. Agu, R. U., Ugwoke, M. I., Armand, M., Kinget, R. & Verbeke, N. The lung as a route for systemic delivery of therapeutic proteins and peptides. *Respir. Res.* **2,** 198–209 (2001).

18. Patton, J. S. & Byron, P. R. Inhaling medicines: delivering drugs to the body through the lungs. *Nat. Rev. Drug Discov.* **6,** 67–74 (2007).

19. Longest, P. W., Tian, G., Li, X., Son, Y. J. & Hindle, M. Performance of Combination Drug and Hygroscopic Excipient Submicrometer Particles from a Softmist Inhaler in a Characteristic Model of the Airways. *Ann. Biomed. Eng.* **40,** 1–15 (2012).

20. Kleinstreuer, C., Zhang, Z. & Donohue, J. F. Targeted Drug-Aerosol Delivery in the Human Respiratory System. *Annu. Rev. Biomed. Eng.* **10,** 195–220 (2008).

21. de Boer, A. H. *et al.* Dry powder inhalation: past, present and future. *Expert Opin. Drug Deliv.* **14,** 499–512 (2017).

22. Smyth, H. D. C. & Hickey, A. J. *Controlled Pulmonary Drug Delivery*. (2011). doi:10.1007/978-1-4419-9745-6

23. Ionescu, C. M. The Human Respiratory System. 13–22 (2013). doi:10.1007/978-1-4471-5388-7_2

24. Labiris, N. R. & Dolovich, M. B. Pulmonary drug delivery. Part I: Physiological factors affecting therapeutic effectiveness of aerosolized medications. *Br. J. Clin. Pharmacol.* **56,** 588–599 (2003).

25. Groneberg, D. A., Witt, C., Wagner, U., Chung, K. F. & Fischer, A. Fundamentals of pulmonary drug delivery. *Respir. Med.* **97,** 382–387 (2003).

26. Folkesson, H. G. *et al.* Alveolar epithelial clearance of protein. *J. Appl. Physiol.* **80,** 1431–1445 (1996).

27. Hastings, R. H., Grady, M., Sakuma, T. & Matthay, M. A. Clearance of different-sized proteins from the alveolar space in humans and rabbits. *J. Appl. Physiol.* **73,** 1310–6 (1992).

28. Edwards, D. A. *et al.* Large Porous Particles for Pulmonary Drug Delivery. *Science.* **276,** 1868–1871 (1997).

29. Tabata, Y. & Ikada, Y. Effect of the size and surface charge of polymer microspheres on their phagocytosis by macrophage. *Biomaterials* **9,** 356–362 (1988).

30. Perry, J. L. *et al.* PEGylated PRINT nanoparticles: the impact of PEG density on protein binding, macrophage association, biodistribution, and pharmacokinetics. *Nano Lett.* **12,** 5304–10 (2012).

31. Evora, C. *et al.* Relating the phagocytosis of microparticles by alveolar macrophages to surface chemistry: The effect of 1,2-dipalmitoylphosphatidylcholine. *J. Control. Release* **51,** 143–152 (1998).

32. Zhang, Z. & Kleinstreuer, C. Airflow structures and nano-particle deposition in a human upper airway model. *J. Comput. Phys.* **198,** 178–210 (2004).

33. Heyder, J., Gebhart, J., Rudolf, G., Schiller, C. F. & Stahlhofen, W. Deposition of particles in the human respiratory tract in the size range 0.005-15 μm. *J. Aerosol Sci.* **17,** 811–825 (1986).

34. Kleinstreuer, C., Zhang, Z. & Li, Z. Modeling airflow and particle transport/deposition in pulmonary airways. *Respir. Physiol. Neurobiol.* **163,** 128–138 (2008).

35. Augusto, L. L. X., Lopes, G. C. & Goncalves, J. A. S. A CFD study of deposition of pharmaceutical aerosols under different respiratory conditions. *Brazilian J. Chem. Eng.* **33,** 549–558 (2016).

36. Byron, P. R. Prediction of Drug Residence Times in Regions of the Human Respiratory Tract Following Aerosol Inhalation. *J. Pharm. Sci.* **75,** 433–438 (1986).

37. Bryan, C. P. *The Papyrus Ebers*. (1930).

38. Labiris, N. R. & Dolovich, M. B. Pulmonary drug delivery. Part II: The role of inhalant delivery devices and drug formulations in therapeutic effectiveness of aerosolized medications. *Br. J. Clin. Pharmacol.* **56,** 600–612 (2003).

39. Claus, S., Weiler, C., Schiewe, J. & Friess, W. How can we bring high drug doses to the lung? *Eur. J. Pharm. Biopharm.* **86,** 1–6 (2014).

40. Lewis, R. A. & Fleming, J. S. Fractional deposition from a jet nebulizer: how it differs from a metered dose inhaler. *Br. J. Dis. Chest* **79,** 361–367 (1985).

41. Newman, S. P., Pavia, D., Morén, F., Sheahan, N. F. & Clarke, S. W. Deposition of pressurised aerosols in the human respiratory tract. *Thorax* **36,** 52–5 (1981).

42. Lenney, J., Innes, J. A. & Crompton, G. K. Inappropriate inhaler use: Assessment of use and patient preference of seven inhalation devices. *Respir. Med.* **94,** 496–500 (2000).

43. Maltesen, M. J. & van de Weert, M. Drying methods for protein pharmaceuticals. *Drug Discov. Today Technol.* **5,** e81–e88 (2008).

44. Nichols, S. C., Mitchell, J. P., Shelton, C. M. & Roberts, D. L. Good Cascade Impactor Practice (GCIP) and considerations for 'in-use' specifications. *AAPS PharmSciTech* **14,** 375–90 (2013).

45. Copley, M. Understanding cascade impaction and its importance for inhaler testing. 1–6 (2007).

46. Vehring, R. Pharmaceutical particle engineering via spray drying. *Pharm. Res.* **25,** 999–1022 (2008).

47. Vehring, R., Foss, W. R. & Lechuga-Ballesteros, D. Particle formation in spray drying. *J. Aerosol Sci.* **38,** 728–746 (2007).

48. Sosnik, A. & Seremeta, K. P. Advantages and challenges of the spray-drying technology for the production of pure drug particles and drug-loaded polymeric carriers. *Adv. Colloid Interface Sci.* **223,** 40–54 (2015).

49. Dolovich, M. B. & Dhand, R. Aerosol drug delivery: Developments in device design and clinical use. *Lancet* **377,** 1032–1045 (2011).

50. Zijlstra, G. S., Hinrichs, W. L. J., de Boer, A. H. & Frijlink, H. W. The role of particle engineering in relation to formulation and de-agglomeration principle in the development of a dry powder formulation for inhalation of cetrorelix. *Eur. J. Pharm. Sci.* **23,** 139–49 (2004).

51. Beteta, O. & Ivanova, S. Cool Down with Liquid Nitrogen. *Chemical Engineering Progress* 30–35 (2015).

52. Rolland, J. P. *et al.* Direct fabrication and harvesting of monodisperse, shape-specific nanobiomaterials. *J. Am. Chem. Soc.* **127,** 10096–10100 (2005).

53. Kelly, J. Y. & DeSimone, J. M. Shape-specific, monodisperse nano-molding of protein particles. *J. Am. Chem. Soc.* **130,** 5438–5439 (2008).

54. Xu, J. *et al.* Rendering protein-based particles transiently insoluble for therapeutic applications. *J. Am. Chem. Soc.* **134,** 8774–8777 (2012).

55. Khodabandehlou, K. *et al.* Silylated Precision Particles for Controlled Release of Proteins. *ACS Appl. Mater. Interfaces* **7,** 5756–5767 (2015).

56. Rahhal, T. B. *et al.* Pulmonary Delivery of Butyrylcholinesterase as a Model Protein to the Lung. *Mol. Pharm.* **13,** 1626–1635 (2016).

57. Enlow, E. M., Luft, J. C., Napier, M. E. & Desimone, J. M. Potent engineered PLGA nanoparticles by virtue of exceptionally high chemotherapeutic loadings. *Nano Lett.* **11,** 808–813 (2011).

CHAPTER 2: HIGH-PERFORMANCE PRINT DRY POWDER AEROSOLS FOR PULMONARY PROTEIN DELIVERY

2.1 Introduction

Pulmonary delivery is an attractive route of administration for therapeutic proteins, as it can be used for the direct administration of therapeutics to the lungs for respiratory conditions or for the non-invasive delivery of low molecular weight proteins to systemic circulation.[1,2] Of the options for inhalation, the formulation of proteins into dry powders for delivery via dry powder inhaler (DPI) is desirable since dried protein formulations are less prone to degradation.[2,3]

Dry powder inhalers utilize patient inhalation to generate an aerosol from the particles contained within the dry powder. However, many DPIs are inefficient at precisely delivering aerosols from the device to the lungs.[4,5] Drug retention in the device and orotracheal impaction can greatly reduce delivery efficiency to the lungs and increase the cost of treatment.[5] High orotracheal impaction can also result in undesirable side effects and potentially increase variability in the dose deposited in the lungs.[4–6] Further, the inability to target aerosol deposition within the lungs limits delivery efficiency to the desired therapeutic region and may limit the safety profile of certain medications.[1,7] Increasing the delivery efficiency of aerosols to specific regions within the lungs would decrease the costs and side effects associated with current inhaled medicines and potentially enable the development of the next generation of inhaled medicines.[1,7]

Particle engineering is a formulation strategy that aims to rationally design particle size, shape, density, and composition in order to generate high-performance aerosols that deposit efficiently and precisely in the lungs.[4,8] Traditional processes, such as spray drying (SD) or spray

freeze drying (SFD), have reasonable control of particle size and density, but generate a distribution of particle sizes and offer limited control of particle shape.[8,9] Incomplete control of particle morphology limits the ability of these formulations to be engineered for efficient and precise lung deposition. These processes also impose stresses on proteins during manufacturing.[3] A method more compatible with protein stability to manufacture precisely engineered particles could be utilized to develop high-performance aerosols of a variety of therapeutic proteins.

Several processes have emerged to manufacture engineered particles that produce high performance dry powder aerosols, some of which are capable of stable protein incorporation.[2,7,8] Some of the most widely investigated methods are based on supercritical fluid drying, of which the gas anti-solvent technique is most common for use with biologics.[2] This process involves atomization of a drug solution into a vessel of supercritical carbon dioxide, after which the supercritical carbon dioxide dissolves into the droplets resulting in drug precipitation and particle formation.[2] Particles produced with this technique are typically low density, which results in readily aerosolizable dry powders.[8] However, the poor miscibility of water and supercritical carbon dioxide requires the presence of an organic solvent in the droplet, which may compromise protein stability.[8,10]

Two novel platforms have leveraged controlled precipitation of protein drug or excipients to produce engineered protein microspheres for inhalation. The Technosphere® (MannKind Corporation, Valencia, CA) platform utilizes pH-dependent crystallization of fumaryl diketopiperazine (FDKP) to generate nanocrystals, which self-assemble into highly porous microsphere templates.[11] Protein drugs are loaded onto the microsphere surface by adsorption, which limits protein loading to the surface area of the particles.[11] Multiple therapeutic proteins have been shown to be compatible with the platform, including insulin (Afrezza®), which was

able to deliver 60 % of the dose emitted from a DPI to the lungs.[12] Further improvement in delivery efficiency via formulation optimization may prove difficult, as the self-assembly process limits control over particle morphology.[8] Promaxx® (Baxter International Inc., Deerfield, IL) technology involves protein dissolution in an aqueous polyethylene glycol (PEG) solution at an elevated temperature followed by cooling, which generates a supersaturated protein solution. The supersaturated solution is conducive to the nucleation and growth of engineered protein microspheres.[13] A Promaxx formulation of alpha-1-antitrypsin was shown to retain protein activity and aerosolize efficiently, with 73 % of the emitted dose appropriate for lung deposition.[8] However, this process requires multiple steps to purify microspheres from solution and is limited to producing spherical particles.[13]

A platform capable of manufacturing respirable engineered particles with complete control of particle morphology while maintaining both the structure and function of the incorporated proteins would be invaluable in the development of high-performance protein aerosols. The Particle Replication in Non-wetting Templates (PRINT) platform has previously been used to manufacture respirable dry powders of monodisperse engineered particles.[14,15] The aerosol performance of dry powders comprised of PRINT particles composed of model polymer hexanediol diacrylate (HDODA) was evaluated *in vitro* from a DPI using an Andersen Cascade Impactor (ACI). Dry powders of PRINT HDODA particles were found to be appropriate for pulmonary delivery with relatively precise deposition profiles when aerosolized from a dry powder inhaler.[16]

The work presented in this chapter represents our efforts to extend the PRINT platform to pulmonary protein delivery and focuses on the development and characterization of dry powders of PRINT protein particles. The specific objective of this chapter was to manufacture dry

powders of PRINT particles containing model proteins bovine serum albumin (BSA) and lysozyme for the purpose of extensively characterizing protein structure and function at each step of the PRINT process. In addition, the aerosol performance of each formulation was evaluated *in vitro* with a cascade impactor.

2.2 Materials and Methods

2.2.1 Materials

Lysozyme from chicken egg white, bovine serum albumin, poly(1-vinylpyrrolidone-co-vinyl acetate) (PVPVA), fluorescamine, and anhydrous isopropanol were purchased from Sigma-Aldrich (St. Louis, MO, USA). α-D-lactose and glycerol were obtained from Acros Organics (Geel, Belgium). Supplies for denaturing gel electrophoresis, including gels, buffers, molecular weight standards, and Coomassie R-250, were obtained from Thermo Scientific (Waltham, MA, USA). The EnzChek® Lysozyme Assay Kit was purchased from Molecular Probes (Eugene, OR, USA). PRINT mold patterned with 1 μm cylinders was acquired from Liquidia Technologies, Inc. (Morrisville, NC, USA). Molykote® 316 silicone spray was obtained from Dow Corning (Midland, MI, USA). Amicon® Ultra 3k molecular weight cutoff (MWCO) centrifugal filters were purchased from EMD Millipore (Billerica, MA, USA).

2.2.2 Methods

2.2.2.1 Fabrication of PRINT Protein Particles

Protein-based PRINT particles of BSA and lysozyme were fabricated using a method adapted from Xu et al.[17] Proteins were purified by dialysis. For both formulations, a 10 wt% (% weight per weight) pre-particle solution (PPS) of protein, lactose, and glycerol in water was cast into a film on a poly(ethylene terephthalate) (PET) sheet. The ratio of protein:lactose:glycerol in the PPS was optimized experimentally. Following film drying, PRINT mold patterned with 1 μm

cylinders (or desired particle geometry) was applied to the film and passed through a heated laminator at 98 °C and 100 psi. Particles were removed from the mold by laminating filled mold to a sheet of PET coated with PVPVA. Particles were collected by dissolving the PVPVA layer with isopropanol, and particles were washed with isopropanol to remove remaining PVPVA.

2.2.2.2 Particle Lyophilization

Particles were centrifuged at 3000 x g for 3 minutes to remove isopropanol. Particles were then resuspended in *tert*-butanol at approximately 1 mg/mL and flash frozen in liquid nitrogen for 1 minute. Particles were then immediately placed on a lyophilizer under maximum vacuum. Samples remained on the lyophilizer for 24 hours, after which the dry powders were removed and stored in a sealed desiccator with desiccant.

2.2.2.3 Scanning Electron Microscopy

Particles were suspended in isopropanol and dried on silicon prior to scanning electron microscopy (SEM). Samples were coated with 3 nm Au/Pd with a Cressington 108 Auto Sputter Coater (Watford, England). Imaging was performed with a Hitachi S-4700 SEM (Tokyo, Japan).

2.2.2.4 Thermogravimetric Analysis

Particle yield and concentration was determined using thermogravimetric analysis (TGA) to measure the particle mass within an isopropanol particle solution. Samples were loaded at 10 μL into disposable aluminum pans that had been tared by the TA Instruments (New Castle, DE, USA) Discovery TGA 5500. Samples were heated to 50 °C at a rate of 5 °C/min followed by an isothermic hold at 50 °C for 20 minutes. The mass of the sample at the end of the isothermic hold was used as the particle mass in 10 μL of solution.

2.2.2.5 Particle Composition Analysis

Particle composition was determined using high-performance liquid chromatography

(HPLC) to measure the lactose and glycerol content of each formulation based on a previously published method.[17] Formulation samples were dissolved in water, and lactose and glycerol were separated from protein using 0.5 mL Amicon® Ultra 3k MWCO centrifugal filters. The filtrate was analyzed on an Agilent 1260 Infinity Quaternary LC with a Hi-Plex Ca column (300 x 7.7 mm, 8 μm) (Agilent, Santa Clara, CA, USA) using a mobile phase of pure water and an evaporative light scattering detector (ELSD). Lactose and glycerol peaks were integrated and compared to standards to determine particle composition.

2.2.2.6 Roll-to-Roll Particle Manufacturing

Fabrication of BSA 1 μm cylinders was scaled for manufacturing on a roll-to-roll system. Design of experiments (DOE) was used along with JMP software (SAS, Cary, NC, USA) to identify fabrication parameters critical to the successful roll-to-roll production of BSA 1 μm cylinders. For each fabrication run, particle yield was determined by TGA and morphology was observed with SEM.

2.2.2.7 Gel Electrophoresis

SDS-PAGE (sodium dodecyl sulfate - polyacrylamide gel electrophoresis) was performed using an XCell™ SureLock™ Mini-Cell (Invitrogen, Waltham, MA, USA) with NuPAGE® Novex® 4 - 12 % Bis-Tris protein gels. Protein was isolated from lyophilized particles by dissolving particles in water followed by separation through a 0.5 mL Amicon® Ultra 3k MWCO centrifugal filter. Two additional water washes were performed on the protein retentate. Samples were denatured and reduced according to the manufacturer's instructions. Stained BenchMark™ protein ladder and unprocessed proteins were used as controls. 5 μg of protein was loaded per well and run for 35 minutes at 200V in NuPAGE® MES SDS running buffer. Gels were stained with Coomassie R-250 prior to imaging.

2.2.2.8 Circular Dichroism

Purified protein was prepared for circular dichroism (CD) in 10 mM potassium phosphate buffer (pH 7.4) in a 1 mm quartz Suprasil® cell (Hellma Analytics, Müllheim, Germany). Protein concentration was adjusted to yield an optical density of 0.8. Heat denatured controls were prepared by incubating proteins at 70 °C for 30 minutes. Spectra were collected in triplicate from 185 to 260 nm in 1 nm steps at 25 °C with a Chirascan™ Plus CD Spectrophotometer (Applied Photophysics, Leatherhead, England). Spectra were deconvoluted using CDPro software (N. Sreerama, Colorado State University) with CONTINLL to determine secondary structure.

2.2.2.9 Intrinsic Fluorescence

Samples and controls for intrinsic fluorescence were prepared at 50 μg/mL protein in the same manner as samples for CD and loaded into a black 96-well microplate in triplicate. Samples were excited at 280 nm and the emission spectra were collected from 320 to 400 nm using a SpectraMax® M5 Microplate Reader (Molecular Devices, Sunnyvale, CA, USA).

2.2.2.10 Lysozyme Activity Assay

Lysozyme enzymatic activity was determined using an EnzChek® Lysozyme Assay Kit according to the manufacturer's directions. Lysozyme was purified from particles as previously described.

2.2.2.11 Storage Stability

The stability of protein in PRINT dry powders was observed over the course of 3 months at multiple temperatures. Lyophilized BSA and lysozyme 1 μm cylinders were stored for 1 week, 1 month, 2 months, and 3 months at -20 °C, 4 °C, 25 °C, and 50 °C at ambient humidity. Purified protein and newly made lyophilized particle samples were used as controls. Following storage, protein was purified and stability was observed via SDS-PAGE as previously described.

2.2.2.12 Fluorescamine Assay

The fluorescamine assay was adapted from Bantan-Polak et al.[18] To each well of an opaque 96-well plate, 100 μL of sample and 50 μL 3 mg/mL fluorescamine in acetonitrile was added. The plate was stored in darkness for 5 minutes and fluorescence was read at λ_{ex} = 390 nm and λ_{em} = 475 nm. Sample fluorescence was compared to a standard curve to determine protein concentration.

2.2.2.13 Cascade Impaction

Aerodynamic performance of both formulations was evaluated from a Penn-Century DP-4M mouse insufflator (Penn-Century, Inc., Wyndmoor, PA) and an RS01 Monodose Dry Powder Inhaler (Plastiape, Italy) with an Andersen Cascade Impactor (ACI) (Copley Scientific, Colwick, England). The ACI was operated at 28.3 L/min for the insufflator and was fitted with a 60 L/min conversion kit (Copley Scientific, Colwick, England) and operated at 60 L/min for the Monodose inhaler. Impactor plates were coated with Molykote® 316 silicone spray to prevent particle re-entrainment. Approximately 5 mg of each dry powder was loaded into a size 3 Quali-V® HPMC Capsule (Qualicaps, Madrid, Spain). The loaded capsule was placed inside of the inhaler and punctured 5 seconds prior to running the ACI at 28.3 L/min for 8.5 seconds or 60 L/min for 4 seconds. Particles in the inhaler, capsule, throat, each of the stages, and the filter were collected in water and quantified with a fluorescamine assay normalized for particle composition as determined by HPLC. The mass median aerodynamic diameter (MMAD) of each formulation was determined by plotting cumulative mass versus aerodynamic diameter for each stage logarithmically. The MMAD is the diameter at which 50 % of particles are larger and 50 % are smaller, by mass. The remaining parameters were calculated as described in the equations below.

$$Geometric\ standard\ deviation\ (GSD) = \sqrt{\frac{d_{86}}{d_{16}}} \tag{2.1}$$

$$Emitted\ dose\ (ED) = 100 * \frac{m_{loaded} - m_{final}}{m_{loaded}} \quad (2.2)$$

$$Fine\ particle\ fraction\ (FPF) = 100 * \frac{Cumulative\ mass\ below\ stage\ 1}{Cumulative\ mass\ collected} \quad (2.3)$$

$$Respirable\ fraction\ (RF) = 100 * \frac{Cumulative\ mass\ stages\ 2-4}{Cumulative\ mass\ collected} \quad (2.4)$$

2.2.2.14 Statistics

Statistical analyses were performed using GraphPad Prism Version 5.1 (GraphPad Software, La Jolla, CA, USA). Data presented as mean ± standard deviation and statistical analyses are one-way analysis of variance (ANOVA) (α=0.05) unless otherwise noted.

2.3 Results

2.3.1 Fabrication of Respirable PRINT Protein Particles

2.3.1.1 Fabrication and Morphological Characterization

A PPS containing 40 % protein, 35 % lactose, and 25 % glycerol by mass in water at 10 wt% was determined to generate a film optimal for the fabrication of both BSA and lysozyme 1 μm cylinder protein particles by SEM **(Figure 2.1)**. Lyophilization of the particles from *tert*-butanol generated flowable dry powders **(Figure 2.2)** that are rapidly water-soluble. Imaging of lyophilized particles resuspended in isopropanol to aid in clear imaging revealed that particles were successfully lyophilized without altering particle morphology **(Figure 2.3)**. Additionally, the 40:35:25 BSA:lactose:glycerol PPS was prepared at 5 wt% to fabricate 80nm x 320 nm rods **(Figure 2.4)**.

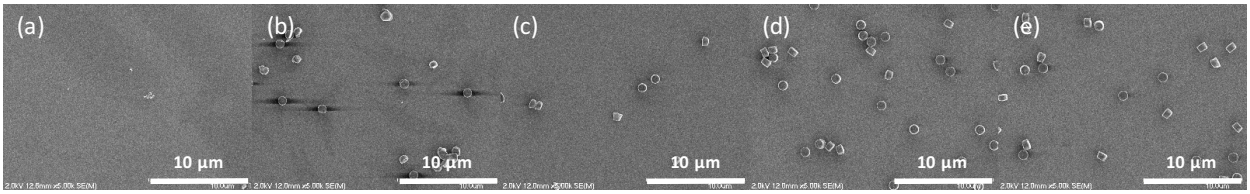

Figure 2.1 Formulation optimization of lysozyme 1 μm cylinders. SEM images of lysozyme 1 μm cylinders fabricated from 10 wt% PPS of lysozyme:lactose:glycerol at (a) 30:40:25, (b) 32.5:42.5:25, (c) 35:40:25, (d) 37.5:37.5:25, and (e) 40:35:25 imaged at 10k magnification.

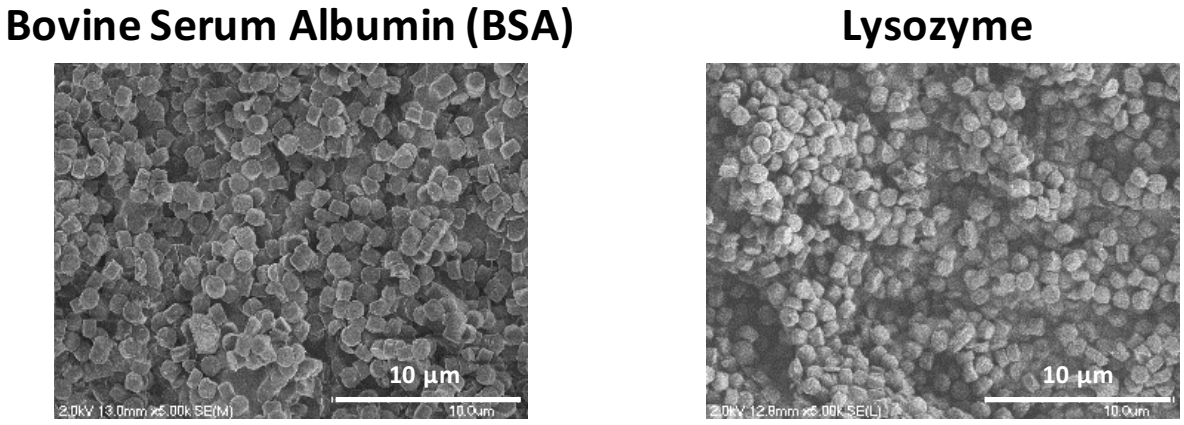

Figure 2.2 SEM of dry powders of BSA and lysozyme 1 µm cylinders. SEM images of lyophilized dry powders of BSA and lysozyme 1 µm cylinders fabricated from a 10 wt% PPS containing 40:35:25 protein:lactose:glycerol.

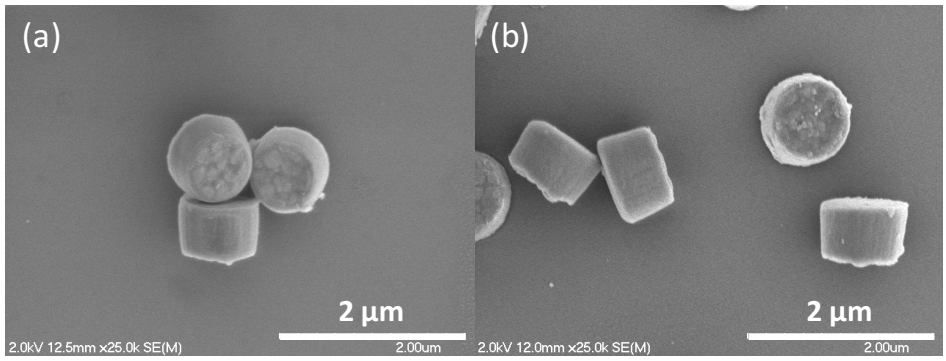

Figure 2.3 SEM of lyophilized BSA and lysozyme 1 µm cylinders.SEM images of lyophilized (a) BSA and (b) lysozyme 1 µm cylinders resuspended in isopropanol imaged at 25k magnification.

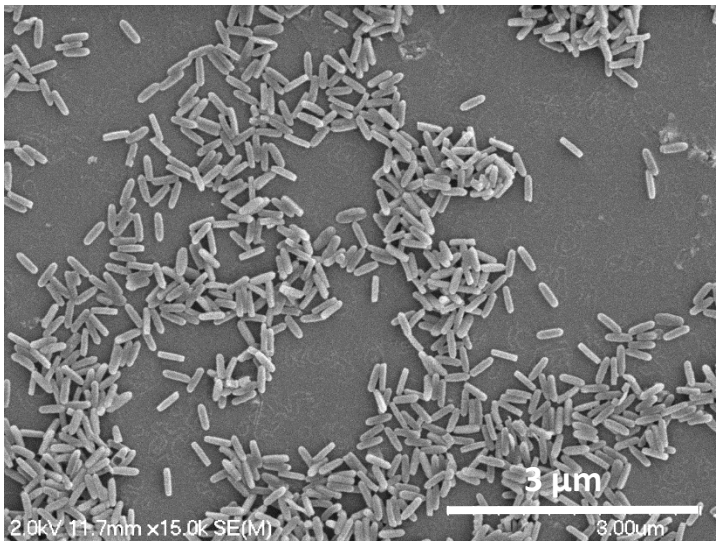

Figure 2.4 SEM of BSA 80x320 nm rods. SEM image of BSA 80nm x 320nm rods in isopropanol at 15k magnification.

2.3.1.2 Particle Composition Analysis

Analysis of particle composition with HPLC determined that BSA and lysozyme 1 μm cylinders have similar relative compositions, as shown in **Figure 2.5**. Lysozyme 1 μm cylinders are composed of 85.8 % ± 1.2 lysozyme by mass and BSA 1 μm cylinders are composed of 84.4 % ± 6.4 BSA by mass. Approximately 15 % of the composition of both formulations was attributed to excipient mass from lactose and glycerol. Further investigation determined that the majority of glycerol and more than half of lactose was removed from the particles during the isopropanol washes due to dissolution **(Figure 2.6)**.

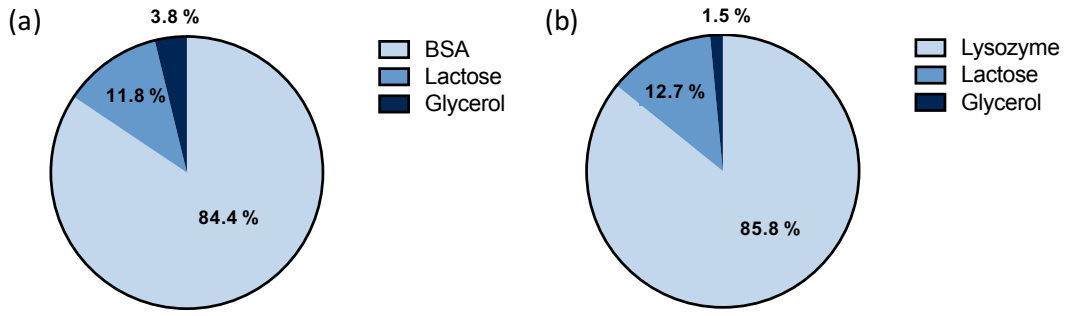

Figure 2.5 Composition of lyophilized BSA and lysozyme 1 μm cylinders. Composition of lyophilized (a) BSA and (b) lysozyme 1 μm cylinders by mass as determined by HPLC (n=3).

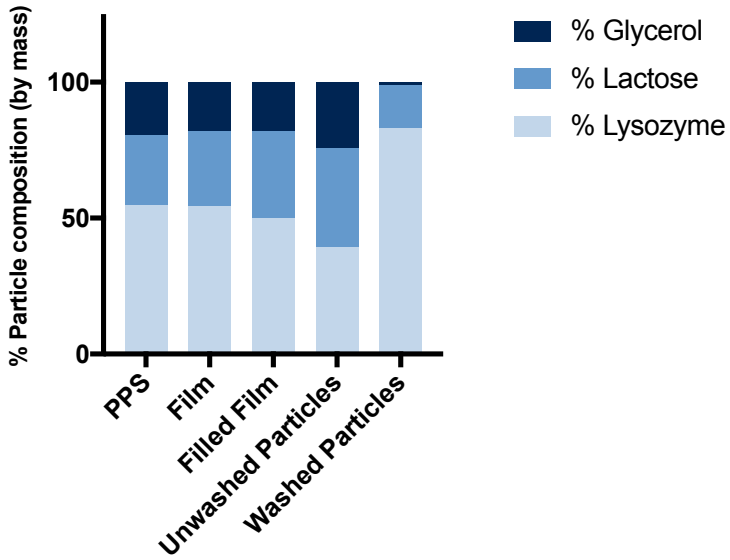

Figure 2.6 Composition of lyophilized BSA and lysozyme 1 μm cylinders. Composition of each step in the fabrication of lysozyme 1 μm cylinders by mass as determined by HPLC (n=1).

2.3.1.3 Roll-to-Roll Particle Manufacturing

Fabrication of BSA 1 μm cylinders was scaled to a roll-to-roll system using the DOE sequence presented in **Table 2.1** generated by JMP. Run 3 and run 7 were terminated early due to overheating of the mold; all other runs successfully fabricated particles **(Figure 2.7)**. Based on particle yield per foot determined by TGA and morphology observed with SEM, the parameters used in Run 8 were identified as optimal.

Table 2.1 DOE for roll-to-roll BSA 1 μm cylinders. Sequence of fabrication parameters for DOE experiment to identify fabrication parameters critical to successful roll-to-roll production scale-up of BSA 1 μm cylinders.

Run	Water Vapor Pressure (mbar)	Fill Temp (C)	Speed (ft/min)	PPS Wt%
1	7.5	77	8	7.5
2	7.5	77	12	10
3	7.5	88	8	10
4	7.5	88	12	7.5
5	9.0	77	8	10
6	9.0	77	12	7.5
7	9.0	88	8	7.5
8	9.0	88	12	10

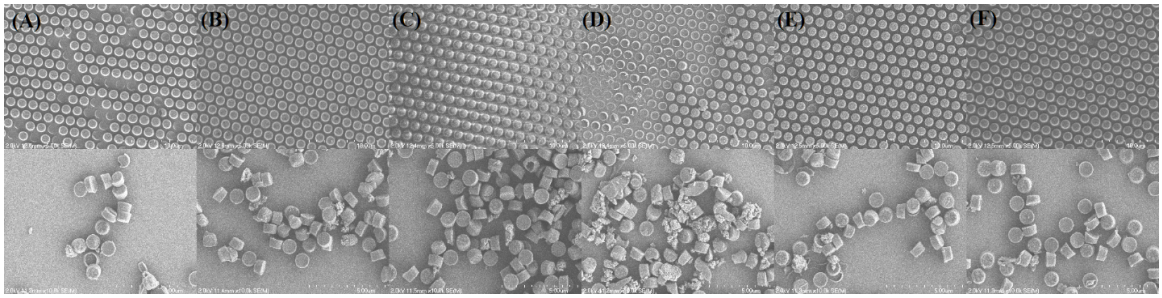

Figure 2.7 SEM of roll-to-roll BSA 1 μm cylinders. SEM images of BSA 1 μm cylinders fabricated with parameters listed in **Table 2.1**. Top row is particles on harvesting layer and bottom row is following isopropanol washes. (A) Run 1, (B) Run 2, (C) Run 4, (D) Run 5, (E) Run 6, and (F) Run 8.

2.3.2 Characterization of Protein Stability

2.3.2.1 Denaturing Gel Electrophoresis

The primary structures of BSA and lysozyme were observed by SDS-PAGE, where the migration of bands in the gel is dependent on protein molecular weight. Protein purified from lyophilized 1 μm cylinders was compared to unprocessed protein and PPS controls. No change in

band migration was observed for either BSA or lysozyme 1 μm cylinders relative to control samples **(Figure 2.8)**.

2.3.2.2 Circular Dichroism

Circular dichroism was used to monitor potential changes in the regional secondary structures of BSA and lysozyme. Changes in the secondary structure of a protein are expected to be observed as a change in CD spectra, which is frequently observed as a decrease in signal intensity. The spectra obtained for protein controls and lyophilized particles overlaid one another, while the heat denatured controls had dramatically reduced signal intensity throughout the spectrum **(Figure 2.9)**. Additionally, the secondary structure content of each protein sample remained similar throughout processing, while the denatured standard displayed altered structure **(Figure 2.10)**.

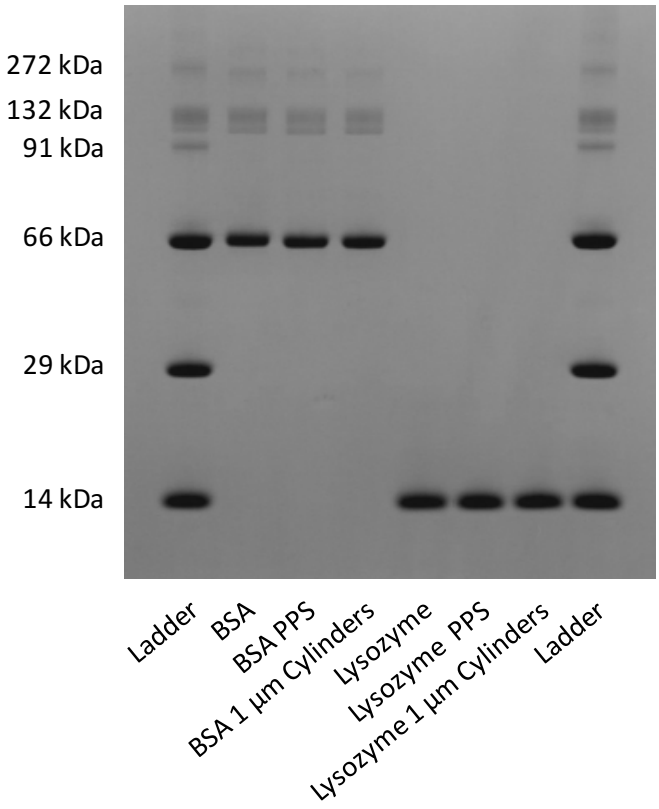

Figure 2.8 SDS-PAGE of lyophilized BSA and lysozyme 1 μm cylinders. SDS-PAGE of protein from each formulation step for lyophilized BSA and lysozyme 1 μm cylinders (n=3).

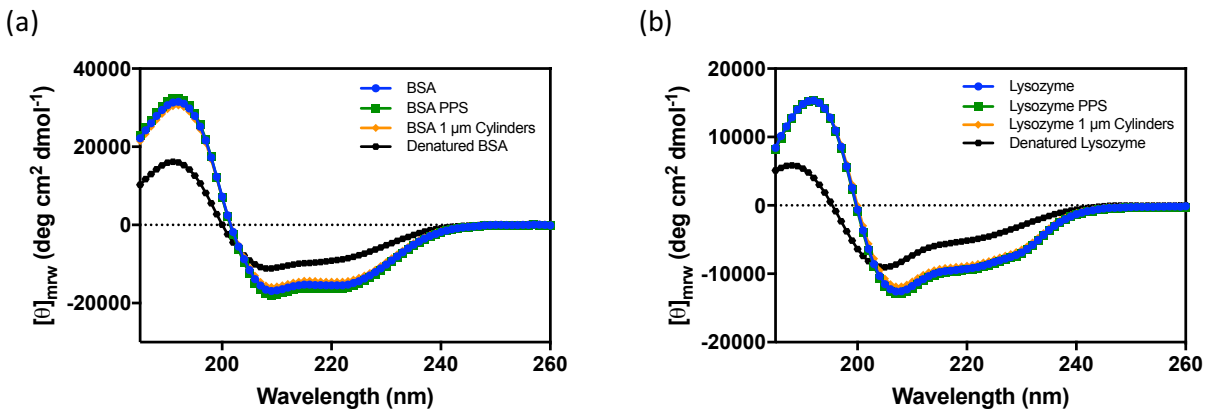

Figure 2.9 Circular dichroism of lyophilized BSA and lysozyme 1 µm cylinders. CD spectra from each formulation step for lyophilized (a) BSA and (b) lysozyme 1 µm cylinders (n=3).

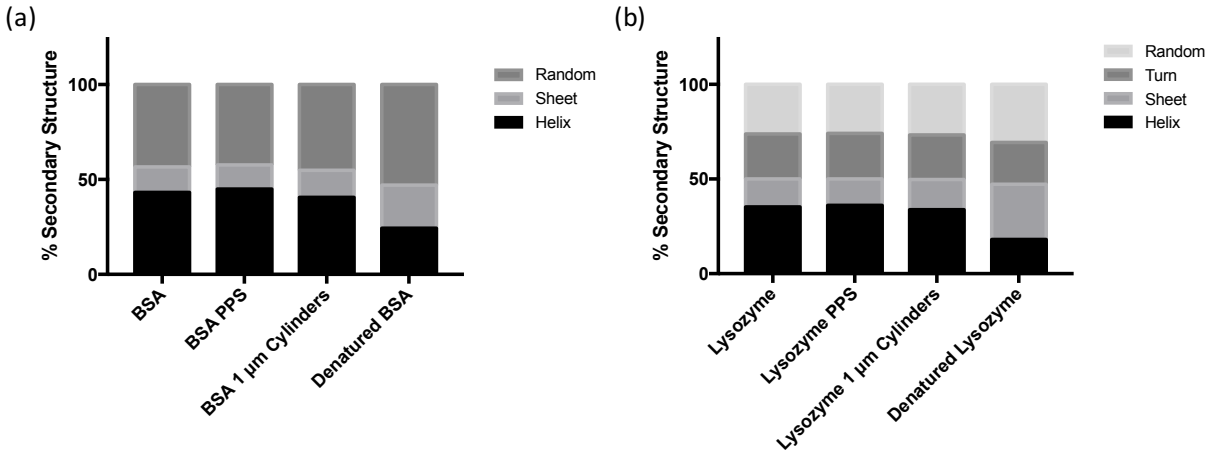

Figure 2.10 Secondary structure of lyophilized BSA and lysozyme 1 µm cylinders. Structure composition calculated from CD spectra from each formulation step for lyophilized (a) BSA and (b) lysozyme 1 µm cylinders (n=3).

2.3.2.3 Intrinsic Fluorescence

The tertiary structures of BSA and lysozyme were observed with intrinsic fluorescence, which monitors the environments of aromatic residues within the three-dimensional conformation of a single polypeptide chain. A change in the tertiary structure of a protein produces a change in the intrinsic fluorescence spectra, often resulting in a decrease in signal intensity at λ_{max} or a shift in λ_{max}. The spectra of lyophilized particles and protein controls overlaid one another, while denatured controls exhibited a red-shift in λ_{max} along with a decrease in signal intensity at λ_{max} **(Figure 2.11)**.

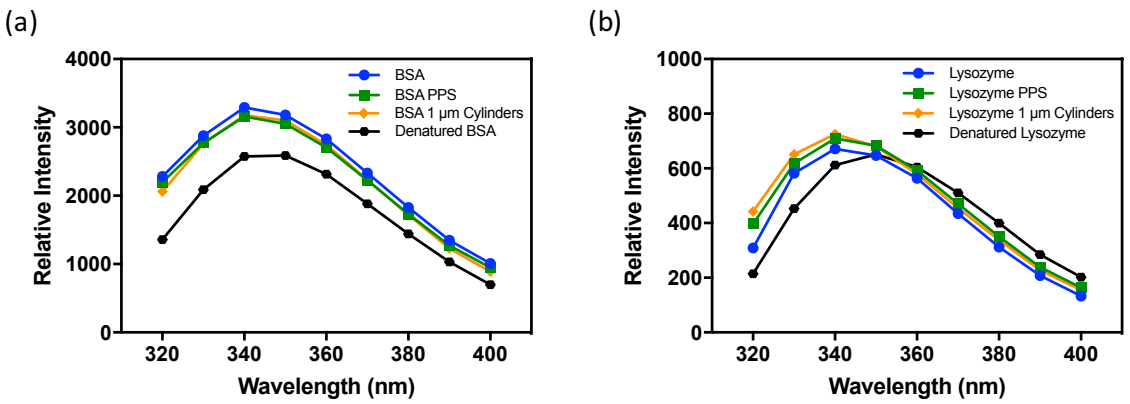

Figure 2.11 Intrinsic fluorescence of lyophilized BSA and lysozyme 1 µm cylinders. Intrinsic fluorescence spectra of protein from each formulation step for lyophilized (a) BSA and (b) lysozyme 1 µm cylinders (n=3).

2.3.2.4 Lysozyme Activity Assay

In addition to structural evaluation, the functional activity of lysozyme was examined. No significant change in lysozyme activity was found following fabrication and lyophilization of particles. In comparison, the denatured control lost more than 50 % of its activity ($p<0.0001$) **(Figure 2.12)**.

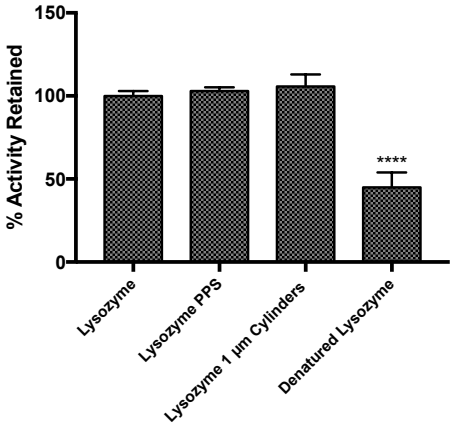

Figure 2.12 Enzymatic activity of lyophilized lysozyme 1 µm cylinders. Activity of lysozyme from each formulation step relative to a lysozyme standard for lyophilized lysozyme 1 µm cylinders (n=3) (**** $p<0.0001$).

2.3.2.5 Storage Stability

In addition to studying post-fabrication protein stability, storage stability studies were performed on lyophilized particles over 3 months at -20, 4, 25, and 50 °C. The molecular weight

of proteins was observed with SDS-PAGE. No changes in the molecular weight of BSA or lysozyme were observed at any point at -20 °C or 4 °C **(Figures 2.13a and 2.13c)**. When stored at 25 °C, both proteins had an increase in molecular weight at 2 and 3 months. All time points had increased high molecular weight species when stored at 50 °C **(Figures 2.13b and 2.13d)**.

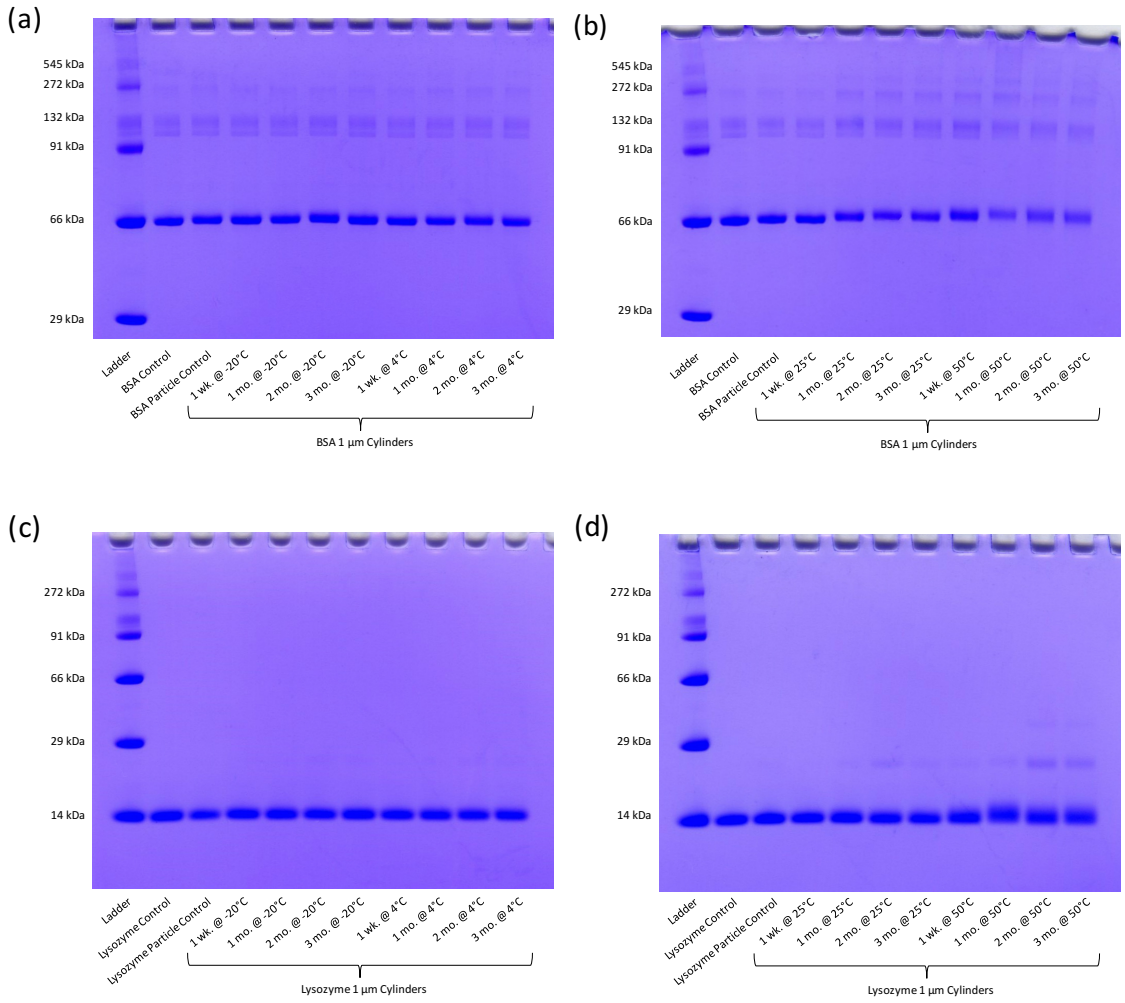

Figure 2.13 SDS-PAGE of lyophilized BSA and lysozyme 1 µm cylinders. SDS-PAGE of lyophilized 1 µm cylinders of BSA stored at (a) -20 °C and 4 °C and (b) 25 °C and 50 °C and of lysozyme stored at (c) -20 °C and 4 °C and (d) 25 °C and 50 °C.

2.3.3 *In Vitro* Aerosol Characterization

2.3.3.1 Penn-Century DP-4M Insufflator

The aerodynamic behavior of dry powder formulations of BSA and lysozyme 1 µm

cylinders was characterized *in vitro* with an ACI at 28.3 L/min using a Penn-Century DP-4M mouse insufflator. The dose deposited on each stage is presented as a fraction of the total collected dose in **Figure 2.14**. The deposition profiles of both formulations were used to calculate several aerosol parameters, summarized in **Table 2.2**. Deposition of both BSA and lysozyme 1 μm cylinders was centered on stage 4 (2.1 – 3.3 μm at 28.3 L/min), with more than 35 % of the collected dose for each formulation depositing on stage 4 alone. The deposition profiles resulted in an MMAD of 3.13 μm ± 0.44 for BSA 1 μm cylinders and 2.84 μm ± 0.35 for lysozyme 1 μm cylinders. The FPF of the collected dose was 88.7 % ± 21.6 and 84.8 % ± 5.9 for BSA and lysozyme 1 μm cylinders, respectively. Both BSA and lysozyme particles had a GSD near 1.5.

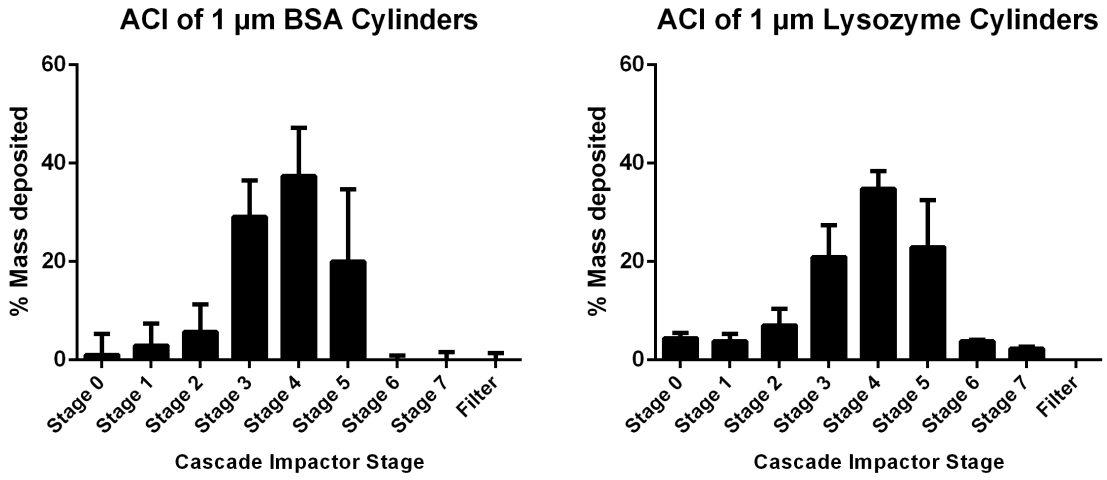

Figure 2.14 Cascade impaction of lyophilized BSA and lysozyme 1 μm cylinders from an insufflator. Distribution of lyophilized BSA and lysozyme 1 μm cylinders from a DP-4M Penn-Century insufflation device at 28.3 L/min (n=3).

Table 2.2 Aerosol parameters of lyophilized BSA and lysozyme 1 μm cylinders from an insufflator. Aerosol parameters of lyophilized BSA and lysozyme 1 μm cylinders from a DP-4M Penn-Century insufflation device at 28.3 L/min (n=3).

Protein	MMAD (μm)	GSD	FPF (%)
BSA	3.13 ± 0.44	1.41 ± 0.01	88.7 ± 21.6
Lysozyme	2.84 ± 0.35	1.56 ± 0.06	84.8 ± 5.9

2.3.3.2 Monodose RS01 Dry Powder Inhaler

The aerodynamic behavior of BSA and lysozyme 1 μm cylinders was characterized *in vitro* with an ACI using a Monodose RS01 inhaler. The dose remaining in the inhaler and the dose deposited in the throat and on each stage is presented as a fraction of the total collected dose in **Figure 2.15**. Both formulations were efficiently emitted from the inhaler, with less than 20 % of the collected dose remaining in the capsule and inhaler following aerosolization. Additionally, both formulations avoided deposition in the artificial throat, with less than 10 % of the collected dose recovered in the throat. The deposition profiles of both formulations were used to calculate several aerosol parameters, summarized in **Table 2.3**. Deposition of both BSA and lysozyme 1 μm cylinders was centered on stage 4 (1.1 – 2.0 μm at 60 L/min), with more than 40 % of the collected dose for each formulation depositing on stage 4 alone. The deposition profiles resulted in an MMAD of 1.77 μm ± 0.06 for BSA particles and 1.83 μm ± 0.12 for lysozyme particles. The FPF of the collected dose was 78.6 % ± 0.3 and 84.6 % ± 4.3 for BSA and lysozyme 1 μm cylinders, respectively. Both formulations had a GSD near 1.5.

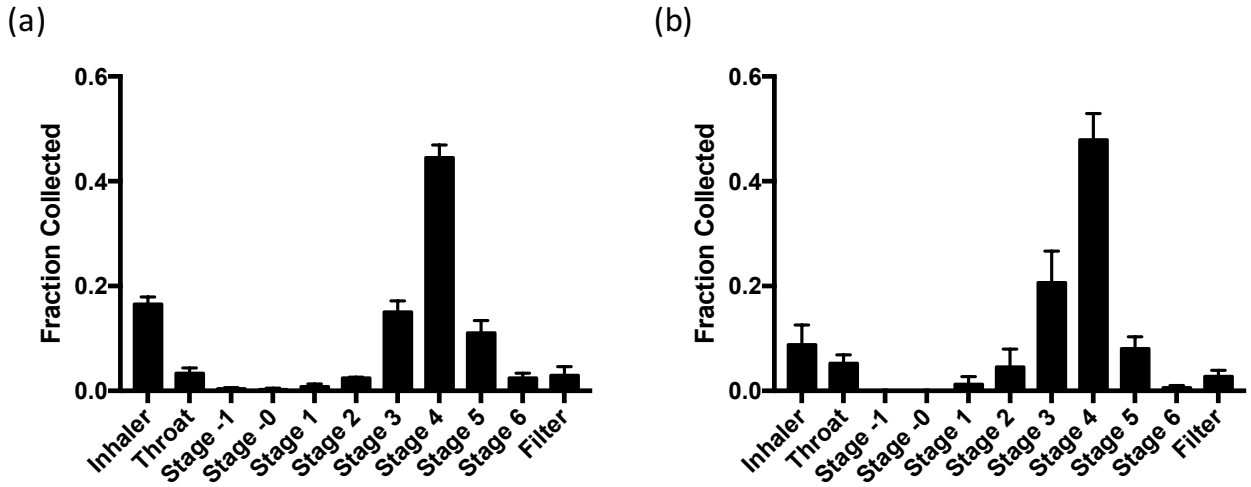

Figure 2.15 Cascade impaction of lyophilized BSA and lysozyme 1 μm cylinders from an inhaler. Cascade impaction distribution of lyophilized (a) BSA and (b) lysozyme 1 μm cylinders from a Monodose RS01 inhaler at 60 L/min (n=3).

Table 2.3 Aerosol parameters of lyophilized BSA and lysozyme 1 μm cylinders from an inhaler. Cascade impaction aerosol parameters of lyophilized BSA and lysozyme 1 μm cylinders from a Monodose RS01 inhaler at 60 L/min (n=3).

Formulation	MMAD (μm)	GSD	ED (%)	FPF Collected (%)	RF (%)
BSA	1.77 ± 0.06	1.51 ± 0.06	94.6 ± 0.9	78.6 ± 0.3	63.0 ± 3.9
Lysozyme	1.83 ± 0.12	1.44 ± 0.03	85.9 ± 1.1	84.6 ± 4.3	74.4 ± 7.7

2.4 Discussion

Pulmonary delivery is a versatile route of administration, as it can be used to non-invasively deliver therapeutics to the lungs for both respiratory indications and systemic distribution.[1,2] Current manufacturing techniques for inhalable dry powder formulations, including spray drying and spray freeze drying, expose proteins to unfavorable thermal and mechanical stresses, which can result in protein instability.[3,19] In addition, both manufacturing techniques have limited control over particle morphology, resulting in formulations composed of particles with a distribution of sizes and poorly defined shape.[4,8,20] This heterogeneous mixture of particles contributes to the poor delivery efficiency and imprecise deposition profiles commonly observed with dry powder inhaler formulations. [4,5,8] In this work, we aimed to evaluate the utility of PRINT as a platform to mold proteins into monodisperse particles that generate high performance respirable dry powders. We have demonstrated that this scalable platform is amenable to the stable incorporation of proteins into engineered particles with precise deposition profiles. We believe this platform will facilitate the development of a wide array of particle-based therapeutic protein formulations for pulmonary delivery.

It is critical that proteins remain stable throughout any manufacturing process used to produce dry powders. Formulations containing destabilized proteins can exhibit a reduction in therapeutic potency or even elicit an immunogenic reaction.[21] One of the primary goals of this study was to closely monitor and thoroughly characterize protein structure at each step involved

in the production of protein dry powders using PRINT. Studies investigating the compatibility of biopharmaceuticals with spray drying and spray freeze drying have reported alterations in the primary[22,23], secondary[23,24], and tertiary[24] structure of proteins along with reduced protein function.[25,26] As such, a set of experiments was designed to observe each structural level of BSA and lysozyme as well as lysozyme function at each step of the PRINT process. Because PRINT involves little physical stress and has a small air-water interface, it was expected that proteins would remain stable throughout the production of PRINT dry powders.

Changes to the primary structure of a protein can occur due to degradation or covalent aggregation, which can be observed with reducing SDS-PAGE.[3] For both BSA and lysozyme, band migration of the protein isolated from pre-particle solution, particles, and lyophilized particles appears to be the same as the control band, suggesting no alteration in primary structure occurs throughout manufacturing. Interaction with air-water interfaces, dehydration, or exposure to elevated temperatures can disrupt intramolecular interactions in proteins, resulting in the unfolding of protein structures.[3,19] Denaturation of these secondary and tertiary structures can be observed by CD and intrinsic fluorescence, respectively.[27,28] The pre-particle solution, particle, and lyophilized particle samples have similar CD profiles to the unprocessed control for both BSA and lysozyme, supporting the retention of secondary structure during each step of manufacturing PRINT protein dry powders. In contrast, the denatured standards showed markedly reduced signal intensity at wavelengths of 195 nm and 205-220 nm, which is indicative of a loss of ordered secondary structure.[27] The global tertiary structure of both proteins was observed by measuring the intrinsic fluorescence of each protein, which is primarily a result of tryptophan (Trp).[28] Protein purified from PPS, particles, and lyophilized particles generated intrinsic fluorescence spectra that overlaid the spectra generated by the control samples,

indicating that the production of PRINT protein dry powders resulted in no alteration of tertiary structure. The denatured standards of both proteins yielded spectra with decreased fluorescence intensity and a shift in λ_{max}, as expected.

Generally, lysozyme is known to be resistant to damage resulting in loss of activity. However, several groups have reported a moderate decrease in lysozyme activity or ordered structure following spray drying.[25,26,29] Given that the protein structure experiments support that lysozyme is in its native state following dissolution from dry powders of lysozyme 1 μm cylinders, we expected lysozyme to fully retain its enzymatic activity throughout manufacturing. Indeed, lysozyme showed no significant difference ($p<0.0001$) in activity at any step in the manufacturing process.

Results from the sequence of protein stability experiments confirm that PRINT can be used to manufacture monodisperse protein dry powders while preserving the native structure and function of the incorporated model proteins. While these particles were intended for respiratory applications, the ability to stably incorporate proteins into highly engineered particles with PRINT could be utilized for a variety of local and systemic routes of drug delivery.

In order to deliver inhalable dry powders to the desired region of the lungs in an efficient and precise manner, the dry powder must aerosolize from the delivery device into individual particles, avoid deposition in the mouth-throat area, and have a narrow distribution of particle diameters.[4,8] A dry powder of monodisperse PRINT particles that fully aerosolizes into discrete particles could be expected to be emitted from the device with high efficiency and deposit in the lungs with high precision.[16] For these studies, the 1 μm cylinder particle geometry was selected in an effort to avoid deposition in the mouth-throat area, as particles in the range of 0.04 – 1.00 μm have been shown to significantly reduce deposition in the mouth-throat area.[30] Images

obtained via SEM of lyophilized BSA and lysozyme 1 μm cylinders confirm the accuracy and homogeneity of particle geometry for both formulations, as is expected with micromolded particles produced with PRINT.[16] Therefore, the ability of our formulations to be efficiently delivered and deposit precisely is expected to primarily be a function of powder fluidization and deagglomeration.[4]

Aerosolization and deposition profiles of both formulations were initially studied *in vitro* using a Penn-Century DP-4M insufflator, as it allows for the aerosolization of sub-milligram doses of powder. Positive results from the pilot studies with the insufflator encouraged scale-up of particle production needed to study aerosolization and deposition of both formulations *in vitro* using a Monodose RS01 dry powder inhaler along with an Andersen Cascade Impactor. A flow rate of 60 L/min was selected as it generated a 4 kPa pressure drop across the inhaler. The first step in efficient and precise delivery of a dry powder to the lungs is fluidization and aerosolization of the powder followed by emission from the device.[4] Both BSA and lysozyme formulations readily aerosolized from the capsule and exited the inhaler, with emission efficiencies of 94.6 % ± 0.9 and 85.9 % ± 1.1, respectively. A recent study by SRB Behara et al defined high efficiency performance from a DPI as an emitted dose >75 %. Both formulations readily exceeded this standard, likely due to the ability of small diameter particles to avoid deposition in the device.[31] The emitted dose could be further improved in this system by increasing the mass loaded into the capsule, as only 2 mg was loaded for these studies.

Following aerosolization and emission from the device, the next step to deliver a dry powder aerosol to the lungs in an efficient and precise manner is the avoidance of extrathoracic airway deposition.[4] Both formulations were largely able to avoid deposition in the artificial throat of the ACI, with <10 % of each formulation lost to throat impaction. This is remarkably

efficient, as deposition in the mouth-throat area can range from 30-95 % of the nominal dose.[22] The ability of PRINT protein aerosols to avoid premature deposition in the throat is likely due to their small diameter, which prevents inertial impaction in the extrathoracic airways.[21] Additionally, the avoidance of deposition in the artificial throat suggests that PRINT protein powders are aerosolizing into discrete particles, as incomplete aerosolization would result in particle agglomerates with sufficient inertia to deposit in the throat.[8]

The final step in the efficient and precise delivery of a dry powder formulation to the lungs is particle deposition.[7] Particle deposition in the lungs occurs most efficiently when the MMAD of the aerosol is between 1 and 5 μm. Aerosols with a smaller MMAD do not have sufficient mass to deposit, while aerosols with a higher MMAD deposit prematurely in the mouth or throat.[32] The aerosols of BSA and lysozyme 1 μm cylinders had MMAD's of 1.77 μm ± 0.06 and 1.83 μm ± 0.12, respectively, which is appropriate for delivery to the lungs via inhalation. The respirable fraction, or the percentage of the collected dose between 1 and 5 μm in aerodynamic diameter, represents the portion of the collected dose that is appropriate for efficient lung deposition. The respirable fraction (RF) of the BSA 1 μm cylinders was 63.0 % ± 3.9 while the respirable fraction of the lysozyme 1 μm cylinders was 74.4 % ± 7.7, indicating that the majority of the aerosol dose is appropriate for lung deposition. While the MMAD of an aerosol can be used to reasonably predict the primary region of deposition in the lungs and the RF estimates the efficiency of deposition in the lungs, neither factor adequately describes the precision with which an aerosol will deposit in a given region.[23] In order to achieve maximum delivery efficiency with a dry powder inhaler, it is desirable to selectively deposit particles in the therapeutic region of interest within lungs.[1,7] GSD describes the precision of the deposition profile of a dry powder formulation *in vitro*.[33] Mathematically, a GSD of 1.0 is perfectly

monodisperse, however, in practice, a monodisperse aerosol will generate a GSD of approximately 1.20 when characterized with an ACI.[34] The GSD was determined to be 1.51 ± 0.06 for BSA 1 μm cylinders and 1.44 ± 0.03 for lysozyme 1 μm cylinders. Although these are not perfectly monodisperse aerosols, they are an improvement over most dry powder aerosols, which often have GSD's near 2.0.[35–37] The observed deposition precision is likely a result of a formulation comprised of monodisperse particles, the ability of the formulation to largely aerosolize into discrete particles, and the carrier-free nature of the formulation. Altogether, the lysozyme and BSA 1 μm cylinder formulations demonstrate that PRINT can be used to manufacture high performance dry powder aerosols that are delivered with high efficiency and precision.

During formulation optimization of BSA and lysozyme 1 μm cylinders, the same PPS formulation was found to be optimal for both proteins. This is likely due to the fact that the T_g of the mixture comprising the film used for particle manufacturing is the primary determinant of mold filling. As the T_g's of different proteins are relatively similar and the proteins only make up 40 % of the film composition, it is reasonable that the same formulation will be optimal for a number of proteins.[38] This feature of PRINT allows for different proteins of interest to readily be incorporated into the formulation and manufactured into particles without requiring re-optimization of the formulation for each protein.

Interestingly, the composition of the final lyophilized particle formulation is different than the original composition of the pre-particle solution. Investigation into this change in composition revealed that nearly the entirety of glycerol and a portion of the lactose was lost during the particle washes in isopropanol as a result of the miscibility of glycerol with isopropanol and the slight solubility of lactose in isopropanol. The resulting particle composition

of more than 85 % protein by mass for both lysozyme and BSA 1 μm cylinders is highly desirable for protein formulations intended for inhalation. Protein drugs frequently require a high dose by mass that may exceed the maximum powder burden that can be delivered to the lung in one dose, so minimizing the excipient mass in a formulation enables the delivery of a higher dose of protein drug.[7,39]

The current study was limited to the evaluation of the stability of two model proteins in the system. Further investigation of therapeutic proteins of interest formulated into PRINT particles is required to fully understand the utility of PRINT as a platform to manufacture dry powder formulations of proteins. Lactose was selected as an excipient in our initial studies as it has been successfully incorporated into many marketed DPI formulations.[39] However, lactose is known to be incompatible with some protein formulations due to Maillard browning.[39] Trehalose, a non-reducing disaccharide with a T_g similar to lactose, can be used in place of lactose with proteins that are incompatible with lactose. Additionally, the current study was designed to evaluate performance of these formulations at the typical flow rate generated by an adult from a standard dry powder inhaler. Further investigation of these formulations at higher and lower flow rates and from different devices is needed to evaluate the dependence of aerosol performance on inhalation flow and pressure. While the particle geometry of 1 μm cylinders selected for this study displayed excellent aerosol performance, the ability to finely tune aerosol properties by precisely changing particle shape also warrants further investigation.

2.5 Conclusions

Current methods of manufacturing particles for dry powder inhalers produce a heterogeneous mixture of particles that are inefficiently delivered to and imprecisely deposit in the lungs. Additionally, these methods expose proteins to undesirable mechanical stresses, which

can lead to denaturation, aggregation, or degradation. The combination of the poor performance of current DPI formulations and the incompatibility of proteins with current manufacturing methods greatly limits the development of protein dry powders for inhalation. To facilitate the development of pulmonary protein formulations, a platform that is compatible with proteins and produces high performance aerosols is needed. The results from this study support our hypothesis that PRINT can be used to manufacture protein dry powders with precise deposition profiles *in vitro*, while preserving the native structure of incorporated proteins. The ability to introduce new proteins of interest without re-optimizing the formulation facilitates rapid formulation development. PRINT's capacity to manufacture precisely engineered respirable particles while maintaining the stability of incorporated proteins is a valuable formulation strategy that could enable the development of the next generation of inhaled medications.

REFERENCES

1. Bäckman, P., Adelmann, H., Petersson, G. & Jones, C. B. Advances in inhaled technologies: understanding the therapeutic challenge, predicting clinical performance, and designing the optimal inhaled product. *Clin. Pharmacol. Ther.* **95,** 509–520 (2014).

2. Hoe, S., Boraey, M. a, Ivey, J. W., Finlay, W. H. & Vehring, R. Manufacturing and Device Options for the Delivery of Biotherapeutics. *J. Aerosol Med. Pulm. Drug Deliv.* **27,** 1–14 (2014).

3. Maltesen, M. J. & van de Weert, M. Drying methods for protein pharmaceuticals. *Drug Discov. Today Technol.* **5,** e81–e88 (2008).

4. Weers, J. G. & Miller, D. P. Formulation Design of Dry Powders for Inhalation. *J. Pharm. Sci.* **104,** 3259–3288 (2015).

5. Longest, P. W., Tian, G., Li, X., Son, Y. J. & Hindle, M. Performance of Combination Drug and Hygroscopic Excipient Submicrometer Particles from a Softmist Inhaler in a Characteristic Model of the Airways. *Ann. Biomed. Eng.* **40,** 1–15 (2012).

6. Borgström, L., Olsson, B. & Thorsson, L. Degree of throat deposition can explain the variability in lung deposition of inhaled drugs. *J. Aerosol Med.* **19,** 473–483 (2006).

7. de Boer, A. H. *et al.* Dry powder inhalation: past, present and future. *Expert Opin. Drug Deliv.* **14,** 499–512 (2017).

8. Chow, A. H. L., Tong, H. H. Y., Chattopadhyay, P. & Shekunov, B. Y. Particle engineering for pulmonary drug delivery. *Pharm. Res.* **24,** 411–437 (2007).

9. Vehring, R. Pharmaceutical particle engineering via spray drying. *Pharm. Res.* **25,** 999–1022 (2008).

10. Winters, M. A. *et al.* Precipitation of proteins in supercritical carbon dioxide. *J. Pharm. Sci.* **85,** 586–594 (1996).

11. Potocka, E. *et al.* Pharmacokinetic characterization of the novel pulmonary delivery excipient fumaryl diketopiperazine. *J. Diabetes Sci. Technol.* **4,** 1164–1173 (2010).

12. Cassidy, J. P. *et al.* Insulin lung deposition and clearance following technosphere ® insulin inhalation powder administration. *Pharm. Res.* **28,** 2157–2164 (2011).

13. Bromberg, L., Rashba-Step, J. & Scott, T. Insulin particle formation in supersaturated aqueous solutions of poly(ethylene glycol). *Biophys. J.* **89,** 3424–3433 (2005).

14. Garcia, A. *et al.* Microfabricated Engineered Particle Systems for Respiratory Drug Delivery and Other Pharmaceutical Applications. *J. Drug Deliv.* **2012,** 1–10 (2012).

15. Mack, P., Horvath, K., Tully, J. & Maynor, B. Particle engineering for inhalation formulation and delivery of biotherapeutics. *Inhalation* **6,** 16–20 (2012).

16. Fromen, C. A. *et al.* Synthesis and Characterization of Monodisperse Uniformly Shaped Respirable Aerosols. *AIChE J.* **59,** 3184–3194 (2013).

17. Xu, J. *et al.* Rendering protein-based particles transiently insoluble for therapeutic applications. *J. Am. Chem. Soc.* **134,** 8774–8777 (2012).

18. Bantan-Polak, T., Kassai, M. & Grant, K. B. A Comparison of Fluorescamine and Naphthalene-2,3-dicarboxaldehyde Fluorogenic Reagents for Microplate-Based Detection of Amino Acids. *Anal. Biochem.* **297,** 128–136 (2001).

19. Ameri, M. & Maa, Y.-F. Spray Drying of Biopharmaceuticals: Stability and Process Considerations. *Dry. Technol.* **24,** 763–768 (2006).

20. Chan, H. K. Dry powder aerosol drug delivery-Opportunities for colloid and surface scientists. *Colloids Surfaces A Physicochem. Eng. Asp.* **284–285,** 50–55 (2006).

21. Frokjaer, S. & Otzen, D. E. Protein drug stability: a formulation challenge. *Nat. Rev. Drug Discov.* **4,** 298–306 (2005).

22. Mumenthaler, M., Hsu, C. C. & Pearlman, R. Feasibility study on spray-drying protein pharmaceuticals: recombinant human growth hormone and tissue-type plasminogen activator. *Pharmaceutical Research* **11,** 12–20 (1994).

23. Costantino, H. R. *et al.* Protein spray-freeze drying. Effect of atomization conditions on particle size and stability. *Pharm. Res.* **17,** 1374–1383 (2000).

24. Shoyele, S. A., Sivadas, N. & Cryan, S. The effects of excipients and particle engineering on the biophysical stability and aerosol performance of parathyroid hormone (1-34) prepared as a dry powder for inhalation. *AAPS PharmSciTech* **12,** 304–311 (2011).

25. Hulse, W. L., Forbes, R. T., Bonner, M. C. & Getrost, M. Do co-spray dried excipients offer better lysozyme stabilisation than single excipients? *Eur. J. Pharm. Sci.* **33,** 294–305 (2008).

26. Yu, Z., Johnston, K. P. & Williams, R. O. Spray freezing into liquid versus spray-freeze drying: Influence of atomization on protein aggregation and biological activity. *Eur. J. Pharm. Sci.* **27,** 9–18 (2006).

27. Capelle, M. A. H., Gurny, R. & Arvinte, T. High throughput screening of protein formulation stability: Practical considerations. *Eur. J. Pharm. Biopharm.* **65,** 131–148 (2007).

28. Garidel, P., Hegyi, M., Bassarab, S. & Weichel, M. A rapid, sensitive and economical assessment of monoclonal antibody conformational stability by intrinsic tryptophan fluorescence spectroscopy. *Biotechnol. J.* **3,** 1201–1211 (2008).

29. Liao, Y. H., Brown, M. B., Nazir, T., Quader, A. & Martin, G. P. Effects of sucrose and trehalose on the preservation of the native structure of spray-dried lysozyme. *Pharm. Res.* **19,** 1847–1853 (2002).

30. Xi, J. & Longest, P. W. Effects of oral airway geometry characteristics on the diffusional deposition of inhaled nanoparticles. *J. Biomech. Eng.* **130,** 11008-1-11008–16 (2008).

31. Behara, S. R. B., Farkas, D. R., Hindle, M. & Longest, P. W. Development of a high efficiency dry powder inhaler: Effects of capsule chamber design and inhaler surface modifications. *Pharm. Res.* **31,** 360–372 (2014).

32. Telko, M. J. & Hickey, A. J. Dry powder inhaler formulation. *Respir. Care* **50,** 1209–1227 (2005).

33. Crowder, T. M., Rosati, J. A., Schroeter, J. D., Hickey, A. J. & Martonen, T. B. Fundamental effects of particle morphology on lung delivery: Predictions of Stokes' law and the particular relevance to dry powder inhaler formulation and development. *Pharm. Res.* **19,** 239–245 (2002).

34. Mitchell, J. P. & Nagel, M. W. Cascade impactors for the size characterization of aerosols from medical inhalers: their uses and limitations. *J. Aerosol Med.* **16,** 341–377 (2003).

35. Finlay, W. H. & Gehmlich, M. G. Inertial sizing of aerosol inhaled from two dry powder inhalers with realistic breath patterns versus constant flow rates. *Int. J. Pharm.* **210,** 83–95 (2000).

36. Bosquillon, C., Lombry, C., Préat, V. & Vanbever, R. Influence of formulation excipients and physical characteristics of inhalation dry powders on their aerosolization performance. *J. Control. Release* **70,** 329–339 (2001).

37. Shur, J., Saluja, B., Lee, S., Tibbatts, J. & Price, R. Effect of Device Design and Formulation on the In Vitro Comparability for Multi-Unit Dose Dry Powder Inhalers. *AAPS J.* **17,** 1105–1116 (2015).

38. Cicerone, M. T., Pikal, M. J. & Qian, K. K. Stabilization of proteins in solid form. *Adv. Drug Deliv. Rev.* **93,** 14–24 (2015).

39. Pilcer, G. & Amighi, K. Formulation strategy and use of excipients in pulmonary drug delivery. *Int. J. Pharm.* **392,** 1–19 (2010).

CHAPTER 3: THE ROLE OF PARTICLE SHAPE IN FLOWABILITY, AEROSOLIZATION, AND DEPOSITION OF DRY POWDER FORMULATIONS

3.1 Introduction

Dry powder inhalers (DPIs) offer many advantages beyond their utility with biologic drugs. In addition to compatibility with nearly any potential therapeutic molecule, DPIs are convenient, portable, and frequently do not require cold chain storage.[1,2] Despite these advantages, DPIs are limited by their poor delivery efficiency and dose consistency.[3,4] Recent advances in both inhaler design and particle engineering have propelled DPIs from notoriously inefficient to devices with potential for high delivery efficiency.[3,5]

Particle engineering is a formulation strategy that designs particles of exquisitely controlled size, shape, and density to improve the performance of dry powder aerosols.[3,6] The performance of dry powder formulations is characterized by three steps – fluidization, aerosolization, and deposition.[7] For a formulation to be considered high performance, it must be able to perform all three steps with high efficiency. The impact of particle size on fluidization, aerosolization, and deposition has been extensively studied and is well understood.[8–10] The role of particle density, though possibly less studied than particle size, is also understood and has frequently been leveraged to improve aerosol performance.[11,12] However, few studies have been performed to understand the role of particle shape.

The most extensive study of particle shape to date characterized the flow and aerosol properties of several particle shapes ranging from 3.7 to 24.1 μm in maximum diameter.[13] Though particles were grouped by diameter and aerodynamic diameter to minimize the effect of

particle size, it is difficult to attribute observed differences in powder performance solely to particle shape. Studies have also been performed to observe the impact of carrier particle shapes on aerosol performance; however, particle shapes were imprecise and particle size was poorly controlled .[14,15] Additionally, the translation of carrier particle performance to drug particles is limited, as carrier particles are in a different size regime and are only intended to aid the performance of smaller drug particles. A systematic study of particle shapes with controlled size and aerodynamic diameter could provide valuable information needed to design high-performance carrier-free dry powders.

Particle Replication in Non-wetting Templates (PRINT) was used to fabricate monodisperse 1 μm cylinders in Chapter 2 and has previously been used to manufacture precisely engineered particle shapes for aerosol formulations.[16–18] This chapter presents work done to fabricate PRINT particle shapes with minimal variation in size and aerodynamic diameter and efforts to advance understanding of the role of particle shape in dry powder flowability, aerosolization, and deposition.

3.2 Materials and Methods

3.2.1 Materials

Lysozyme, poly(1-vinylpyrrolidone-co-vinyl acetate) (PVPVA), fluorescamine, anhydrous isopropanol, lactose, glycerol, lysozyme assay kit, silicone spray, PRINT mold, centrifugal filters, and hydroxypropyl methylcellulose (HPMC) capsules were obtained from the same suppliers detailed in Chapter 2. The stainless-steel 18 Mesh sieve was obtained from Alfa Aesar (Haverhill, MA, USA). Shallow aluminum pans were acquired from TA Instruments (New Castle, DE, USA). Glass 1 mL tuberculin syringes were obtained from Cadence Science (Cranston, RI, USA).

3.2.2 Methods

3.2.2.1 Fabrication of Lysozyme PRINT Particle Shapes

Particle shapes for this study were selected from a library of PRINT particle geometries. Particle geometries were chosen in an effort to study particle shape as independently as possible from other particle factors, including particle diameter, surface area, and volume. The particle shapes selected include 1x1 μm cylinders, 0.5x1 μm cylinders, 1 μm pollen, and 1.5 μm donuts **(Figure 3.1)**. Lysozyme PRINT particle shapes were fabricated using a method adapted from Xu et al as previously described in Chapter 2.[19] The ratio of lysozyme to excipients and the concentration of the pre-particle solution (PPS) were optimized for each shape.

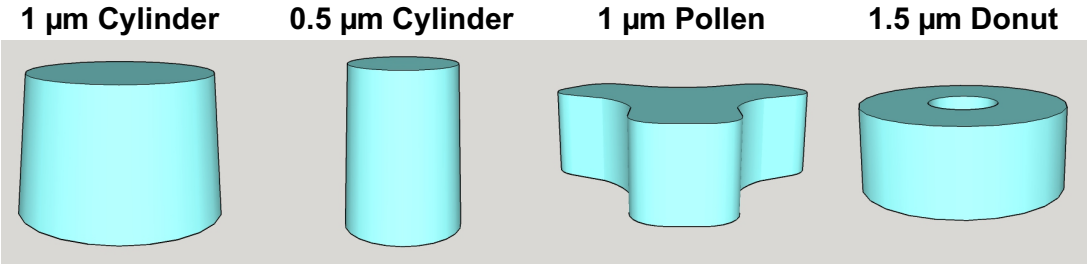

Figure 3.1 Models of lysozyme particle shapes. Models of selected particle shapes, including 1x1 μm cylinder, 0.5x1 μm cylinder, 1 μm pollen, and 1.5 μm donut.

3.2.2.2 Particle Lyophilization

Particles were resuspended in *tert*-butanol at 1 mg/mL, flash frozen in liquid nitrogen, and lyophilized for 24 hours, as described in Chapter 2.

3.2.2.3 Scanning Electron Microscopy

Particles were resuspended in isopropanol and imaged as described in Chapter 2.

3.2.2.4 Image Analysis

Particles were prepared for scanning electron microscopy (SEM) as described in the protocol in Chapter 2. Particles were imaged with high contrast to aid in particle border detection by ImageJ software (National Institutes of Health, Bethesda, MD, USA). Images were imported

into ImageJ and converted to binary. The binary images underwent the Fill Hole function, which resulted in a white two-dimension (2D) projection of three-dimensional (3D) particles on a black background. ImageJ software then automatically measures particle dimensions. Boundaries were set to ensure ImageJ did not measure overlapping particles. A minimum of 10 images with 10+ particles were measured for each shape. A diagram of the process is in **Figure 3.2**.

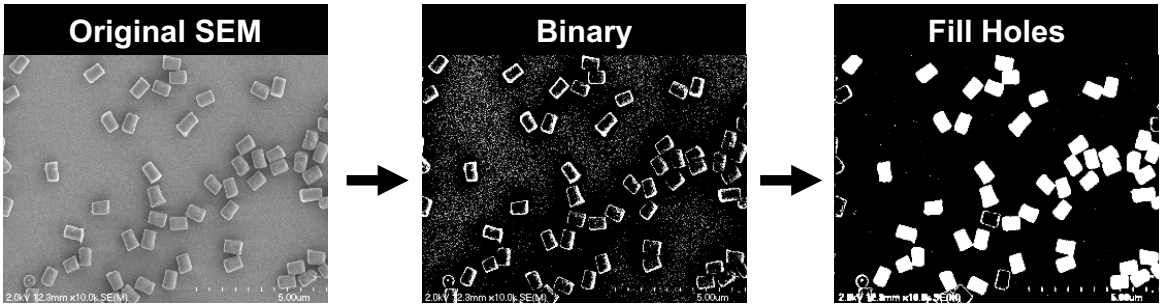

Figure 3.2 Image analysis process. Diagram of image analysis process for 0.5x1 μm cylinders, including the original SEM, conversion to binary, the application of the Fill Hole function.

In addition to particle dimensions, parameters describing particle shape were obtained during image analysis, including projected area (A), maximum Feret diameter ($x_{F,max}$), minimum Feret diameter ($x_{F,min}$), and perimeter (P). Surface area (SA) and volume (V) were determined by inputting particle measurements into SketchUp (Trimble, Inc., Boulder, CO, USA), a 3D modeling software used to create the particle models in **Figure 3.1**. Particle parameters including surface area-to-volume (SA/V), aspect ratio (AR), circularity, and surface volume mean diameter (SVMD) were calculated using the equations below (Equations 3.1 – 3.4).

$$SA/V = \frac{SA}{V} \tag{3.1}$$

$$AR = \frac{x_{F,min}}{x_{F,max}} \tag{3.2}$$

$$Circularity = \frac{4\pi * A}{P^2} \tag{3.3}$$

$$SVMD = 2 * \sqrt{\frac{A}{\pi}} \tag{3.4}$$

3.2.2.5 Thermogravimetric Analysis

Particle concentration was determined using thermogravimetric analysis (TGA) as described in Chapter 2.

3.2.2.6 Particle Composition Analysis

Particle composition was determined via high-performance liquid chromatography (HPLC) as described in Chapter 2.

3.2.2.7 Lysozyme Activity Assay

The enzymatic activity of lysozyme molded into each particle shape both before and after lyophilization was measured with the lysozyme activity assay explained in Chapter 2.

3.2.2.8 Angle of Repose

The flowability of powders of the four particle shapes was studied by determining the angle of repose using a fixed height funnel and fixed diameter base method. A stainless-steel funnel was fixed at a height of 1 cm above an aluminum pan base with a 1 mm lip to control the diameter of the base of the powder cone. The width of the metal pan was measured with digital calipers and used as the diameter of the base. Powder was passed through an 18 Mesh sieve to break up large agglomerates before being gently placed in the funnel. Once a cone had formed, the height of the cone was measured with digital calipers. The angle of repose (α) was calculated from the base diameter and cone height using Equation 3.5. Each sample was measured in triplicate.

$$\tan(\alpha) = \frac{height}{0.5 * base} \tag{3.5}$$

3.2.2.9 Powder Density and Compressibility

The bulk (ρ_{bulk}) and tapped (ρ_{tap}) densities of powders of lysozyme particle shapes were determined in a 1 mL glass tuberculin syringe with a method adapted from Hassan and Lau.[13]

Powder was added to the syringe on a balance until the powder volume reached the 1 mL calibration (V_0 = 1 mL) . The mass of powder in 1 cm^3 was recorded to calculate the bulk density (Equation 3.6). To measure the tapped density, the glass syringe was tapped by hand against a tabletop at a rate of two taps per second for 500 taps, after which no further powder compression was observed. Each sample was measured in triplicate. The volume of the compressed powder (V_f) was recorded and used to calculate the tapped density (Equation 3.7). In addition to bulk and tapped density, the compressibility index (CI) of each shape was calculated (Equation 3.8).

$$\rho_{bulk} = \frac{Powder\ mass\ (g)}{V_0} \tag{3.6}$$

$$\rho_{tap} = \frac{Powder\ mass\ (g)}{V_f} \tag{3.7}$$

$$CI = 100 * \frac{V_0 - V_f}{V_0} \tag{3.8}$$

3.2.2.10 Cascade Impaction

The aerosol properties of lysozyme particle shapes were evaluated *in vitro* using an Andersen Cascade Impactor (ACI) operated at 60 L/min and a Monodose RS01 dry powder inhaler with 5 mg of powder loaded into the HPMC capsule. Further experimental details and definitions of aerosol parameters are available in Chapter 2. A fluorescamine assay normalized to the composition of each particle shape was used to quantify particle deposition on each stage, as in Chapter 2.

3.2.2.11 Statistics

Statistical analyses were performed using GraphPad Prism Version 5.1 (GraphPad Software, La Jolla, CA, USA). Data presented as mean ± standard deviation. Statistical analyses were performed as one-way analysis of variance (ANOVA) with post hoc Tukey's test at significance level α = 0.05 unless stated otherwise.

3.3 Results

3.3.1 Fabrication and Characterization of Lysozyme Particle Shapes

3.3.1.1 Fabrication and Morphological Characterization

A PPS of composed of 40 % lysozyme, 35 % lactose, and 25 % glycerol in water, which had previously been identified as optimal for PRINT protein particles, was used to optimize the concentration of solids in PPS for lysozyme particle shapes. Particles of each shape were fabricated from 5, 7.5, 10, 12.5, and 15 wt% PPS and, following isopropanol washes, were observed by SEM **(Figure 3.3)**. The 10 wt% PPS resulted in optimal particle morphology for 1x1 μm cylinders, 0.5x1 μm cylinders, and 1 μm pollen lysozyme particles, while the 12.5 wt% PPS was optimal for lysozyme 1.5 μm donuts. Lyophilization of the particles from *tert*-butanol at 1 mg/mL generated dry powders that were rapidly water soluble. Imaging of lyophilized particles resuspended in isopropanol prior to imaging revealed no change in particle morphology following lyophilization **(Figure 3.4)**.

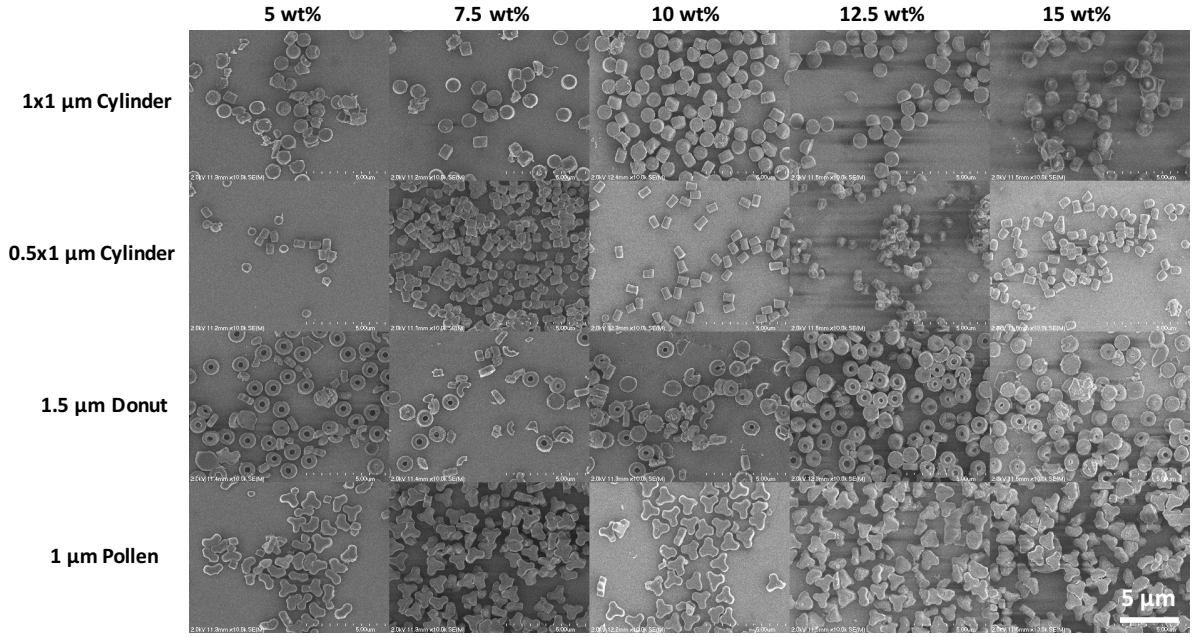

Figure 3.3 Formulation optimization of lysozyme particle shapes. SEM images at 10k magnification of lysozyme particle shaped fabricated from 5 wt%, 7.5 wt%, 10 wt%, 12.5 wt%, and 15 wt% lysozyme:lactose:glycerol 40:35:25 PPS.

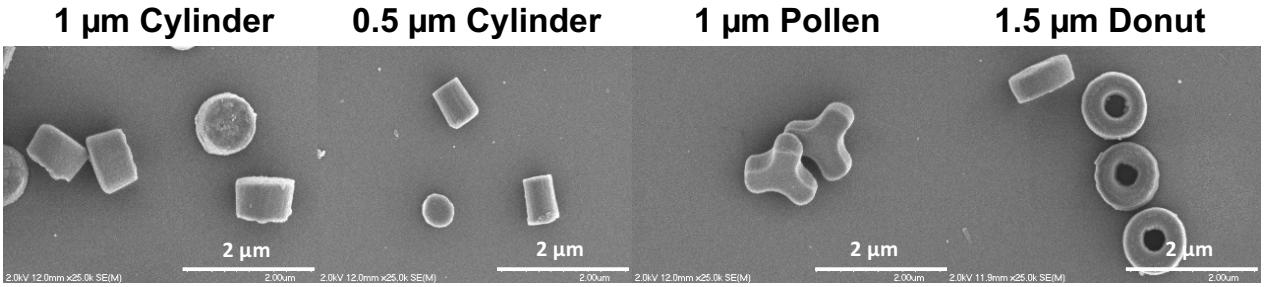

Figure 3.4 SEM of lysozyme particle shapes. Representative SEM images at 25k magnification of 1x1 µm cylinders, 0.5x1 µm cylinders, 1 µm pollen, and 1.5 µm donut lysozyme particles resuspended in isopropanol following lyophilization.

3.3.1.2 Image Analysis

Image analysis was used to obtain dimension measurements for each particle shape. The measured dimensions for each particle shape are diagramed in **Figure 3.5**. The results of image analysis are presented in **Table 3.1**.

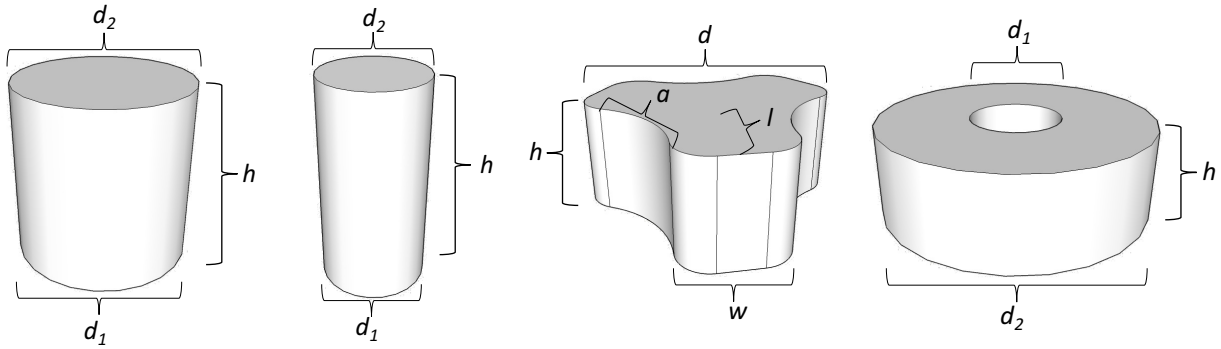

Figure 3.5 Particle dimensions. Diagrams of dimensions measured during image analysis.

Particles were found to be of similar size, ranging from 0.60 – 1.23 µm in minimum diameter and from 0.91 – 1.40 µm in maximum diameter. The maximum diameter of each particle shape was found to be significantly different than every other particle shape ($p<0.0001$). The dimensions from image analysis were used to build a 3D model of each particle shape **(Figure 3.1)**. The models were then used to compute the SA and V of each particle shape, which were found to be reasonably similar for each shape **(Table 3.2)**. Using parameters from image analysis in addition to the 3D models, further descriptors of particle shape were calculated, including SA/V, AR, circularity, and SVMD **(Table 3.3)**.

Table 3.1 Particle dimensions. Measurements from image analysis of lysozyme particle shapes.

Dimension	1x1 µm Cylinder	0.5x1 µm Cylinder	1 µm Pollen	1.5 µm Donut
Height (h)	0.613 ± 0.003 µm	0.713 ± 0.022 µm	0.440 ± 0.014 µm	0.397 ± 0.017 µm
Small Diameter (d_1)	0.823 ± 0.016 µm	0.467 ± 0.007 µm	-	-
Large Diameter (d_2)	0.926 ± 0.007 µm	0.518 ± 0.015 µm	-	-
Inner Diameter (d_1)	-	-	-	0.339 ± 0.038 µm
Outer Diameter (d_2)	-	-	-	0.991 ± 0.024 µm
Arm Width (w)	-	-	0.497 ± 0.007 µm	-
Arm Length (l)	-	-	1.007 ± 0.015 µm	-
Arc (a)	-	-	0.069 ± 0.008 µm	-
Perimeter (P)	3.42 ± 0.13 µm	2.61 ± 0.18 µm	4.60 ± 0.17 µm	3.77 ± 0.12 µm
Feret Min ($x_{F,min}$)	1.01 ± 0.04 µm	0.60 ± 0.04 µm	1.23 ± 0.04 µm	1.11 ± 0.03
Feret Max ($x_{F,max}$)	1.08 ± 0.05 µm	0.91 ± 0.06 µm	1.40 ± 0.04 µm	1.18 ± 0.03 µm

Table 3.2 Surface area and volume of particle shapes. Calculated values for particle shapes.

Particle Shape	Surface Area (µm²)	Volume (µm³)
1 µm Cylinder	2.88	0.364
0.5 µm Cylinder	1.48	0.134
1 µm Pollen	3.85	0.422
1.5 µm Donut	3.00	0.267

Table 3.3 Shape descriptor values. Calculated shape descriptors for lysozyme particle shapes.

Particle Shape	SA/V	AR	Circularity	SVMD (µm)
1 µm Cylinder	7.90	0.94	0.87	1.02
0.5 µm Cylinder	11.00	0.66	0.75	0.72
1 µm Pollen	9.12	0.88	0.60	1.13
1.5 µm Donut	11.23	0.94	0.77	1.05

3.3.1.3 Particle Composition Analysis

Particle composition analysis determined that all lyophilized lysozyme particle shapes have reasonably similar compositions, as shown in **Figure 3.6**. Lysozyme 1x1 µm cylinders are 85.8 % ± 1.2 lysozyme by mass, 0.5x1 µm cylinders are 93.6 % ± 3.7 lysozyme by mass, 1 µm pollen are 86.6 % ± 4.1 lysozyme by mass, and 1.5 µm donuts are 94.5 % ± 2.6 lysozyme by

mass. Excipient mass ranged from 7-15 % of the composition for all particle shapes.

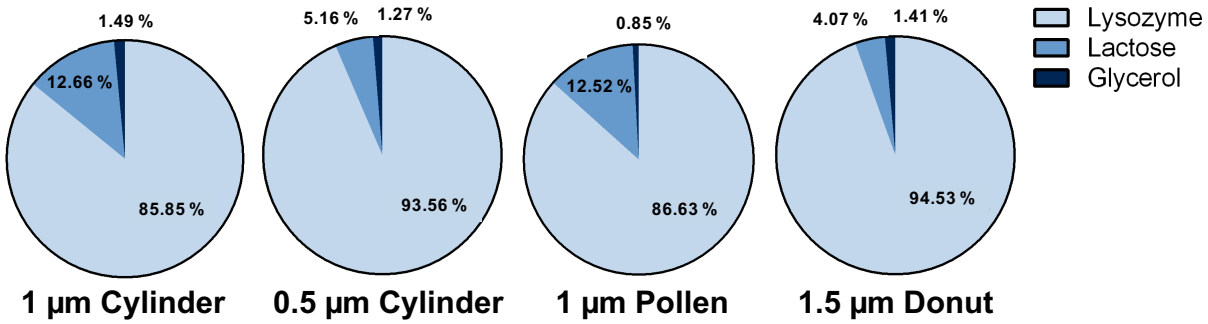

Figure 3.6 Composition of lyophilized lysozyme particle shapes. Composition of lyophilized lysozyme particle shapes as determined by HPLC (n=3).

Lysozyme purified from samples prior to composition analysis by HPLC was used to measure the enzymatic activity in each of the particle shapes both before and after lyophilization **(Figure 3.7)**. No change in enzymatic activity relative to the lysozyme control was observed. The denatured control lost more than 50 % activity relative to the lysozyme control.

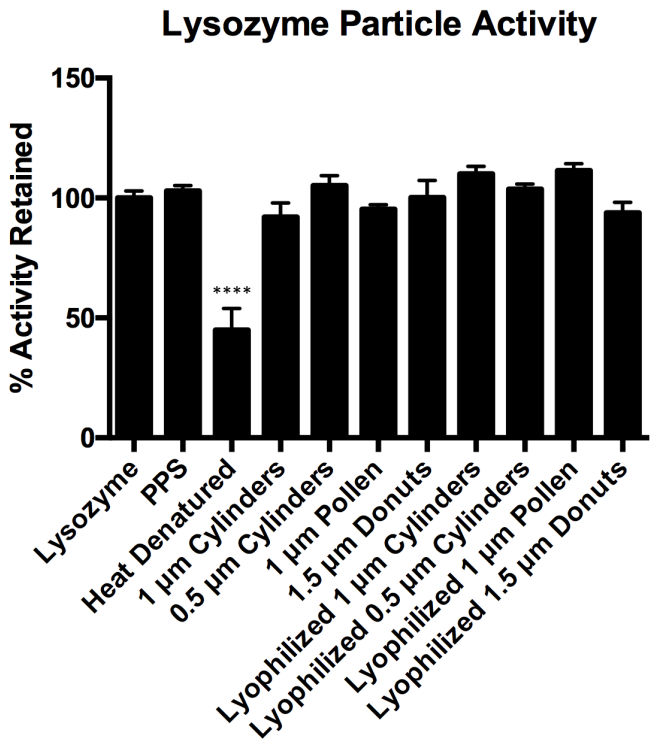

Figure 3.7 Enzymatic activity of lysozyme particle shapes. Enzymatic activity of lysozyme purified from 1x1 µm cylinder, 0.5x1 µm cylinder, 1.5 µm donut, and 1 µm pollen lysozyme particles (n=3) (****$p<0.0001$).

3.3.2 Characterization of Bulk Powder Properties

3.3.2.1 Angle of Repose

Powder cones formed from sieved powders of each particle shape using a fixed height funnel are in **Figure 3.8**. Powders were sieved through an 18 Mesh sieve to break apart large agglomerates (>1 mm) without disturbing the bulk properties of each of the powders. The angle of repose calculated for each lysozyme particle shape is in **Table 3.4**. The values of angle of repose were not found to be significantly different (p=0.2265).

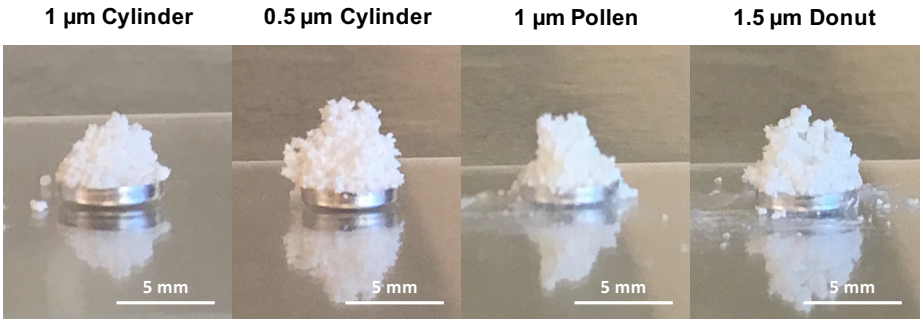

Figure 3.8 Powder cones for angle of repose. Powder cones of lysozyme particle shapes for angle of repose determination (n=3).

Table 3.4 Angle of repose of lysozyme particle shapes. Angle of repose values for powders of 1x1 µm cylinder, 0.5x1 µm cylinder, 1.5 µm donut, and 1 µm pollen lysozyme particles (n=3).

Particle Shape	Angle of Repose (°)
1 µm Cylinders	65.89 ± 2.04
0.5 µm Cylinders	70.93 ± 3.28
1 µm Pollen	64.52 ± 5.00
1.5 µm Donuts	67.15 ± 3.31

3.3.2.2 Bulk and Tapped Density

The bulk and tapped density of powders of each lysozyme particle shape were determined, along with the CI **(Table 3.5)**. While the bulk and tapped density of powders of each lysozyme particle shape were quite different, the CI was found to be similar for all particle shapes. The CI of 0.5x1 µm cylinders was found to be statistically different than both the 1 µm pollen and 1.5 µm donuts ($p<0.05$).

Table 3.5 Density and compressibility of lysozyme particle shapes. Powder density and compressibility of 1x1 μm cylinder, 0.5x1 μm cylinder, 1 μm pollen, and 1.5 μm donut lysozyme particles (n=3).

Particle Shape	Bulk Density (g/cm^3)	Tapped Density (g/cm^3)	Compressibility Index
1 μm Cylinders	1.05 ± 0.04	1.69 ± 0.07	38.21 ± 0.60
0.5 μm Cylinders	0.68 ± 0.04	1.28 ± 0.02	46.86 ± 3.91
1 μm Pollen	0.94 ± 0.04	1.44 ± 0.02	34.76 ± 3.66
1.5 μm Donuts	0.50 ± 0.02	0.74 ± 0.03	33.13 ± 6.49

3.3.3 Aerosol Characterization of Lysozyme Particle Shapes

The aerosol performance of particle shapes was characterized *in vitro* via ACI. The dose remaining in the inhaler and the dose deposited in the throat and on each stage is presented as a fraction of the total collected dose in **Figure 3.9**. All shapes were efficiently emitted, with less than 15 % of the collected dose remaining in the capsule and inhaler following aerosolization. While emitted dose (ED) values were similar for all shapes, the ED of 1x1 μm cylinders was significantly lower than the ED of 1 μm pollen ($p<0.05$). All particle shapes avoided deposition in the artificial throat, with less than 10 % of the collected dose recovered in the throat.

Deposition profiles for each shape were used to calculate aerosol parameters, summarized in **Table 3.6**. Deposition of all particle shapes was centered on stage 4 (1.1 – 2.0 μm at 60 L/min), with more than 30 % of the collected dose for each shape depositing on stage 4. Geometric standard deviation (GSD) ranged from 1.44 for 1x1 μm cylinders to 1.86 for 0.5x1 μm cylinders. The deposition profiles of each particle shape resulted in a mass median aerodynamic diameter (MMAD) of 1.83 μm ± 0.12 for 1x μm cylinders, 1.77 μm ± 0.14 for 0.5x1 μm cylinders, 1.77 μm ± 0.10 for 1 μm pollen, and 1.90 μm ± 0.08 for 1.5 μm donuts. The fine particle fraction (FPF) of the collected dose was between 78 % and 85 % for all particle shapes. There was no significant difference between the FPF values for the particle shapes ($p=0.0978$).

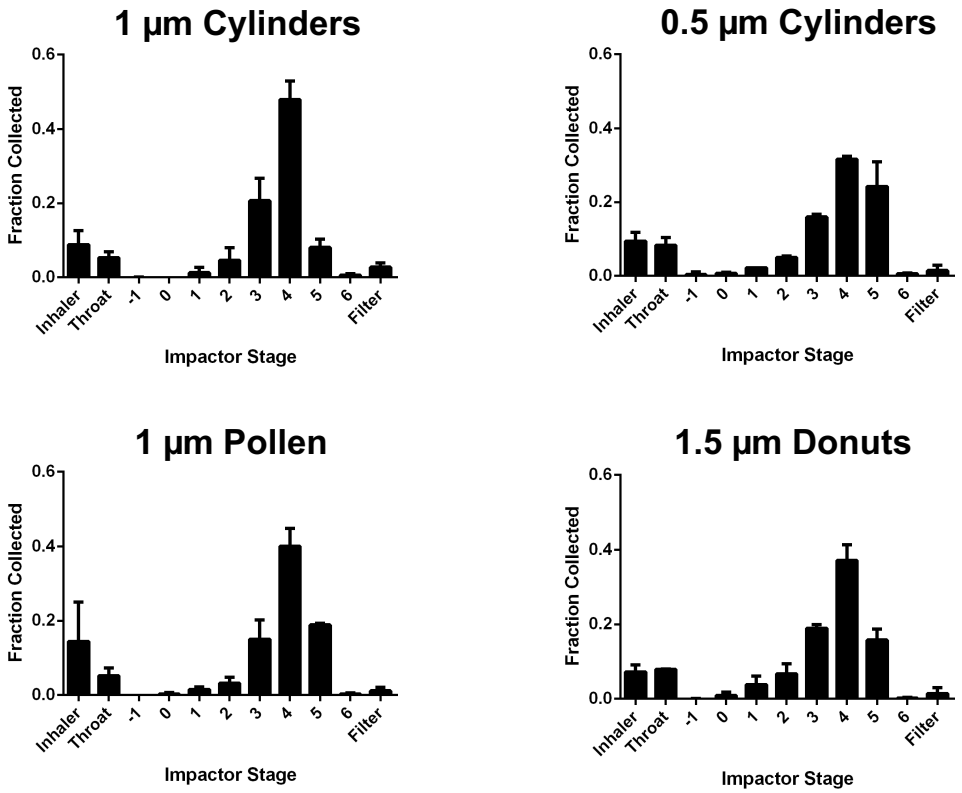

Figure 3.9 Cascade impaction of lysozyme particle shapes. Cascade impaction of lyophilized lysozyme particle shapes from a Monodose RS01 inhaler at 60 L/min (n=3).

Table 3.6 Aerosol parameters of lysozyme particle shapes. Aerosol parameters of lyophilized lysozyme particle shapes as determined by cascade impaction from a Monodose RS01 inhaler at 60 L/min (n=3).

Particle Shape	MMAD (µm)	GSD	ED (%)	FPF Collected(%)
1 µm Cylinders	1.83 ± 0.12	1.44 ± 0.03	85.8 ± 1.1	84.6 ± 4.3
0.5 µm Cylinders	1.77 ± 0.14	1.86 ± 0.13	89.2 ± 2.3	78.9 ± 2.3
1 µm Pollen	1.77 ± 0.10	1.60 ± 0.06	89.4 ± 0.4	85.0 ± 3.3
1.5 µm Donuts	1.90 ± 0.08	1.61 ± 0.07	88.0 ± 0.9	80.1 ± 2.1

3.3.4 Powder and Aerosol Properties as a Function of Particle Morphology

Parameters including CI, angle of repose, ED, and FPF, which are dependent on particle shape, describe the flowability, aerosolization, and deposition properties of powders. Therefore, these powder parameters were plotted as a function of parameters describing particle shape in an effort to observe relationships between the two groups of parameters and further understand the role of particle shape in aerosol performance **(Figures 3.10 – 3.15)**.

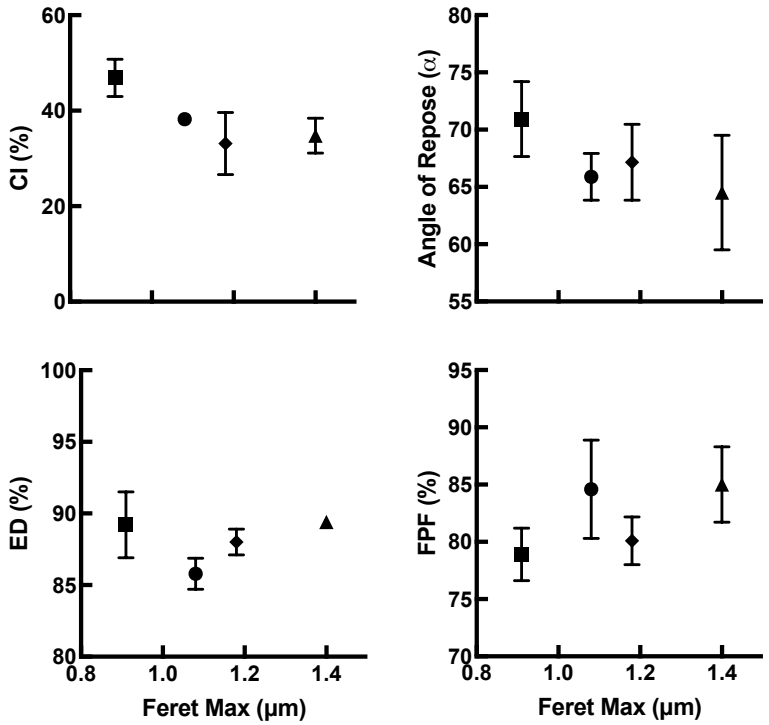

Figure 3.10 Powder parameters as a function of Feret max. Flowability, aerosolization, and deposition as a function of their $x_{F,max}$ of lyophilized lysozyme particles shapes, including 1x1 μm cylinders (●), 0.5x1 μm cylinders (■), 1 μm pollen (▲), and 1.5 μm donuts (◆).

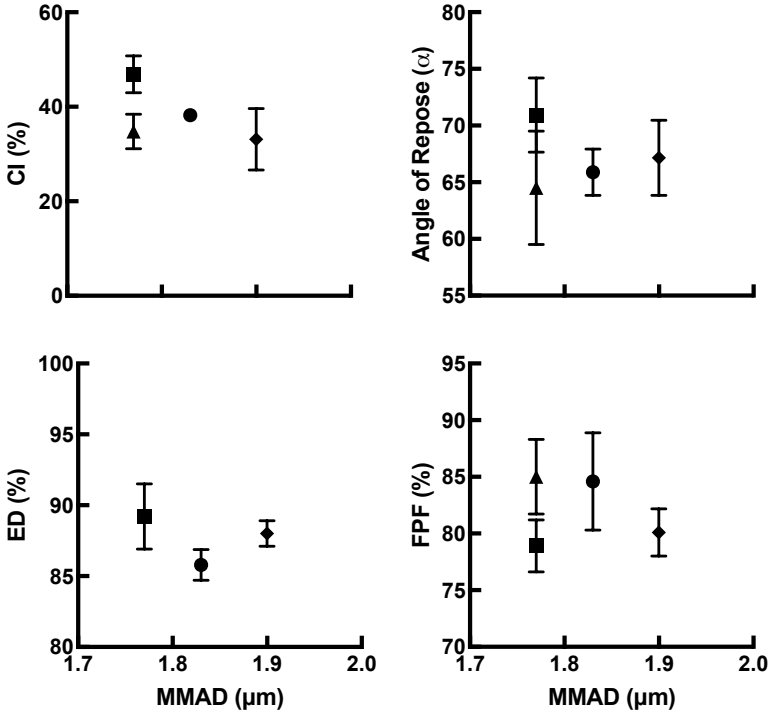

Figure 3.11 Powder parameters as a function of MMAD. Flowability, aerosolization, and deposition as a function of their MMAD of lyophilized lysozyme particles shapes, including 1x1 μm cylinders (●), 0.5x1 μm cylinders (■), 1 μm pollen (▲), and 1.5 μm donuts (◆).

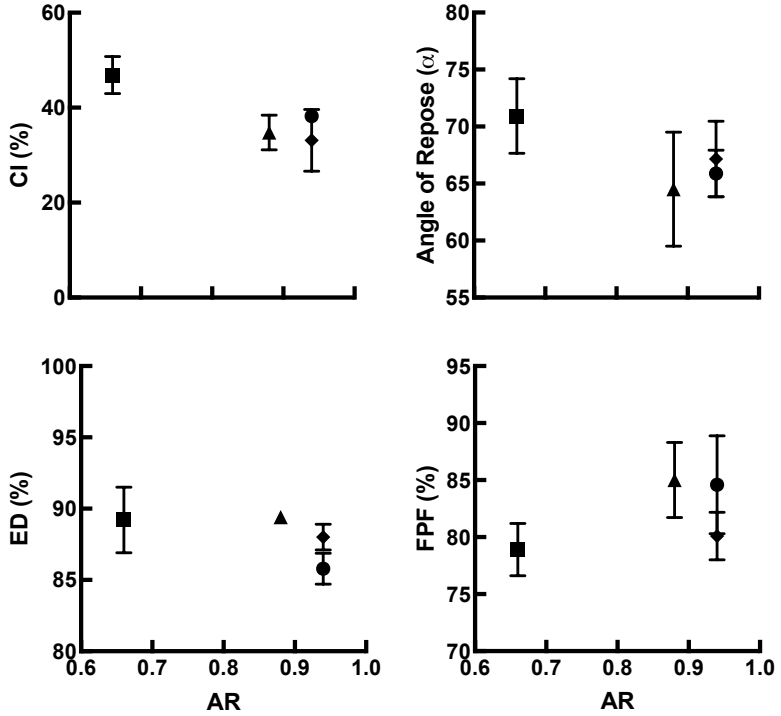

Figure 3.12 Powder parameters as a function of AR. Flowability, aerosolization, and deposition as a function of their AR of lyophilized lysozyme particles shapes, including 1x1 μm cylinders (●), 0.5x1 μm cylinders (■), 1 μm pollen (▲), and 1.5 μm donuts (◆).

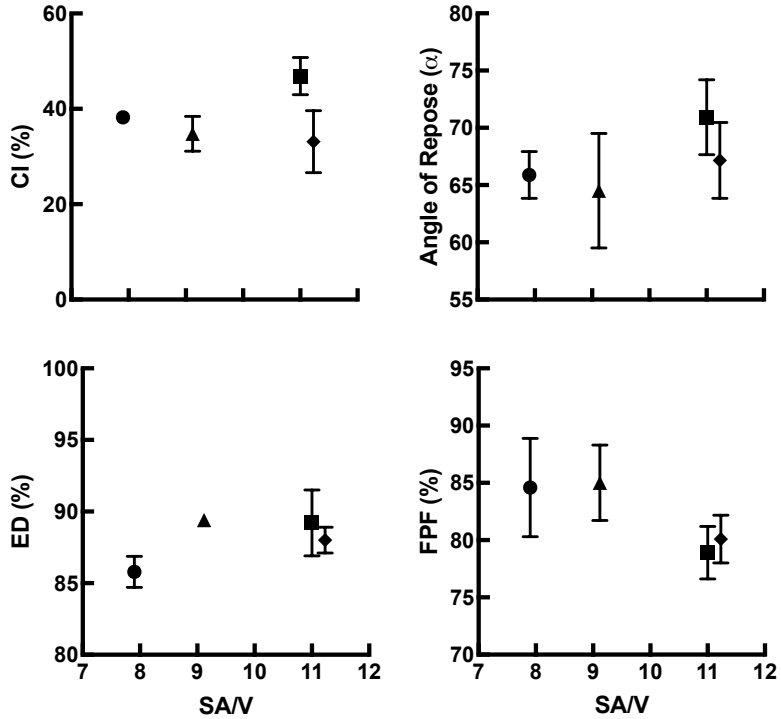

Figure 3.13 Powder parameters as a function of SA/V. Flowability, aerosolization, and deposition as a function of their SA/V of lyophilized lysozyme particles shapes, including 1x1 μm cylinders (●), 0.5x1 μm cylinders (■), 1 μm pollen (▲), and 1.5 μm donuts (◆).

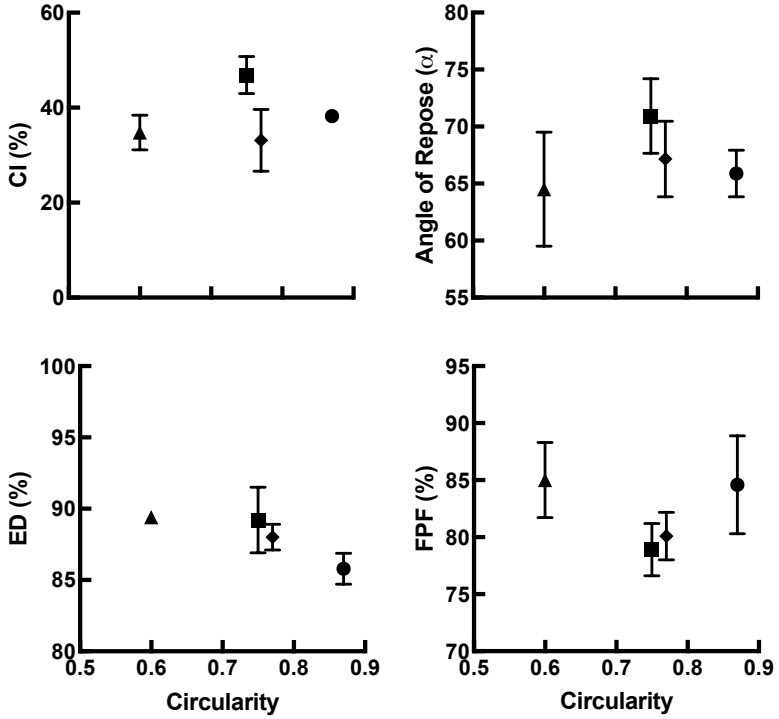

Figure 3.14 Powder parameters as a function of circularity. Flowability, aerosolization, and deposition as a function of their circularity of lyophilized lysozyme particles shapes, including 1x1 μm cylinders (●), 0.5x1 μm cylinders (■), 1 μm pollen (▲), and 1.5 μm donuts (◆).

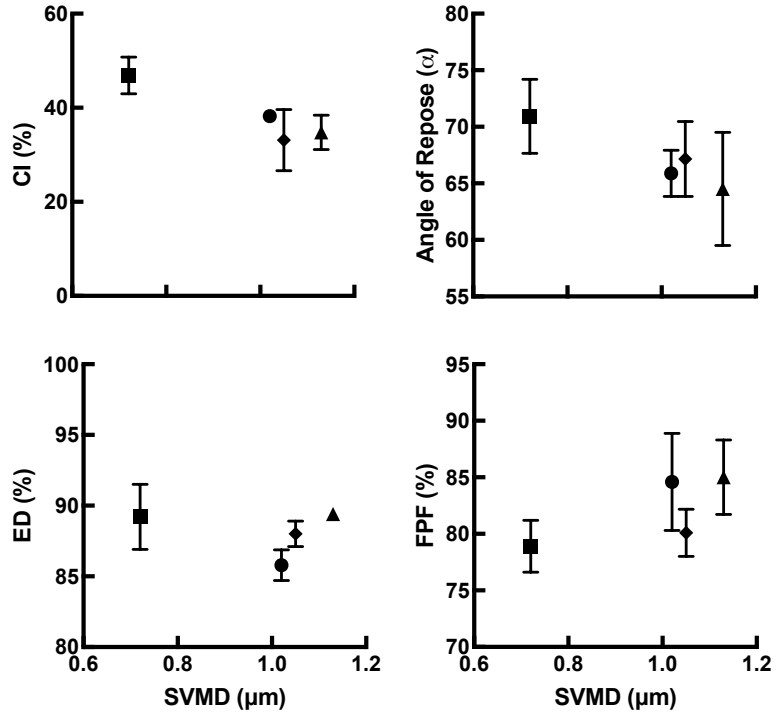

Figure 3.15 Powder parameters as a function of SVMD. Flowability, aerosolization, and deposition as a function of their SVMD of lyophilized lysozyme particles shapes, including 1x1 μm cylinders (●), 0.5x1 μm cylinders (■), 1 μm pollen (▲), and 1.5 μm donuts (◆).

3.4 Discussion

Pulmonary administration is a popular route of drug delivery with numerous potential therapeutic applications.[20,5] However, inhalable formulations frequently suffer from poor delivery efficiency, which limits the utility of the route.[3,4] Recent advances in both particle and device engineering for dry powder inhalers have increased performance potential and demand for dry powder aerosols.[3,21,22] Several particle engineering studies have been performed where investigators studied the effects of particle size and density to increase the delivery efficiency of dry powder formulations, as reviewed elsewhere.[3,6,23] Although particle shape is also known to be an important factor in aerosol performance, few studies have been performed in an effort to understand the role of particle shape, likely due to the difficulty of fabricating particles of precisely defined shape.[13,18] The objective of this work was to fabricate monodisperse PRINT particles in multiple shapes in order to study the role of particle shape in dry powder flowability, aerosolization, and deposition. Further understanding of the effects of particle shape will contribute to the improvement of high-performance dry powder aerosols.

In order to independently investigate the role of particle shape in flowability, aerosolization, and deposition, it is important that the particle shapes studied have the same maximum diameter, density, and composition.[13,21] Constant particle diameter, density, and composition ensure that particle shape is the primary variable responsible for observed changes in powder and aerosol behavior. The most comprehensive particle shape study to date by Hassan et al controlled for differences in particle size and aerodynamic diameter by grouping particles according to diameter and aerodynamic diameter prior to analyses.[13] Although this study was successful in interpreting grouped data and provided valuable insight into the role of particle shape, it would be more ideal to use particles of controlled size and aerodynamic diameter to

allow for the analysis of all particle shapes as a single group. As such, the initial goal for this study was to fabricate multiple particle shapes with minimal variation in maximum diameter and aerodynamic diameter between shapes. An extensive search through a library of available PRINT molds identified a group of four particle shapes with similar maximum diameters that were expected to generate similar aerodynamic diameters based on previous studies.[18] The formulation used for lysozyme 1x1 μm cylinders in Chapter 2 was adapted and successfully micromolded into PRINT molds of each particle shape, generating flowable dry powders following lyophilization. Image analysis determined that all particle shapes were of similar maximum diameter (0.90 – 1.40 μm), though each statistically different from the others ($p<0.0001$). The statistically significant difference in maximum diameter is due to the low error values obtained from image analysis, which are a result of the monodispersity of PRINT particles. The small differences in maximum diameter between particle shapes was deemed acceptable for our study. Particle composition analysis showed that all particle shapes are of similar composition, and thus, similar density. Together, these results supported the use of four lysozyme particle shapes, including 1x1 μm cylinders, 0.5x1 μm cylinders, 1 μm pollen, and 1.5 μm donuts, in the investigation of the role of particle shape in the powder and aerosol properties of dry powder formulations.

To study the relationship of particle shape with flowability, aerosolization, and deposition, particle shape must be quantified. The most frequent descriptors of particle shape in literature are diameter, SA, and AR.[24,14] In this study, we opted to describe particle shape with five factors, including $x_{F,max}$, AR, SA/V, circularity, and SVMD. The major dimensions of particle shape are described by $x_{F,max}$, the maximum distance between two parallel planes enclosing an object, and AR. SA/V, circularity, and SVMD describe the particle surface and its

deviation from sphericity. Little work has been done to date to understand the intricate interplay of all of these factors in regards to powder and aerosol properties.[13]

Bulk powder properties, including angle of repose and CI, were studied as measures of powder flowability. Flow is important for dry powder formulations, as it aids in powder handling and dispersion from the capsule and inhaler.[21,14] Flowability was first measured by angle of repose, which represents the ease of which a powder overcomes interparticle adhesion to achieve flow.[13] The lower the angle of repose, the higher propensity for the powder to flow.[25] Generally, an angle of repose smaller than 40° indicates good powder flow, though the angle is dependent on the method used.[25] All powders of lysozyme particle shapes had angle of repose values greater than 64°, indicating poor flowability. The high angle of repose suggests that the particles within these powders are forming aggregates that are resistant to flow.[13] Flowability was also measured by powder density and compressibility. Compressibility is a result of interparticle forces that cause particles to remain distant from one another and form low-density powders while in the bulk state.[26] The interparticle forces are overcome upon application of force, resulting in significant compression and increased density of the powder.[26] A CI value less than 25 % is considered ideal for particle flow.[13] The poor flowability observed in the angle of repose experiment was also observed in the compressibility experiment, with values of CI ranging from 35.2 to 47.1 % for lysozyme particle shapes. Results for individual particle shapes were consistent between both angle of repose and CI values. The 1 μm pollen powder had both the lowest angle of repose and CI, suggesting that is has the best flowability, while the 0.5x1 μm cylinders exhibited the poorest flowability for both angle of repose and CI. Although all particle shapes were found to flow poorly, it has been suggested that compressible dry powder formulations are well-suited for efficient pulmonary delivery, as they have weak interparticle

interactions that are readily overcome upon aerosolization.[26] In contrast, aggregates with strong interparticle interactions are not disrupted upon compression and will display a low CI, but fail to deagglomerate upon aerosolization.[26] This idea is supported by results from Chapter 2, which suggest that PRINT 1x1 μm cylinders fully disperse upon aerosolization for both efficient and precise delivery.

The aerosolization and deposition of particle shapes was studied *in vitro* via cascade impaction with a Monodose RS01 inhaler at 60 L/min. A flow rate of 60 L/min was selected because it produced a pressure drop of 4 kPa across the inhaler, which is the pressure drop required for a medium resistance device, such as the Monodose RS01 inhaler. Efficient delivery of inhalable dry powders requires fluidization and aerosolization of powders in the inhaler followed by aerosol emission.[3] All particle shapes were efficiently aerosolized from the inhaler, with emitted doses ranging from 85.8 to 89.4 % of the loaded dose. The high ED of 1 μm pollen particles may be explained by its superior flowability, though the poor flowability of 0.5x1 μm cylinders did not result in a significantly lower ED. This may suggest that even particles in the form of aggregates are readily fluidized. Deposition of particles in the lungs occurs most efficiently when the aerodynamic diameter is between 1 and 5 μm.[26] Aerosols of all particle shapes had MMAD values between 1.77 and 1.90 μm, which are ideal for efficient lung deposition. Importantly, the MMAD's of the particle shapes were not significantly different, which was one of the initial goals in selecting particle shapes. The FPF is the percentage of the collected dose that is below 5 μm in aerodynamic diameter. All particle shapes had FPF values between 78.9 and 85.0 %, indicating that the majority of the dose of all particle shapes is appropriate for pulmonary delivery. There was no significant difference between the FPF of particles shapes, likely because the particles are sufficiently small upon aerosolization to deposit

in stages below the 5 μm cutoff. The lower FPF value for 0.5 x 1 μm cylinders may indicate that, although the ED is not hindered by poor flowability, the particles are unable to fully deagglomerate following fluidization.

Together, the angle of repose, CI, ED, and FPF describe powder flowability, aerosolization, and deposition.[13] To interrogate the impact that particle shape has on these factors, powder parameters were plotted as a function of parameters describing particle shape in **Figures 3.10-3.15**.

The maximum diameter of particles plays an important role in powder flow, aerosolization, and deposition.[27] Within the 1-10 μm range of particle diameters, smaller diameter particles tend to have stronger interparticle forces and form aggregates, which results in poor powder flow.[27] Larger particles within this size range would be expected to have weaker interparticle forces, resulting in lower values for angle of repose and CI. Although few significant differences in the angle of repose and CI between particle shapes were observed, there appears to be a general trend that shapes of larger $x_{F,max}$ exhibit better flowability **(Figure 3.10)**. The ED and FPF appear to be minimally impacted by differences in $x_{F,max}$, which may suggest that all particle shapes fluidize as aggregates and are readily aerosolized into individual particles with aerodynamic diameters below the FPF cutoff of 5 μm.

By definition, the aerodynamic diameter of particles is a combination of particle diameter, density, and shape.[28] As particles in this study are assumed to be of equivalent density, any differences in MMAD can be attributed to diameter and particle shape. The relationships that were observed between $x_{F,max}$ and flow parameters are less apparent or absent when plotted against MMAD **(Figure 3.11)**. This could be due to the shape factor included in the calculation of aerodynamic diameter, which may obscure any effects due to particle shape. There appears to

be no relationship between MMAD and ED. The ED is expected to primarily be influenced by powder properties prior to aerosolization. Additionally, no trend between MMAD and FPF was observed, as all particle shapes had MMAD values well below 5 μm.

Particles with a smaller $x_{F,min}$ to $x_{F,max}$, or AR, are expected to be more compressible and exhibit poor flowability.[27] This is because particles with small AR's form loose aggregates that readily deagglomerate and compress when pressure is applied.[27] Indeed, the shape with the lowest AR, 0.5x1 μm cylinders, had the highest CI and angle of repose. CI and angle of repose for the other three shapes were similar, as there was little variation in AR among them **(Figure 3.12)**. No trend in ED or FPF was observed relative to AR, suggesting that the poor flowability of 0.5x1 μm cylinders is not strongly affecting aerosolization.

Particles with higher SA/V may be expected to have stronger interparticle interactions, however, SA/V does not describe the availability of the surface for interaction with neighboring particles. As such, no trend was observed between SA/V and CI, angle of repose, or ED (**Figure 3.13)**. Interestingly, particle shapes with greater SA/V tended to have a lower FPF, which may suggest incomplete deagglomeration upon aerosolization due to stronger interparticle interactions.

Particle circularity was measured in an effort to describe the morphology of the surface of the particle shapes. However, no trends were observed for any of the powder parameters relative to circularity **(Figure 3.14)**. SVMD was measured to describe the 2D surface of each particle shape that would experience drag forces upon aerosolization. Unfortunately, the close grouping of SVMD values for three particle shapes makes it difficult to observe any potential relationship between powder parameters and SVMD **(Figure 3.15)**.

Although some relationships were observed in the current study, the study was limited to

four particle shapes based on the availability of PRINT molds that would generate particles of similar particle diameters and aerodynamic diameters. The design and manufacture of additional PRINT molds of different particles shapes near 1 μm in diameter and a series of shapes of larger diameter will allow for further investigation into the role of particle shape. Additionally, this study evaluated the role of particle shape at a single flow rate of 60 L/min. Particle shape could potentially have different importance at lower and higher flow rates, which are relevant for different inhalers and patients with respiratory insufficiencies. The results of this study support utilizing PRINT particles to further investigate the role of particle shape in powder flow, aerosolization, and deposition.

3.5 Conclusions

Advances in particle and device engineering have increased both expectations and potential for the performance of dry powder aerosols. The ability to manufacture particles in precisely engineered shapes presents an excellent opportunity to improve dry powder performance. However, the role of particle shape in powder flowability, aerosolization, and deposition is not well understood, and thus currently cannot be leveraged into an advance in aerosol performance. To facilitate further understanding of the impact of particle shape, a series of four similarly sized PRINT particle shapes were developed as dry powders, all of which displayed excellent aerosol properties. Particle shapes with a larger $x_{F,max}$ were observed to improve flowability, however, this effect was negated in particle shapes of low AR. Additionally, it was shown that shapes with higher SA/V values produced lower FPF's, as the particles were unable to completely aerosolize. Interestingly, we observed that PRINT dry powders fluidize as large particle aggregates, leading to efficient emission of all particle shapes from the device. While additional studies will be required to fully elucidate the role of particle

shape in flowability, aerosolization, and deposition, it is clear from these studies that shape is an important aspect of developing high-performance dry powder aerosols. Further knowledge of the impact of particle shape on dry powder performance could yield important improvements in the performance of dry powder formulations.

REFERENCES

1. Saluja, V. *et al.* A comparison between spray drying and spray freeze drying to produce an influenza subunit vaccine powder for inhalation. *J. Control. Release* **144,** 127–133 (2010).

2. Licalsi, C., Christensen, T., Bennett, J. V., Phillips, E. & Witham, C. Dry powder inhalation as a potential delivery method for vaccines. *Vaccine* **17,** 1796–1803 (1999).

3. Weers, J. G. & Miller, D. P. Formulation Design of Dry Powders for Inhalation. *J. Pharm. Sci.* **104,** 3259–3288 (2015).

4. Longest, P. W., Tian, G., Li, X., Son, Y. J. & Hindle, M. Performance of Combination Drug and Hygroscopic Excipient Submicrometer Particles from a Softmist Inhaler in a Characteristic Model of the Airways. *Ann. Biomed. Eng.* **40,** 1–15 (2012).

5. de Boer, A. H. *et al.* Dry powder inhalation: past, present and future. *Expert Opin. Drug Deliv.* **14,** 499–512 (2017).

6. Chow, A. H. L., Tong, H. H. Y., Chattopadhyay, P. & Shekunov, B. Y. Particle engineering for pulmonary drug delivery. *Pharm. Res.* **24,** 411–437 (2007).

7. Saiful Hassan, M. & Lau, R. Effect of Particle Formulation on Dry Powder Inhalation Efficiency. *Curr. Pharm. Des.* **16,** 2377–2387 (2010).

8. Carstensen, J. T. & Chan, P. C. Relation between particle size and repose angles of powders. *Powder Technol.* **15,** 129–131 (1976).

9. Visser, J. Van der Waals and other cohesive forces affecting powder fluidization. *Powder Technol.* **58,** 1–10 (1989).

10. Heyder, J., Gebhart, J., Rudolf, G., Schiller, C. F. & Stahlhofen, W. Deposition of particles in the human respiratory tract in the size range 0.005-15 μm. *J. Aerosol Sci.* **17,** 811–825 (1986).

11. Edwards, D. A. *et al.* Large Porous Particles for Pulmonary Drug Delivery. *Science (80-.).* **276,** 1868–1871 (1997).

12. Vanbever, R. *et al.* Formulation and physical characterization of large porous particles for inhalation. *Pharmaceutical Research* **16,** 1735–1742 (1999).

13. Hassan, M. S. & Lau, R. W. M. Effect of particle shape on dry particle inhalation: study of flowability, aerosolization, and deposition properties. *AAPS PharmSciTech* **10,** 1252–1262 (2009).

14. Zeng, X. M., Martin, G. P., Marriott, C. & Pritchard, J. The influence of carrier morphology on drug delivery by dry powder inhalers. *Int. J. Pharm.* **200,** 93–106 (2000).

15. Kaialy, W., Alhalaweh, A., Velaga, S. P. & Nokhodchi, A. Effect of carrier particle shape on dry powder inhaler performance. *Int. J. Pharm.* **421,** 12–23 (2011).

16. Garcia, A. *et al.* Microfabricated Engineered Particle Systems for Respiratory Drug Delivery and Other Pharmaceutical Applications. *J. Drug Deliv.* **2012,** 1–10 (2012).

17. Mack, P., Horvath, K., Tully, J. & Maynor, B. Particle engineering for inhalation formulation and delivery of biotherapeutics. *Inhalation* **6,** 16–20 (2012).

18. Fromen, C. A. *et al.* Synthesis and Characterization of Monodisperse Uniformly Shaped Respirable Aerosols. *AIChE J.* **59,** 3184–3194 (2013).

19. Xu, J. *et al.* Rendering protein-based particles transiently insoluble for therapeutic applications. *J. Am. Chem. Soc.* **134,** 8774–8777 (2012).

20. Bäckman, P., Adelmann, H., Petersson, G. & Jones, C. B. Advances in inhaled technologies: understanding the therapeutic challenge, predicting clinical performance, and designing the optimal inhaled product. *Clin. Pharmacol. Ther.* **95,** 509–520 (2014).

21. Yang, M. Y., Chan, J. G. Y. & Chan, H. K. Pulmonary drug delivery by powder aerosols. *J. Control. Release* **193,** 228–240 (2014).

22. Dolovich, M. B. & Dhand, R. Aerosol drug delivery: Developments in device design and clinical use. *Lancet* **377,** 1032–1045 (2011).

23. Lin, Y.-W., Wong, J., Qu, L., Chan, H. K. & Zhou, Q. T. Powder production and particle engineering for dry powder inhaler formulations. *Curr. Pharm. Des.* **21,** 3902–3916 (2015).

24. Hassan, M. S. & Lau, R. Inhalation performance of pollen-shape carrier in dry powder formulation: Effect of size and surface morphology. *Int. J. Pharm.* **413,** 93–102 (2011).

25. Geldart, D., Abdullah, E. C., Hassanpour, A., Nwoke, L. C. & Wouters, I. Characterization of powder flowability using measurement of angle of repose. *China Particuology* **4,** 104–107 (2006).

26. Seville, P. C., Learoyd, T. P., Li, H. Y., Williamson, I. J. & Birchall, J. C. Amino acid-modified spray-dried powders with enhanced aerosolisation properties for pulmonary drug delivery. *Powder Technol.* **178,** 40–50 (2007).

27. Louey, M. D., Van Oort, M. & Hickey, A. J. Aerosol dispersion of respirable particles in narrow size distributions using drug-alone and lactose-blend formulations. *Pharm. Res.* **21,** 1207–1213 (2004).

28. Mortensen, N. P., Durham, P. & Hickey, A. J. The role of particle physico-chemical properties in pulmonary drug delivery for tuberculosis therapy. *J. Microencapsul.* **31,** 265–2048 (2014).

CHAPTER 4: THERAPEUTIC APPLICATIONS OF PRINT DRY POWDERS[1]

4.1 Introduction

The ability to manufacture protein dry powders with PRINT with complete control of particle size, shape, and composition affords a unique opportunity to create innovative high-performance inhaled therapies. In previous chapters, we demonstrated that dry powders of monodisperse PRINT protein particles efficiently fluidize and aerosolize from an inhaler and deposit in a cascade impactor with remarkably high precision. The high delivery efficiency and precision possible with PRINT dry powders is particularly ideal for pulmonary protein delivery, as the high cost of biopharmaceuticals necessitates a highly efficient delivery technique for commercial viability.[1] Additionally, the low excipient mass possible with PRINT is beneficial for proteins, which frequently require a high dose by mass, as excipient mass reduces the amount of protein that can be delivered without causing respiratory tract irritation.[2] The advantages of PRINT protein dry powders motivated the development of respirable formulations of two therapeutic proteins, deoxyribonuclease I (DNase) and butyrylcholinesterase (BuChE).

Cystic fibrosis (CF) is an autosomal recessive disorder that is characterized by viscous secretions in the lungs and other organs.[3] The viscous secretions cause obstructions in the lungs, which lead to inflammation, infection, and tissue damage.[3] Lung disease due to obstruction is the primary cause of morbidity in patients with CF.[3] Currently, CF therapy aims to minimize the

[1]Parts of this chapter previously published in: Rahhal TB, Fromen CA, Wilson EM, Kai MP, Shen TW, Luft JC, DeSimone JM. Pulmonary delivery of butyrylcholinesterase as a model protein to the lung. Molecular Pharmaceutics. 13, 1626-1635 (2016).

complications caused by lung obstruction with airway clearance techniques, broad-spectrum antibiotics, and removal of endobronchial biofilms.[4] Dornase alfa (recombinant human deoxyribonuclease I) is a widely-used inhaled therapeutic protein that aids in airway clearance by reducing mucus viscosity, thereby encouraging mucociliary and cough clearance of the mucus.[5] Currently, dornase alfa is administered once daily via nebulizer.[5,6] Although dornase alfa therapy has proven beneficial for many patients, it contributes nearly 30 minutes to the daily treatment burden of CF patients, which averages 108 minutes per day.[6] A dry powder formulation of DNase could be rapidly administered and therefore decrease the treatment burden for CF patients. Few reports of DNase dry powders have been published, potentially due to the sensitivity of DNase to physical denaturation.[7–9] The reported formulations were observed to have full retention of DNase activity in the final dry powder formulation, however, no further stability testing was reported.[7,8] Because PRINT imparts little physical force during manufacturing, we hypothesized that PRINT could be used to produce a dry powder formulation of DNase without altering the native structure of DNase.

The second therapeutic protein discussed in this chapter is BuChE, which is a protein of interest for the prophylactic treatment of organophosphate poisoning by inhalation.[10,11] Organophosphates, which are often present in insecticides, herbicides, and nerve agents, are readily internalized by several routes, including ingestion, skin absorption, and inhalation.[12] Upon internalization, organophosphates rapidly inhibit acetylcholinesterase, which leads to a toxic accumulation of acetylcholine, resulting in neurotoxic effects or death.[12] Protection of military personnel against organophosphate exposure by inhalation nerve agents is of high interest, as inhalation is the primary route of exposure.[11] An inhaled pretreatment of BuChE has been shown to protect against inhaled organophosphates in macaques by effectively binding

organophosphates in the lungs prior to entry into systemic circulation.[11] Based on the macaque data, Rosenberg et al. proposed that a "pulmonary bioshield" of BuChE could be used to protect military personnel from nerve agents prior to exposure.[11,13] However, studies by Rosenberg et al. were performed with liquid formulations that are intended for delivery by nebulizater.[11,13] For military applications, a delivery system for BuChE administration must be highly portable and stable over a range of ambient temperatures, which is not feasible with liquid formulations.[1] A dry powder formulation of BuChE would more readily meet the requirements for military applications, and thus, a dry powder formulation of BuChE was developed using PRINT.

In this chapter, we describe the formulation of two different therapeutic proteins into PRINT dry powder formulations intended for local respiratory applications. The stability of DNase and BuChE in PRINT dry powders was evaluated and the aerosol performance of both formulations was characterized *in vitro* via cascade impaction. In addition, the residence time of BuChE dry powders were determined *in vivo*.

4.2 Materials and Methods

4.2.1 Materials

Deoxyribonuclease I (DNase) from bovine pancreas was purchased from EMD Millipore (Billerica, MA, USA). Butyrylcholinesterase (BuChE) from equine serum was obtained from Sigma-Aldrich (St. Louis, MO, USA). The DetectX® Butyrylcholinesterase Fluorescent Activity Kit was purchased from Arbor Assays (Ann Arbor, MI, USA). DyLight™ 680 NHS-Ester was acquired from Thermo Fisher Scientific (Waltham, MA, USA). Poly(1-vinylpyrrolidone-co-vinyl acetate) (PVPVA), fluorescamine, isopropanol, lactose, glycerol, silicone spray, PRINT mold, centrifugal filters, supplies for gel electrophoresis, and hydroxypropyl methylcellulose (HPMC) capsules were obtained from the same suppliers detailed in Chapter 2.

4.2.2 Methods

4.2.2.1 Fabrication of PRINT Protein Particles

Protein-based PRINT particles of DNase and BuChE were fabricated using a method adapted from Xu et al.[14] Proteins were used as received. For both 1 μm cylinder formulations, a 10 wt% pre-particle solution (PPS) of 40:35:25 protein:lactose:glycerol was prepared in water and cast into a film on poly(ethylene terephthalate) (PET). BuChE nanoparticles were fabricated with the same method from a 5 wt% PPS. Following film drying, PRINT mold was applied to the film and passed through a heated laminator at 98°C and 100 psi. Particles were harvested and washed as described in Chapter 2.

4.2.2.2 Particle Lyophilization

Particles were resuspended in *tert*-butanol at 1 mg/mL, flash frozen in liquid nitrogen, and lyophilized for 24 hours, as described in Chapter 2.

4.2.2.3 Scanning Electron Microscopy

Particles were suspended in isopropanol and imaged on a silicon wafer, as in Chapter 2.

4.2.2.4 Thermogravimetric Analysis

Particle concentration was determined using thermogravimetric analysis (TGA) as explained in Chapter 2.

4.2.2.5 Particle Composition Analysis

Particle composition was determined via high-performance liquid chromatography (HPLC) as detailed in Chapter 2.

4.2.2.6 Gel Electrophoresis

SDS-PAGE (sodium dodecyl sulfate – polyacrylamide gel electrophoresis) was performed as described in Chapter 2.

4.2.2.7 Circular Dichroism

Protein for circular dichroism (CD) was purified into 10 mM potassium phosphate buffer (pH 7.4) and prepared at 250 μg/mL to yield an optical density of 0.8 at 185 nm. Spectra were collected in triplicate and deconvoluted according to the protocol in Chapter 2.

4.2.2.8 Intrinsic Fluorescence

Samples for intrinsic fluorescence were prepared in the same manner as CD samples and analyzed according to the method in Chapter 2.

4.2.2.9 Butyrylcholinesterase Activity Assay

BuChE enzymatic activity was determined using a DetectX® Butyrylcholinesterase Fluorescent Activity Kit according to manufacturer's instructions. BuChE was purified from particles by dissolving particles in water followed by separation through a 0.5 mL Amicon® Ultra 3k MWCO centrifugal filter. Two additional water washes were performed on the protein retentate. The enzymatic activity of particle samples was compared to the activity of a BuChE control.

4.2.2.10 Fluorescamine Assay

A fluorescamine assay was performed to quantify cascade impaction deposition and normalized to the composition of each particle shape, as in Chapter 2.

4.2.2.11 Cascade Impaction

The aerosol properties of DNase and BuChE 1 μm cylinders were evaluated *in vitro* using an Andersen Cascade Impactor (ACI) operated at 28.3 L/min. DNase 1 μm cylinders were aerosolized from a Monodose RS01 dry powder inhaler with 5 mg of particles in an HPMC capsule. BuChE 1 μm cylinders were aerosolized from a Penn-Century DP-4M insufflator. Further experimental details and definitions of aerosol parameters are available in Chapter 2.

4.2.2.12 Animals

Male C57BL/6 mice were obtained from The Jackson Laboratory (Bar Harbor, ME, USA) at 4 weeks of age and housed in a pathogen-free facility at the University of North Carolina at Chapel Hill. Standard guidelines and approved protocols for the care and use of laboratory mice were followed as set forth by the UNC Institution of Animal Care and Use Committee (IACUC). Mice were treated at 6 weeks of age.

4.2.2.13 Conjugation of Fluorescent Label to Butyrylcholinesterase

BuChE was labeled with DyLight™ 680 using an NHS-Ester of DyLight at a 3-fold molar excess of dye to BuChE. No activity loss was observed, as previously published.[15]

4.2.2.14 Detection of BuChE in Biological Media

DyLight 680-conjugated BuChE was added to three biologically relevant mediums, including PBS, blood, and plasma to develop and validate an assay to quantify BuChE. Fluorescent BuChE was added to PBS, blood, and plasma from 0 to 10 mg/mL and fluorescence was measured at 0, 1, 4, and 24 hours after addition of fluorescent BuChE. Samples were excited at 675 nm and emission was read at 712 nm.

4.2.2.15 Orotracheal Administration by Insufflation

Dry powders of fluorescently-tagged BuChE 1 μm cylinders (fabricated with 3 % fluorescently-tagged BuChE) were orotracheally administered to mice with a Penn-Century DP-4M insufflator and a laryngoscope to aid in insufflator placement. Prior to administration, mice were anesthetized with ketamine and placed on a board at an incline of 45 degrees held by their upper incisors. The insufflator, loaded with 2 mg of BuChE 1 um cylinders, was inserted into the trachea and the device was actuated 5 consecutive times with 200 μL of air. Following administration, the insufflator was removed and mice were given Antisedane® (Zoetis,

Parsippany, NJ, USA) to reverse anesthesia and placed on a heated pad. The insufflator was weighed following dosing to determine the actual dose delivered from the device.

4.2.2.16 Determination of Residence Time

The residence time of insufflated BuChE 1 μm cylinder powders were determined in C57BL/6 mice. Mice were euthanized with ketamine followed by cardiac puncture at 24, 48, 72, 96, 144, and 168 hours after BuChE administration in addition to PBS treated control mice at 24 hours. Mice were then perfused with 10 mL 1X PBS. Bronchoalveolar lavage (BAL) was then performed with 1 mL of 1X PBS to collect bronchoalveolar lavage fluid (BALF) from the lungs for determination of BALF residence time. Following BAL, lungs were resected from the mice for determination of lung residence time. The harvested lungs and BALF were imaged with an IVIS-Lumina (PerkinElmer, Waltham, MA, USA) ($\lambda_{ex}/\lambda_{em}$: 675/712 nm) to measure radiant efficiency of BuChE per gram of each sample. The BuChE activity present in each BALF sample was determined with the BuChE activity assay summarized earlier.

4.2.2.17 Statistics

Statistical analyses were performed using GraphPad Prism Version 5.1 (GraphPad Software, La Jolla, CA, USA). Data presented as mean ± standard deviation. Statistical analyses were performed using a one-way analysis of variance (ANOVA) with post hoc Tukey's test with $\alpha = 0.05$ unless stated otherwise.

4.3 Results

4.3.1 Fabrication and Characterization of DNase 1 μm Cylinders

4.3.1.1 Fabrication and Morphological Characterization of Particles

A pre-particle solution (PPS) of 10 wt% in water with the solids component comprised of 40 % DNase, 35 % lactose, and 25 % glycerol by mass was determined to be ideal for the

fabrication of DNase 1 μm cylinders, as observed by scanning electron microscopy (SEM). Resuspension of DNase particles in *tert*-butanol followed by flash-freezing and lyophilization yielded a dry powder that was rapidly water-soluble. Observation of particle morphology by SEM following lyophilization confirmed that DNase 1 μm cylinders were successfully micromolded and no change in particle morphology occurred during lyophilization **(Figure 4.1)**.

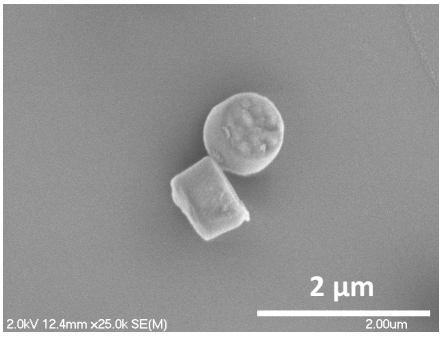

Figure 4.1 SEM of DNase 1 μm cylinders. SEM image of lyophilized DNase 1 μm cylinders resuspended in isopropanol at 25k magnification.

4.3.1.2 Composition of DNase 1 μm Cylinders

Analysis of the composition of lyophilized DNase 1 μm cylinders by high-performance liquid chromatography (HPLC) determined that particles are composed of 81.27 % ± 1.57 DNase, 13.95 % ± 0.72 lactose, and 4.77 % ± 0.85 glycerol by mass **(Figure 4.2)**. Less than 20 % of particle mass was attributed to excipients.

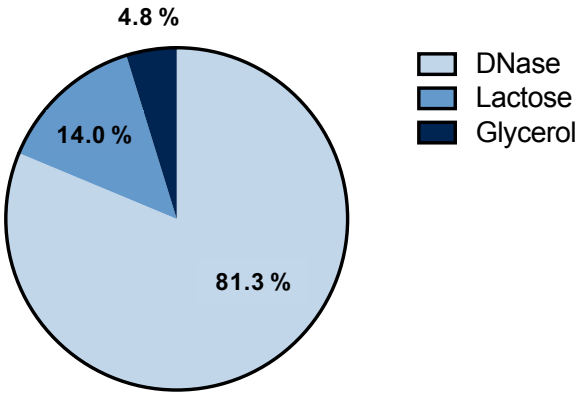

Figure 4.2 Composition of DNase 1 μm cylinders. Composition of lyophilized DNase 1 μm cylinders by mass as determined by HPLC (n=3).

4.3.2 Characterization of DNase Stability

4.3.2.1 Gel Electrophoresis

Potential changes in the primary structure of DNase were observed by monitoring molecular weight with SDS-PAGE **(Figure 4.3)**. The DNase samples appear to be comprised of a mixture of proteins from 10 to 66 kDa in molecular weight. The most intense band near the 29 kDa ladder standard belongs to DNase, which has a molecular weight near 30 kDa. Although changes in the DNase band are somewhat obscured by other bands, there appears to be no change in the primary DNase band at any step in the PRINT process.

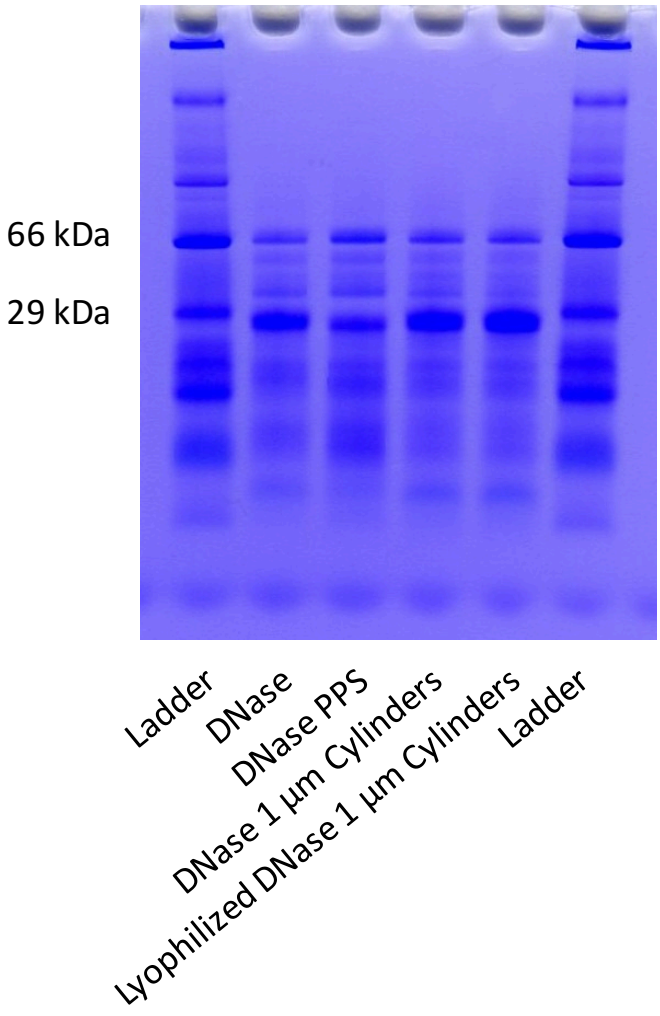

Figure 4.3 SDS-PAGE of DNase 1 µm cylinders. SDS-PAGE of DNase from each formulation step for lyophilized DNase 1 µm cylinders (n=3).

4.3.2.2 Circular Dichroism

The secondary structure of DNase was monitored with circular dichroism (CD). Any changes in the secondary structure of DNase during PRINT would be observed as a change in CD spectra. The spectra obtained for lyophilized DNase 1 µm cylinders deviated from the DNase and DNase PPS control spectra slightly, though the heat-denatured standard was dramatically different from the control samples **(Figure 4.4)**. The calculated secondary structure content of each sample showed a small loss of α helices for lyophilized DNase 1 µm cylinders relative to controls, while denatured DNase lost nearly all α helices relative to controls **(Figure 4.5)**.

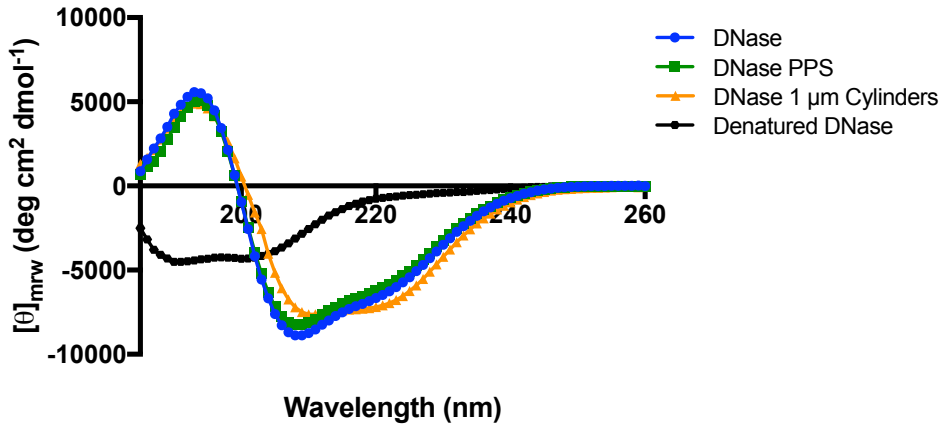

Figure 4.4 Circular dichroism of DNase 1 µm cylinders. CD spectra of DNase from each formulation step for lyophilized DNase 1 µm cylinders (n=3).

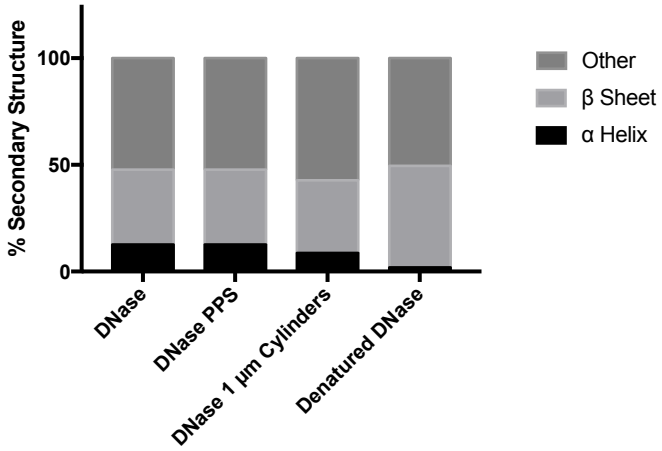

Figure 4.5 Secondary structure of DNase 1 µm cylinders. Secondary structure composition calculated from CD of DNase from each step for lyophilized DNase 1 µm cylinders (n=3).

4.3.2.3 Intrinsic Fluorescence

The tertiary structure, or global folding, of DNase was observed with intrinsic fluorescence spectroscopy. Changes in folding result in a change in the environment of fluorescent residues, which alters protein intrinsic fluorescence. The spectra of lyophilized DNase 1 μm cylinders overlaid the spectra of DNase and DNase PPS controls **(Figure 4.6)**. The denatured DNase control showed a dramatic reduction in signal intensity and a shift in the wavelength of maximum emission.

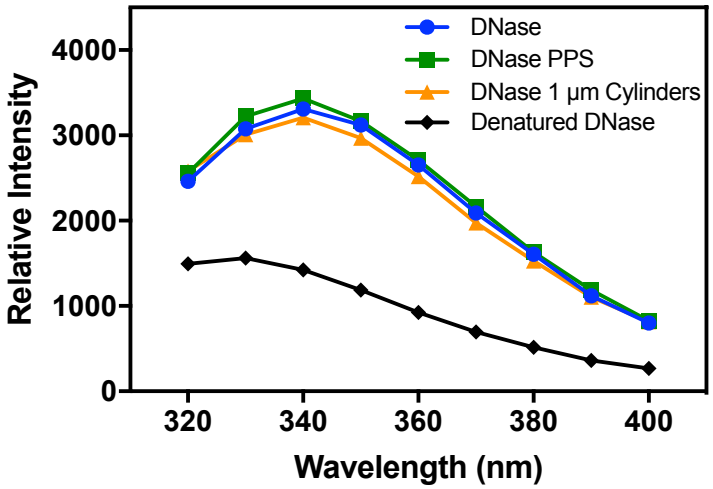

Figure 4.6 Intrinsic fluorescence of DNase 1 μm cylinders. Intrinsic fluorescence spectra of DNase from each formulation step for lyophilized DNase 1 μm cylinders (n=3).

4.3.3 *In Vitro* Aerosol Characterization of DNase 1 μm Cylinders

The aerosol performance of lyophilized DNase 1 μm cylinders was evaluated *in vitro* with an Andersen Cascade Impactor (ACI) using a Monodose RS01 inhaler at 28.3 L/min. Dose retained in the device and deposited in the throat and on stages of the ACI are plotted as a fraction of the total collected dose in **Figure 4.7**. Powder and aerosol parameters calculated from cascade impaction data are presented in **Table 4.1**. Less than 3 % of the collected dose was recovered from the HPMC capsule or the inhaler, resulting in an emitted dose (ED) of 98.9 %. The aerosol was largely able to bypass the artificial throat, with approximately 10 % of the

collected dose recovered in the throat. Deposition of DNase 1 μm cylinders occurred largely on stages 3 and 4, resulting in a mass median aerodynamic diameter (MMAD) of 2.73 μm with a geometric standard deviation (GSD) of 1.62. The fine particle fraction (FPF) of the formulation, or percent of the formulation appropriately sized for lung deposition, was determined to be 75.4 %.

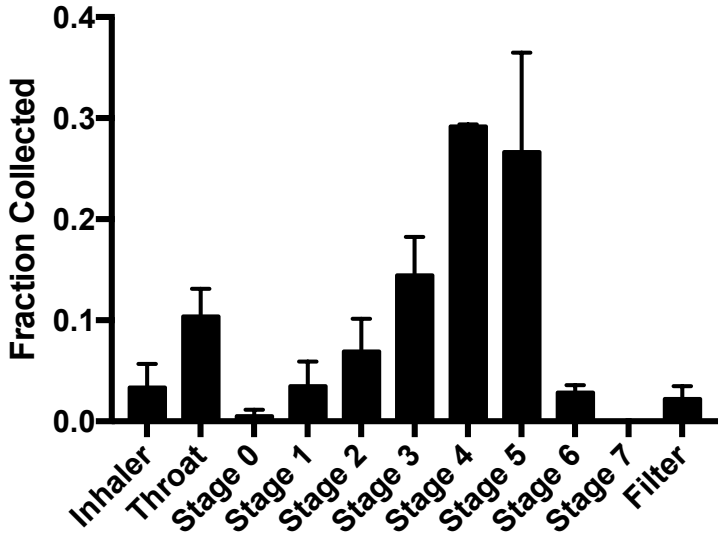

Figure 4.7 Cascade impaction of DNase 1 μm cylinders. Cascade impaction distribution of lyophilized DNase 1 μm cylinder from a Monodose RS01 inhaler at 28.3 L/min (n=3).

Table 4.1 Aerosol parameters of DNase 1 μm cylinders. Cascade impaction parameters of lyophilized DNase 1 μm cylinders from a Monodose RS01 inhaler at 28.3 L/min (n=3).

Formulation	MMAD (μm)	GSD	ED (%)	FPF Collected (%)
DNase	2.91 ± 0.69	1.66 ± 0.14	98.9 ± 0.9	75.4 ± 6.7

4.3.4 Fabrication and Characterization of PRINT BuChE Particles

4.3.4.1 Fabrication and Morphological Characterization

A PPS of 40 % BuChE, 35 % lactose, and 25 % glycerol by mass at 10 wt% in water was found to produce the optimal film for the fabrication of BuChE 1 μm cylinders. Rapidly water-soluble dry powders were produce upon lyophilization of the particles from *tert*-butanol. Observation of lyophilized BuChE 1 μm cylinders resuspended in isopropanol by SEM found the

particles to retain the proper 1 μm cylinder morphology throughout lyophilization **(Figure 4.8)**.

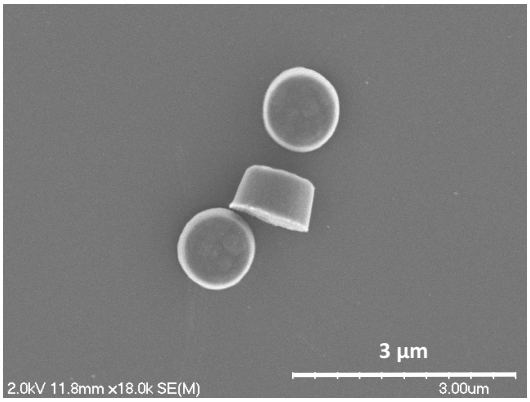

Figure 4.8 SEM of BuChE 1 μm cylinders. SEM image of lyophilized BuChE 1 μm cylinders resuspended in isopropanol at 18k magnification.

4.3.4.2 Composition of BuChE 1 μm Cylinders

Analysis of particle composition by HPLC determined that lyophilized BuChE 1 μm cylinders are composed of 88.8 % BuChE, 1.0 % lactose, and 10.2 % glycerol **(Figure 4.9)**. Less than 15 % of the particle mass was attributed to excipients.

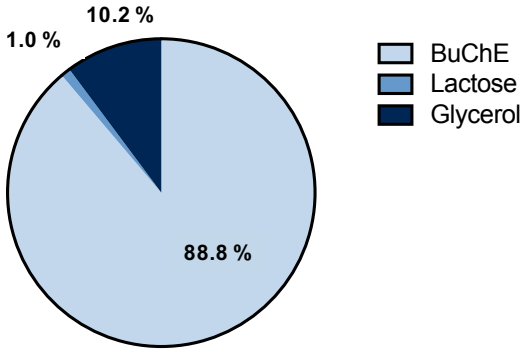

Figure 4.9 Composition of BuChE 1 μm cylinders. Composition of lyophilized BuChE 1 μm cylinders by mass as determined by HPLC (n=3).

4.3.4.3 Characterization of BuChE Stability

The functional stability of BuChE was observed at each step of the PRINT process, as its enzymatic activity is responsible for its therapeutic effect. The BuChE activity assay found no significant difference between the activity of lyophilized BuChE 1 μm cylinders and both the BuChE and BuChE PPS controls **(Figure 4.10)**.

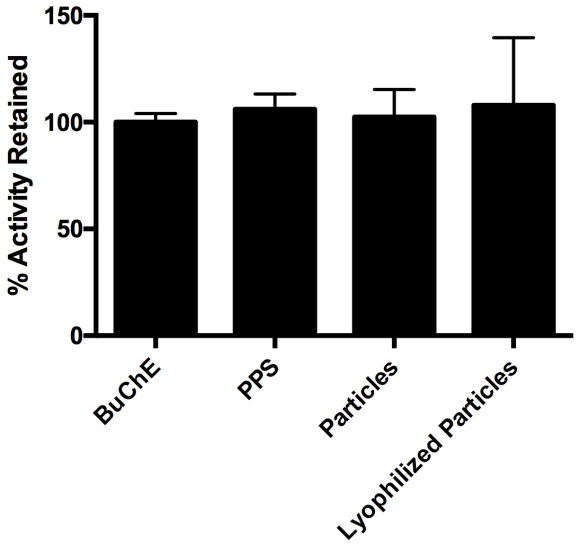

Figure 4.10 Enzymatic activity of BuChE 1 μm cylinders. Activity of BuChE from each formulation step relative to a BuChE standard for lyophilized BuChE 1 μm cylinders (n=3).

4.3.4.4 Fabrication of BuChE Nanoparticles

A PPS of 40 % BuChE, 35 % lactose, and 25 % glycerol was used to fabricate BuChE nanoparticles. A 5 wt% PPS was identified as optimal to fabricate 80x320 nm rods, while a PPS of 2.5 wt% was optimal for 55x70 nm cylinders **(Figure 4.11)**.

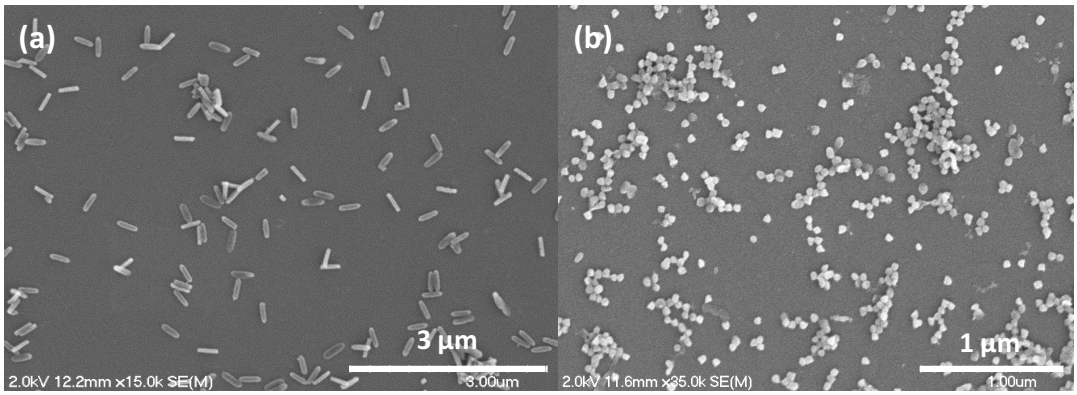

Figure 4.11 SEM of BuChE nanoparticles. SEM images of (a) 80x320 nm rod and (b) 55x70 nm cylinder BuChE particles.

4.3.5 In Vitro Aerosol Characterization of BuChE 1 μm Cylinders

Cascade impaction was used to characterize the aerosol performance of lyophilized BuChE 1 μm cylinders from a Penn-Century DP-4M insufflator at 28.3 L/min. The dose deposited on each stage as a fraction of the total collected dose is presented in **Figure 4.12**. The

deposition profile was used to calculate the aerosol parameters in **Table 4.2**. Deposition of BuChE 1 μm cylinders was centered on stage 4, which collects particles between 2.1 and 3.3 μm in aerodynamic diameter at 28.3 L/min. More than 45 % of the collected dose was on stage 4. BuChE 1 μm cylinders were found to have an MMAD of 2.73 μm with a GSD of 1.39. The FPF of the collected dose was 95.13 %.

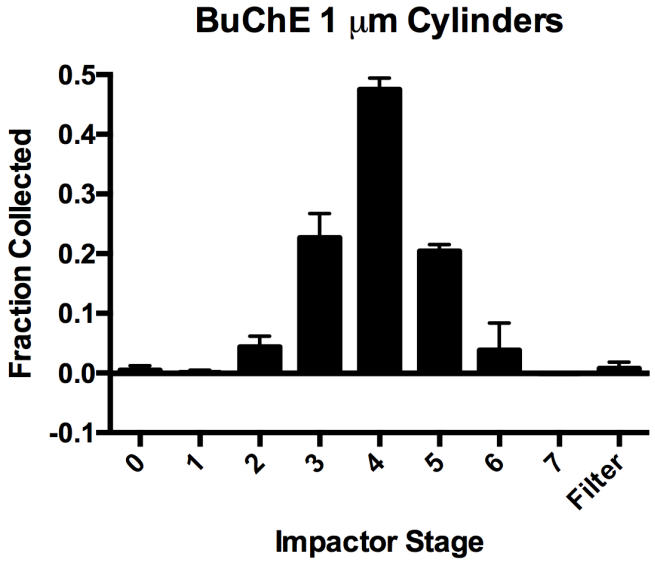

Figure 4.12 Cascade impaction of BuChE 1 μm cylinders. Cascade impaction distribution of lyophilized BuChE 1 μm cylinders from a Penn-Century DP-4M insufflator at 28.3 L/min (n=3).

Table 4.2 Aerosol parameters of BuChE 1 μm cylinders. Cascade impaction parameters of lyophilized BuChE 1 μm cylinders from a Penn-Century DP-4M insufflator at 28.3 L/min (n=3).

Protein	MMAD (μm)	GSD	FPF (%)
BuChE	2.73	1.39	95.13

4.3.6 Insufflation of BuChE 1 μm Cylinders

4.3.6.1 Fluorescent BuChE Assay

An assay was developed to quantify the mass of fluorescent BuChE present in PBS, whole blood, and plasma. In addition, fluorescent BuChE was allowed to incubate in the biological fluids for 0, 1, 4, and 24 hours to account for time between sample collection and analysis. The relative fluorescence of each sample plotted against the fluorescent BuChE

concentration for each fluid is presented in **Figure 4.13**. All samples in PBS produced a clear linearly positive relationship between fluorescent BuChE concentration and relative fluorescence. Additionally, the fluorescence of each sample did not change with longer incubation times. Samples in whole blood showed a similar linearly positive relationship at 0 and 1 hours of incubation, but the fluorescence dramatically increased after incubation for 4 or 24 hours. In contrast, samples in plasma generated a linearly positive relationship and produced a consistent relative fluorescence at each of the incubation times. The limit of detection for fluorescent BuChE in PBS, plasma, and whole blood was 7.8 μg/mL. Fluorescent BuChE saturated the fluorescence signal in PBS and plasma above 2 mg/mL, while fluorescence was not saturated in blood at 8 mg/mL.

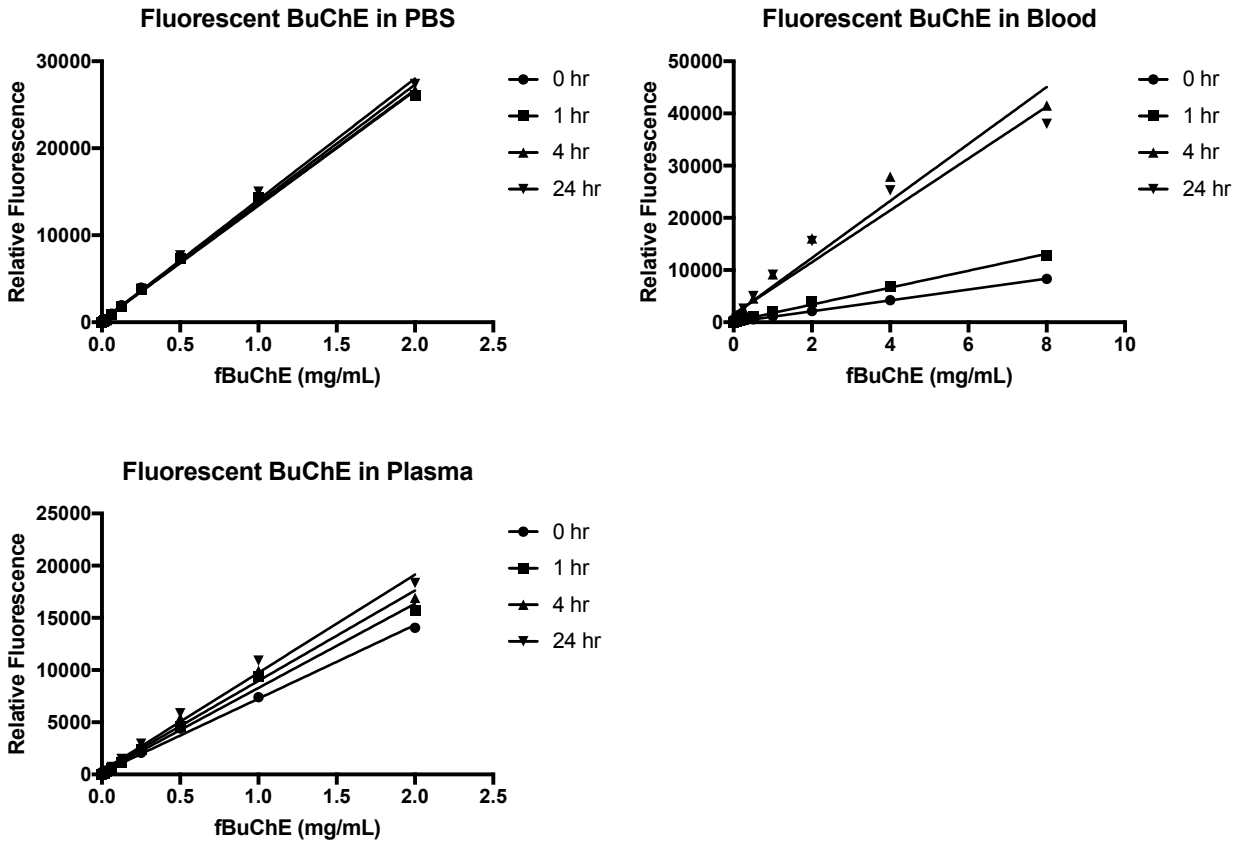

Figure 4.13 BuChE assay development. Assay development for the determination of the mass of DyLight 680-labeled BuChE in media relevant to *in vivo* mouse studies.

4.3.6.2 Insufflation of BuChE 1 μm Cylinders

Dry powders of fluorescently-tagged BuChE 1 μm cylinders were administered to mice by insufflation to observe the residence time of BuChE in murine lungs. Following insufflation and euthanization at the designated time point, BALF was collected and lungs were resected. Representative IVIS images of the lungs resected at each time point following the administration of BuChE 1 μm cylinders by insufflation are shown in **Figure 4.14**. The gain of the instrument was set to avoid any autofluorescence in the PBS control lung. At both 24 and 48 hours following administration, fluorescence is clearly visible in the lungs, though the signal appears to be restricted to one side. No fluorescence was detected in the lungs at further time points, including 72, 96, 144, and 168 hours.

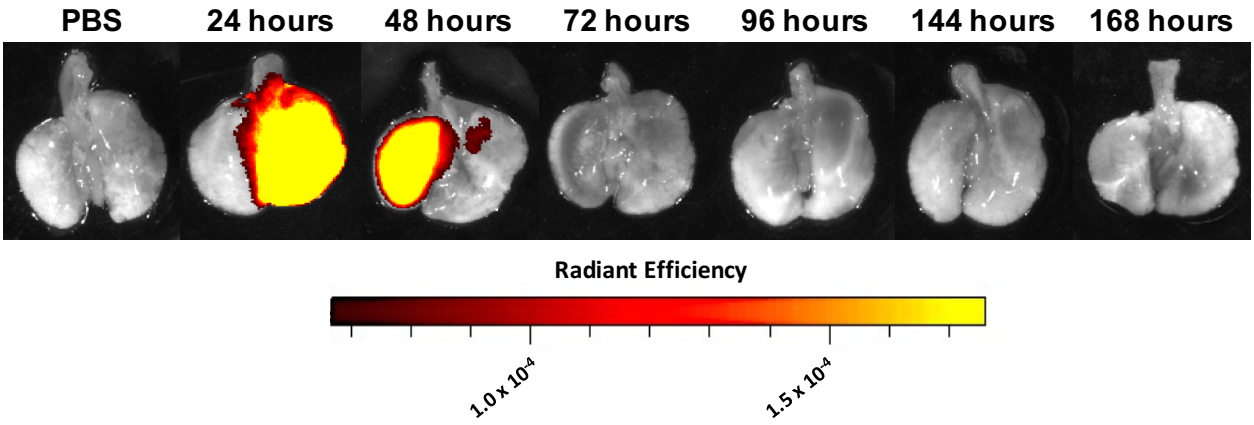

Figure 4.14 IVIS of BuChE 1 μm cylinders. IVIS images of resected murine lungs of a PBS treated control and multiple time points following administration of fluorescently-labeled lyophilized BuChE 1 μm cylinders from a Penn-Century DP-4M insufflator (n=3 per time).

The radiant efficiency of each lung observed by IVIS was normalized to the mass of the lung and is plotted in **Figure 4.15a**. The lungs resected at 24 and 48 hours following insufflation have significantly higher fluorescence than the PBS controls, while the remaining time points were not found to be significantly different than the PBS control. The BALF collected from each lung prior to IVIS imaging was also imaged under IVIS and the radiant efficiency measured was

normalized to the mass of each sample **(Figure 4.15b)**. A similar trend was observed in the BALF, with fluorescence at 24 and 48 hours being significantly different than the PBS control, while the later time points were not found to be significantly different. The activity of BuChE in each of the BALF samples was also measured, and a trend similar to BALF fluorescence was observed **(Figure 4.15c)**.

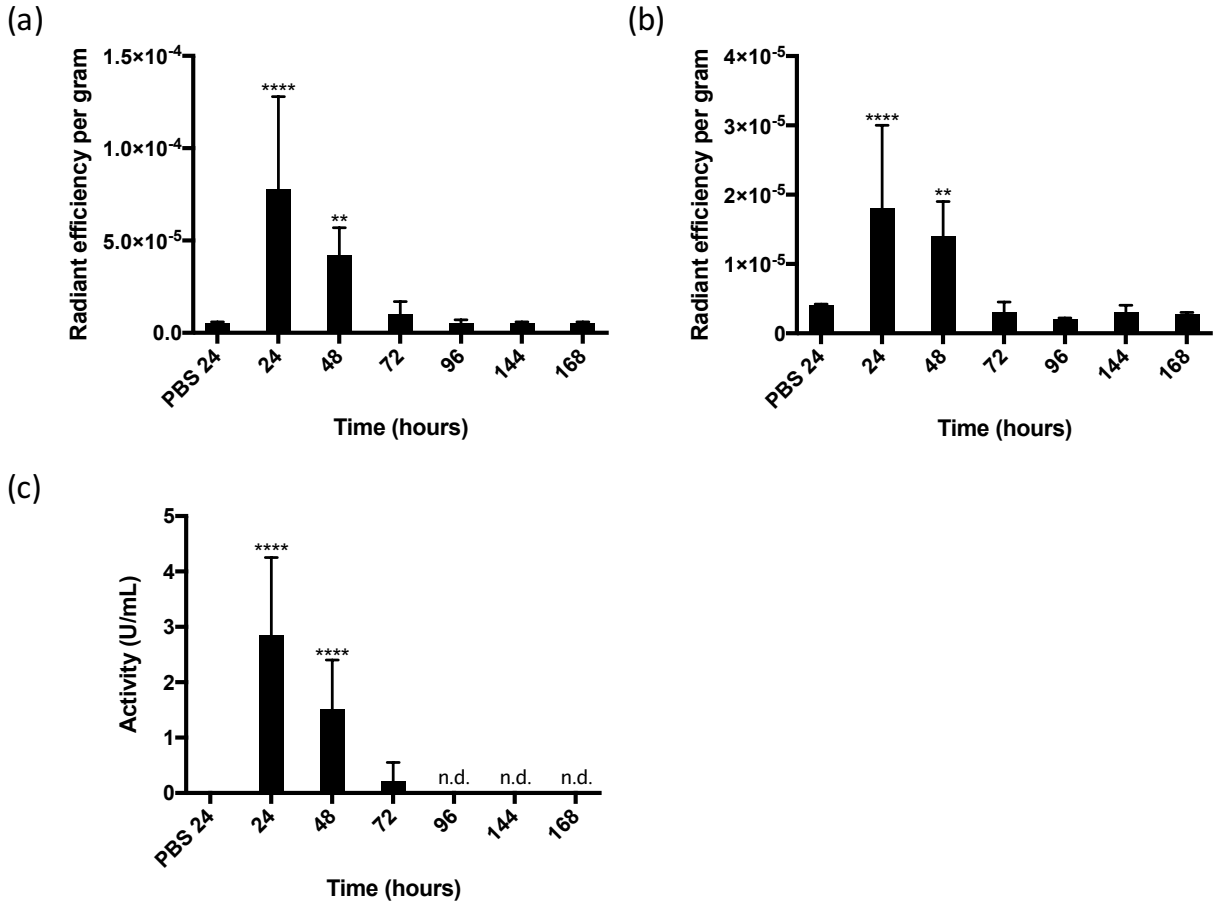

Figure 4.15 Residence time of BuChE 1 μm cylinders. Residence time of fluorescent BuChE in murine lungs following administration of lyophilized BuChE 1 μm cylinders with a Penn-Century DP-4M insufflator. (a) Fluorescence of resected mouse lungs normalized to BuChE dose and lung mass, (b) Fluorescence of BALF normalized to BuChE dose and BALF mass, and (c) activity of BuChE in BALF normalized to BuChE dose (n=3 per time) (n.d. = not detected).

4.4 Discussion

Respirable protein formulations allow for the localization of therapeutics for respiratory conditions to the lungs, resulting in higher local drug concentrations and minimized systemic

exposure.[16] Despite these advantages, respirable biologics have achieved little commercial prosperity, with dornase alfa remaining the only definitive success.[1] Dornase alfa, along with most inhalable biologics, is administered as a liquid formulation via nebulizer.[1,17] Liquid formulations delivered by nebulization are more rapid to develop due to their simplicity, but they frequently exhibit low delivery efficiency, which greatly limits opportunities to achieve commercial success with liquid formulations of inhaled biologics.[1,18,19] In Chapter 2, we demonstrated the ability to rapidly develop high-performance dry powder formulations of proteins using PRINT. In this chapter, we aimed to employ the utility of PRINT to develop high-performance dry powder aerosols of two therapeutic proteins of interest – DNase and BuChE. We believe the ability to rapidly formulate high-performance dry powder aerosols of nearly any therapeutic protein of interest with PRINT will facilitate the development and successful commercialization of novel inhalable protein formulations.

The first formulation discussed, DNase, is used as a mucolytic in CF therapy. DNase from bovine pancreas was used due to cost and availability. DNase cleaves the DNA present in airway mucus, thereby decreasing mucus viscosity and aiding in mucociliary and cough clearance of sputum.[17] Currently, DNase is administered once daily via nebulizer, which poses a major treatment burden to patients.[5,17] A dry powder formulation, which would decrease the time required for DNase administration, would improve patient compliance and improve quality of life for CF patients.[6] Because PRINT involves little physical stress, we hypothesized that PRINT could be used to formulate a high-performance dry powder of DNase while maintaining DNase stability.

Multiple groups have observed a positive correlation between forced expiratory volume (FEV), a marker of lung function, and deposition of DNase in lower airways.[20,21] The particle

shape selected for PRINT dry powders of DNase was informed by results from Chapter 3, which suggested 1 μm cylinders would maximize deposition efficiency in the lower airways. Because PRINT mold filling is primarily dependent on the T_g of the film, and the T_g of different proteins is relatively similar, the same formulation that was optimized for bovine serum albumin and lysozyme 1 μm cylinders was used for DNase 1 μm cylinders.[22] Particles were successfully micromolded into the 1 μm cylinder geometry and maintained the precisely engineered geometry expected with PRINT following lyophilization, as observed by SEM.[23] The composition of lyophilized 1 μm DNase cylinders was more than 80 % DNase by mass, with the remaining mass attributed to excipients. The low excipient mass of this formulation enables 2.5 mg of DNase to be delivered as about 3 mg of particles, which minimizes the powder burden for patients with already compromised lung function.

As one of the primary goals of formulating DNase as a PRINT dry powder was to maintain protein stability, a set of experiments was performed to evaluate each structural level of DNase throughout the PRINT process. It is critical that therapeutic proteins retain their native structure in their final formulation, as denatured proteins can have decreased therapeutic efficacy or even elicit immunogenic reactions.[24] The primary structure of DNase was observed by monitoring changes in molecular weight detectable by SDS-PAGE. Changes to the primary structure of a protein can occur as a result of covalent aggregation or degradation, which results in a corresponding increase or decrease in molecular weight, respectively.[25] Although additional bands present in all samples obscures interpretation of the results, it appears that the primary DNase band near 30 kDa is similar in lyophilized DNase 1 μm cylinders and DNase controls, suggesting retention of the primary structure of DNase. The disruption of intramolecular interactions in proteins, often a result of elevated temperatures, dehydration, or interaction with

interfaces, results in the unfolding of both local and global protein structure.[25,26] In this study, the local secondary structure was observed by CD while the global tertiary structure was observed with intrinsic fluorescence.[27,28] Changes in the secondary structure of proteins result in altered CD spectra, frequently observed as a decrease in signal intensity.[27] Spectra obtained from lyophilized DNase 1 μm cylinders were observed to have a mild decrease in signal intensity near 210 nm and a mild increase in intensity near 225 nm, suggesting a small alteration in the secondary structure of DNase may be occurring during manufacturing. The change observed in lyophilized particles is minimal relative to heat-denatured DNase, which displayed a dramatic alteration in CD spectra, including inversion of the signal from 185 to 200 nm. In order to better understand the magnitude of secondary structural change occurring within lyophilized DNase 1 μm cylinders, the secondary structure composition was determined for each sample. Both DNase and DNase PPS were found to be composed of 12.5 % alpha helices, while lyophilized DNase 1 μm cylinders contained 8.6 % alpha helices and heat-denatured DNase contained 1.82 % alpha helices. Though the small change in secondary structure observed is not ideal, a local structural change of this magnitude can likely be addressed with further formulation optimization, potentially including alteration of excipients, particle washing method, filling temperature, or lyophilization cycle.[24,29] The native tertiary structure of a protein generates a characteristic intrinsic fluorescence spectra that is dependent on the environment of tryptophan residues present in the protein. Any change in the global structure of a folding results in a change in intrinsic fluorescence, often observed as a change in λ_{max} or decreased fluorescence intensity at λ_{max}.[28] In contrast to CD, no alteration of intrinsic fluorescence spectra was observed for lyophilized DNase 1 μm cylinders relative to DNase and DNase PPS controls, suggesting no alteration in tertiary structure occurs during manufacturing. The heat-denatured DNase control

displayed a shift of λ_{max} from 340 nm to 330 nm and had major reduction in fluorescence intensity at $\lambda_{max.}$ Overall, while further formulation optimization is required, results from protein stability experiments show that PRINT is a promising platform for the development of a dry powder of DNase.

The aerosol properties of lyophilized DNase 1 μm cylinders were studied *in vitro* via cascade impaction. Cascade impaction of DNase particles was run at 28.3 L/min, which more closely models the impaired respiratory function observed in CF patients.[21] The decreased flow rate was expected to generally decrease formulation performance relative to other dry powders of 1 μm cylinders, as powder fluidization and aerosolization become less efficient at lower flow rates.[30] Lyophilized DNase 1 μm cylinders readily aerosolized from a Monodose RS01 inhaler, with 98.9 % of the loaded dose being emitted. The high ED of DNase particles, even at a low flow rate, may be explained by results from Chapter 3, which suggest that PRINT protein dry powders fluidize as low density aggregates. Large, low density particles and aggregates tend to readily fluidize, even when flow rates are decreased.[31] DNase particles were largely able to avoid impaction in the artificial throat, with only 10.4 % of the dose depositing there, suggesting that particle aggregates are readily aerosolized, even at a decreased flow rate. The deposition profile of DNase 1 μm cylinders in the cascade impactor resulted in a MMAD of 2.91 μm and a GSD of 1.66. The MMAD and GSD of DNase 1 μm cylinders are slightly elevated relative to 1 μm cylinders from Chapter 2, potentially due to incomplete aerosolization of particle aggregates at the lower flow rate. Regardless, the MMAD is appropriate for efficient deposition in the lower airways, which is critical to obtain clinically significant improvements in FEV.[20,21] The FPF of the DNase 1 μm cylinders was determined to be 75.4 %, indicating that the majority of the aerosol generated is sized for lung deposition.

Altogether, results from protein stability studies and aerosol characterization indicate that PRINT can be used to manufacture a dry powder DNase formulation that exhibits high-performance aerosol properties even under impaired flow conditions frequently present in CF patients.[21] Though further formulation optimization is required, the potential to dramatically reduce the daily therapy burden for CF patients with a dry powder formulation of DNase motivates continued development.

The second formulation development project discussed in this chapter is a PRINT dry powder of BuChE. Studies by Rosenberg at al have shown that aerosol delivery of BuChE creates a "pulmonary bioshield" that captures organophosphates in a stoichiometric manner upon inhalation exposure, thereby limiting organophosphate access to systemic circulation.[11,13] A dry powder formulation of BuChE would be most ideal for military applications, as it would be portable and potentially stable in ambient storage conditions in a variety of climates. Herein, we report on the development and *in vitro* and *in vivo* evaluation of a PRINT dry powder formulation of BuChE.

To form the most effective BuChE bioshield possible, it is critical that an inhaled BuChE formulation is able to reach the lower airways.[11] For this reason, we selected the 1 μm cylinder geometry based on the aerosol parameters described in Chapter 3. Once again, we were able to use the formulation optimized for other compositions of 1 μm cylinders, as the T_g of different proteins does not vary enough to require reformulation.[22] The BuChE formulation was successfully micromolded into the 1 μm cylinder geometry and retained the proper geometry following lyophilization, as was observed by SEM. The composition of DNase 1 μm cylinders was found to be 88.8 % BuChE by mass, with less than 12 % of particle mass due to excipients. It is important to minimize excipient mass in this formulation, as the stoichiometric mechanism

of organophosphate inactivation by BuChE necessitates as large dose of BuChE by mass to form an effective bioshield. Based on macaque data, inhaled dosages for humans are estimated to be between 250 and 750 mg per 70 kg to form an effective bioshield.[11] Importantly, no loss of BuChE enzymatic activity, which is responsible for inactivating organophosphates, was observed at any formulation step.[13] In addition to BuChE microparticles, two different geometries of BuChE nanoparticles were fabricated as a prospective formulation to increase the residence time of BuChE in the lungs, potentially via controlled-release or by avoiding clearance by alveolar macrophages.[32] Further formulation development is required for these particles to have an aerodynamic diameter appropriate for lung deposition.

The aerosol performance of dry powders of BuChE 1 μm cylinders was studied via cascade impaction at 28.3 L/min with a Penn-Century DP-4M insufflator. The DP-4M insufflator was used in preparation for future *in vivo* mouse studies. When actively aerosolized from the insufflator, BuChE 1 μm cylinders produce an MMAD of 2.73 μm and deposit precisely on stage 4 (2.1 – 3.3 μm at 28.3 L/min). The precise deposition profile results in a GSD of 1.39. Likely aided by active aerosolization from the insufflator, the FPF of the collected dose was 95.13 %, indicating nearly all of the aerosolized dose is an appropriate size for lung deposition.

An assay to quantify fluorescent BuChE was successfully developed in three different relevant fluids, including PBS, whole blood, and plasma. In all three fluids, there was a simple linear relationship between fluorescent BuChE concentration and fluorescence intensity, which will allow for the quantification of fluorescent BuChE in blood and bronchoalveolar lavage fluid (BALF) collected in PBS.

The residence time of fluorescent BuChE was observed in mice following administration of a dry powder of BuChE 1 μm cylinders by insufflation. The residence time of BuChE in the

lungs is a critical aspect of its therapeutic effect as a bioshield for organophosphates, as BuChE must be present at a sufficiently high concentration to have a protective effect.[11] Imaging of resected mouse lungs with IVIS shows a clear fluorescent BuChE signal at 24 and 48 hours, with no signal present at further time points. Fluorescence signal is isolated to one side of the lungs, suggesting that the insufflator was placed below the carina of the trachea and entered one of the primary bronchi. Although deposition throughout the lungs would be more ideal, residence time can still be observed. Fluorescence measured from both the lungs and BALF by IVIS imaging was normalized to BuChE dose administered and lung or BALF mass. Once again, fluorescent BuChE concentration was significantly higher than baseline up to 48 hours. As BuChE activity is responsible for its bioshield effect against organophosphates, the activity of BuChE present in each BALF sample was also measured. Activity data detected significantly elevated levels of BuChE activity for 48 hours, which was in agreement with fluorescence data. Altogether, *in vivo* data suggest that the maximum protection time for a bioshield delivered with the BuChE 1 μm cylinder formulation is 48 hours.

In this study, we successfully fabricated a high-performance dry powder of BuChE that retains its full therapeutic activity in the final formulation and can be administered to mice by insufflation. Currently, the maximum protection time possible with this formulation is 48 hours, though residence time in the lungs could potentially be increased by modifying BuChE release from the particles or by incorporating polymer-modified BuChE into the PRINT particles, which would lengthen the prophylactic protection time of the BuChE lung bioshield.[33]

4.5 Conclusions

Currently, inhalable formulations of protein therapeutics are frequently developed as liquid formulations intended for delivery by nebulizers, largely due to the simplicity and rapidity

of formulation design.[1] However, nebulized formulations are well-known to have poor delivery efficiencies and are inconvenient to patients, which limits the potential for these formulations to achieve commercial success.[1,19] In Chapter 2, we developed and characterized a formulation strategy that enables the rapid development of protein dry powder formulations with PRINT. In this chapter, we used the same formulation strategy to demonstrate the utility of PRINT and successfully develop formulations of high-performance DNase and BuChE dry powders. The unique ability of PRINT to manufacture precisely engineered respirable protein particles with little optimization needed for new proteins could facilitate the improvement of current inhaled protein formulations and the development of a multitude of new formulations.

REFERENCES

1. Hertel, S. P., Winter, G. & Friess, W. Protein stability in pulmonary drug delivery via nebulization. *Adv. Drug Deliv. Rev.* **93,** 79–94 (2015).

2. Pilcer, G. & Amighi, K. Formulation strategy and use of excipients in pulmonary drug delivery. *Int. J. Pharm.* **392,** 1–19 (2010).

3. Cutting, G. R. Cystic fibrosis genetics: from molecular understanding to clinical application. *Nat. Rev. Genet.* **16,** 45–56 (2014).

4. Conrad, D. *et al.* Cystic fibrosis therapy: A community ecology perspective. *Am. J. Respir. Cell Mol. Biol.* **48,** 150–156 (2013).

5. Yang, C. *et al.* Dornase alfa for cystic fibrosis (Review). *Cochrane Database Syst. Rev. 2016* 1–75 (2016). doi:10.1002/14651858.CD001127.pub3.Copyright

6. Sawicki, G. S., Sellers, D. E. & Robinson, W. M. High treatment burden in adults with cystic fibrosis: Challenges to disease self-management. *J. Cyst. Fibros.* **8,** 91–96 (2009).

7. Chan, H. K., Clark, A., Gonda, I., Mumenthaler, M. & Hsu, C. Spray dried powders and powder blends of recombinant human deoxyribonuclease (rhDNase) for aerosol delivery. *Pharmaceutical Research* **14,** 431–437 (1997).

8. Yang, Y. *et al.* Inhalable antibiotic delivery using a dry powder co-delivering recombinant deoxyribonuclease and ciprofloxacin for treatment of cystic fibrosis. *Pharm. Res.* **27,** 151–160 (2010).

9. Worthington, K. & Worthington, V. *Worthington Enzyme Manual*. (1993).

10. Reed, B. A., Sabourin, C. L. & Lenz, D. E. Human butyrylcholinesterase efficacy against nerve agent exposure. *J. Biochem. Mol. Toxicol.* **31,** (2017).

11. Rosenberg, Y. J. *et al.* Pulmonary delivery of an aerosolized recombinant human butyrylcholinesterase pretreatment protects against aerosolized paraoxon in macaques. *Chem. Biol. Interact.* **203,** 167–171 (2013).

12. Marrs, T. C. Organophosphate anticholinesterase poisoning. *Toxic Subst. Mech.* **15,** 357–388 (1996).

13. Rosenberg, Y. J. & Fink, J. B. Creation of a protective pulmonary bioshield against inhaled organophosphates using an aerosolized bioscavenger. *Ann. N. Y. Acad. Sci.* **1374,** 151–158 (2016).

14. Xu, J. *et al.* Rendering protein-based particles transiently insoluble for therapeutic applications. *J. Am. Chem. Soc.* **134,** 8774–8777 (2012).

15. Rahhal, T. B. *et al.* Pulmonary Delivery of Butyrylcholinesterase as a Model Protein to the Lung. *Mol. Pharm.* **13,** 1626–1635 (2016).

16. Pilcer, G. & Amighi, K. Formulation strategy and use of excipients in pulmonary drug delivery. *Int. J. Pharm.* **392,** 1–19 (2010).

17. Cipolla, D., Gonda, I. & Shire, S. J. Characterization of Aerosols of Human Recombinant Deoxyribonuclease I (rhDNase) Generated by Jet Nebulizers. *Pharm. Res. An Off. J. Am. Assoc. Pharm. Sci.* **11,** 491–498 (1994).

18. Wildhaber, J. H., Dore, N. D., Wilson, J. M., Devadason, S. G. & LeSouëf, P. N. Inhalation therapy in asthma: nebulizer or pressurized metered-dose inhaler with holding chamber? In vivo comparison of lung deposition in children. *J. Pediatr.* **135,** 28–33 (1999).

19. Lewis, R. A. & Fleming, J. S. Fractional deposition from a jet nebulizer: how it differs from a metered dose inhaler. *Br. J. Dis. Chest* **79,** 361–367 (1985).

20. Geller, D. E. *et al.* Effect of smaller droplet size of dornase alfa on lung function in mild cystic fibrosis. *Pediatr. Pulmonol.* **25,** 83–87 (1998).

21. Diot, P. *et al.* RhDNase I aerosol deposition and related factors in cystic fibrosis. *Am. J. Respir. Crit. Care Med.* **156,** 1662–1668 (1997).

22. Cicerone, M. T., Pikal, M. J. & Qian, K. K. Stabilization of proteins in solid form. *Adv. Drug Deliv. Rev.* **93,** 14–24 (2015).

23. Fromen, C. A. *et al.* Synthesis and Characterization of Monodisperse Uniformly Shaped Respirable Aerosols. *AIChE J.* **59,** 3184–3194 (2013).

24. Frokjaer, S. & Otzen, D. E. Protein drug stability: a formulation challenge. *Nat. Rev. Drug Discov.* **4,** 298–306 (2005).

25. Maltesen, M. J. & van de Weert, M. Drying methods for protein pharmaceuticals. *Drug Discov. Today Technol.* **5,** e81–e88 (2008).

26. Ameri, M. & Maa, Y.-F. Spray Drying of Biopharmaceuticals: Stability and Process Considerations. *Dry. Technol.* **24,** 763–768 (2006).

27. Capelle, M. A. H., Gurny, R. & Arvinte, T. High throughput screening of protein formulation stability: Practical considerations. *Eur. J. Pharm. Biopharm.* **65,** 131–148 (2007).

28. Garidel, P., Hegyi, M., Bassarab, S. & Weichel, M. A rapid, sensitive and economical assessment of monoclonal antibody conformational stability by intrinsic tryptophan fluorescence spectroscopy. *Biotechnol. J.* **3,** 1201–1211 (2008).

29. Kamerzell, T. J., Esfandiary, R., Joshi, S. B., Middaugh, C. R. & Volkin, D. B. Protein-excipient interactions: Mechanisms and biophysical characterization applied to protein formulation development. *Adv. Drug Deliv. Rev.* **63,** 1118–1159 (2011).

30. Zhou, Q. T., Armstrong, B., Larson, I., Stewart, P. J. & Morton, D. A. V. Understanding the influence of powder flowability, fluidization and de-agglomeration characteristics on the aerosolization of pharmaceutical model powders. *Eur. J. Pharm. Sci.* **40,** 412–421 (2010).

31. Chew, N. Y. K. & Chan, H. K. Use of solid corrugated particles to enhance powder aerosol performance. *Pharm. Res.* **18,** 1570–1577 (2001).

32. Shen, T. W. *et al.* Distribution and Cellular Uptake of PEGylated Polymeric Particles in the Lung Towards Cell-Specific Targeted Delivery. *Pharm. Res.* **32,** 3248–3260 (2015).

33. Cohen, O. *et al.* Comparison of polyethylene glycol-conjugated recombinant human acetylcholinesterase and serum human butyrylcholinesterase as bioscavengers of organophosphate compounds. *Mol. Pharmacol.* **70,** 1121–1131 (2006).

CHAPTER 5: SUMMARY AND FUTURE DIRECTIONS

5.1 Summary

The primary objectives of this work were to (1) develop a formulation strategy using PRINT to manufacture micromolded protein particles that produce high-performance dry powder aerosols, (2) expand the formulation strategy to generate a series of particles with precisely controlled geometries to study the role of particle shape in aerosol performance, and (3) integrate knowledge from formulation development and particle shape studies to rapidly develop high-performance formulations of two therapeutic proteins of interest.

The exquisite control of particle geometry and mild processing conditions afforded by PRINT allowed us to establish a "plug-and-play" platform to rapidly develop new respirable protein formulations while maintaining the integrity of proteins. We successfully developed a generalizable formulation strategy to fabricate PRINT protein particles that consistently produce high-performance dry powder aerosols, regardless of the incorporated protein (Chapter 2). After demonstrating that PRINT protein particles could produce high-performance dry powder aerosols, multiple shapes of protein particles with minimal variation in particle size were fabricated to study the role of particle shape in dry powder fluidization, aerosolization, and deposition (Chapter 3). Results of the particle shape study informed the selection of particle shape for our therapeutic applications and will further improve performance of PRINT dry powder aerosols. The respirable protein particle formulation strategy and the optimal particle shape identified in particle shape studies were used to successfully develop dry powder formulations of two therapeutic proteins, and deliver one formulation to mice *in vivo* (Chapter 4).

5.2 Impact and Future Directions

5.2.1 PRINT as a Platform for Pulmonary Protein Delivery

The precise control of particle shape and size afforded by PRINT enables respirable dry powders to be manufactured with minimal variability in particle geometry within or between batches.[1–3] The homogeneous geometry of PRINT particles results in dry powders that exhibit consistent and reproducible high-performance aerosol properties.[1] In Chapter 2, the PRINT protein dry powder formulations were found to produce aerosols with highly efficient and precise deposition profiles. These high-performance dry powder formulations are particularly valuable for costly protein-based therapeutics, as an improvement in delivery efficiency could dramatically reduce drug cost.

PRINT protein particles were found to be composed primarily of protein, which minimizes the amount of excipient that would be delivered with each dose. As high powder masses have the potential to cause upper airway irritation, coughing, or bronchospasms, limiting excipient mass to the amount needed to stabilize the incorporated protein is desirable.[4,5] In combination with high delivery efficiency and precision, the low excipient mass possible with PRINT enables the delivery of higher drug doses, which are frequently required for protein therapeutics.[4]

Because PRINT is a micromolding technique, particle geometry is determined solely by the shape of cavities patterned into the mold and is independent of particle composition.[1,6,7] This allows for particle composition to be manipulated independent of particle geometry. In contrast, for bottom-up particle manufacturing methods used to fabricate dry powders, such as spray drying, particle composition and geometry are intrinsically linked.[8] As particle geometry is the primary determinant of dry powder aerosol properties, it is reasonable to expect PRINT protein

dry powders of the same geometry to display similar aerosol properties, regardless of the incorporated protein, as was observed with two compositions of 1 μm cylinders in Chapter 2.[9–11] The ability to select the ideal particle geometry prior to developing a novel protein formulation from a library of potential particle geometries with known aerosol properties could improve the efficiency of formulation optimization and enable the rapid development of novel inhaled formulations.

Future studies aimed at furthering the development of PRINT as a platform for respirable protein formulations should aim to establish the aerosol parameters of additional particle shapes fabricated from multiple proteins. Due to the extensive number of PRINT particle geometries available, efforts should focus on geometries most likely to generate aerosols with aerodynamic diameters between 1 and 5 μm, which are appropriate for pulmonary delivery. Examples of potential particle geometries are in **Figure 5.1**. Particle shapes with surfaces that minimize the surface area available for interparticle interactions are of particular interest.

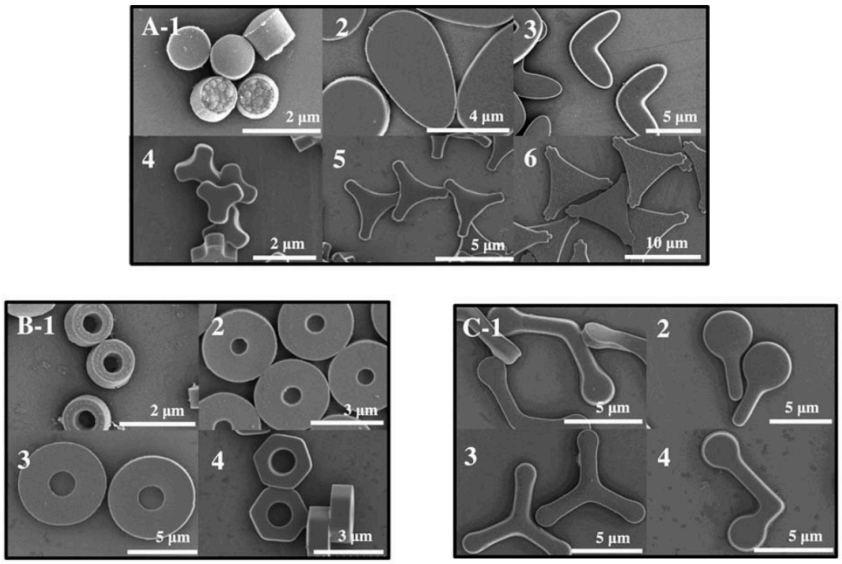

Figure 5.1 Examples of PRINT particle shapes. Examples of PRINT particle shapes to generate protein dry powders appropriate for pulmonary delivery. A1) cylinder, A2) ellipsoid, A3) Lorenz, A4) small pollen mimic, A5) medium pollen mimic, A6) large pollen mimic, B1) small toroid, B2) medium toroid, B3) large toroid, B4) hexnut, C1) V boomerang, C2) lollipop, C3) helicopter, C4) L dumbbell. Adapted from Fromen et al.[2] with permission.

Several studies in Chapter 2 were performed to demonstrate the stability of two model proteins in respirable PRINT dry powders. While these studies provided a solid foundation, further studies investigating protein stability in PRINT should be performed, including size exclusion chromatography (SEC) for molecular weight, capillary electrophoresis (CE) to observe reduction of proteins by lactose, and differential scanning calorimetry (DSC) to measure the glass transition temperature of dry powder formulations. These experiments will allow for further optimization of the PRINT process and aid in proper excipient selection for each protein.

Ultimately, the primary objective of Chapter 2 was establishing PRINT as a platform for pulmonary protein delivery, and thus the majority of efforts should be focused on identifying additional respirable therapeutic protein candidates and studying PRINT protein dry powder formulations *in vivo*. Studies in larger animals with lung anatomy more similar to human lung anatomy, such as guinea pigs or canines, would aid in establishing PRINT as a viable method to precisely deliver respirable dry powders.

5.2.2 Role of Particle Shape in Respirable Dry Powders

PRINT provides a unique opportunity to study the role of particle shape in the fluidization, aerosolization, and deposition of dry powders. Bottom-up fabrication methods, which are frequently used to fabricate respirable dry powders, are unable to independently control particle size, shape, and composition.[8] Thus, to date, studies aimed at investigating the role of particle shape in dry powder formulations have been limited.[11] In Chapter 3, a series of four protein particle shapes with minimal variation in particle size and composition was fabricated to investigate the role of particle shape in dry powder performance.

To our knowledge, this is the first report of a study utilizing particles of controlled size and composition to investigate the role of drug particle shape in the fluidization, aerosolization,

and deposition of dry powders. The impact of particle size and density on dry powder performance has been extensively characterized and is frequently leveraged to engineer dry powder formulations with superior delivery efficiency and precision.[12–16] The investigation of the role of shape in Chapter 3 identified particle shape parameters that impact dry powder performance, indicating that particle shape could be an important particle parameter to modulate when engineering particles for high-performance dry powder formulations. Further knowledge of the role of particle shape, along with the ability to precisely engineer particle geometry with PRINT, could be used to more specifically and efficiently deliver therapeutics to the lungs, facilitating the development of novel inhaled therapies.[17]

The studies in Chapter 3 provide evidence that differences in particle shape, even on the nanoscale, result in noticeable differences in dry powder performance. These results provide a solid foundation and rationale to further study the impact of particle shape on fluidization, aerosolization, and deposition of dry powders. Additional particle shapes with aerodynamic diameters closer to 5 μm with controlled maximum diameters and compositions should be fabricated to study the importance of particle shape across the range of aerodynamic diameters relevant to pulmonary delivery.

For particle shape studies, the shapes were selected from previously designed and readily available PRINT molds. The selected particle shapes were chosen in an effort to minimize differences in maximum diameter and volume between shapes. These studies could be improved by designing new particle geometries and manufacturing PRINT molds with shapes of equivalent maximum diameter and volume. This would allow for particle shape to be studied as independently as possible from particle size.

Future studies should also further interrogate the impact particle shape has on bulk

powder properties and on interparticle interactions. In a pair of reviews, leading experts in dry powder formulations made recommendations to standardize dry powder characterization techniques to aid in the identification of relationships between specific dry powder properties and formulation performance.[18,19] While many of these experiments were performed in Chapter 3, there are additional experiments to be performed to further characterize the particle shape formulations. Recommended experiments include measurement of electrostatic properties of the particle surface with a Faraday cage method, thermal analysis of solid state composition by DSC to ensure equivalent composition for each shape, and moisture content with Karl Fischer titration to observe differences in hygroscopicity due to particle shape. Additionally, the study of individual interparticle interactions by colloid probe atomic force microscopy (AFM) could provide valuable insight on the orientations of particle shapes that minimize and maximize interactions. The recommended studies provide an excellent opportunity to quantify the impact of particle shape on dry powder formulations and observe potential correlations between different shape parameters and dry powder performance descriptors. This could eventually enable the predictive design of novel particle shapes to yield significant improvements in the performance of dry powder aerosols.[18,19]

One particularly impactful application of respirable engineered particles is for targeted delivery of therapeutics to the lungs. Improved targeting of therapeutic particles to specific sites within the lungs is an area of intense research focus.[20,21] Specifically delivering therapeutics to the desired site of action in the lungs could improve drug efficacy, minimize potential side effects, and reduce the cost of a therapy.[17,20]

Ruge et al. proposed three levels of targeting within the respiratory tract in a recent review, including (1) central or peripheral respiratory tract deposition, (2) deposition at the site

of disease, and (3) targeting of specific cell populations **(Figure 5.2)**.[20] Current particle engineering strategies are typically limited to the first level of targeting, and thus aim to selectively deposit therapeutics in either the central or peripheral region of the respiratory tract.[20] Experiments presented in this dissertation and in previous studies in the DeSimone lab have shown that formulations of PRINT dry powders can efficiently target both the central and peripheral regions.[2] Additional studies have also shown that PRINT particles can be used to achieve the third level of targeting, successfully targeting and de-targeting various cell populations in the lung epithelium.[22] Although many of the particles used for cell-specific delivery were nanometer-sized, further formulation of these nanoparticles within larger PRINT particles could be used to efficiently deliver these particles to the desired region, where they could rapidly release the encapsulated nanoparticles.

The second level of targeting, delivering aerosols directly to the site of disease, remains a major challenge for pulmonary delivery.[20,21,23] Advances in the theory of particle engineering, including further understanding of particle shape provided by PRINT, could improve drug targeting to the site of disease.

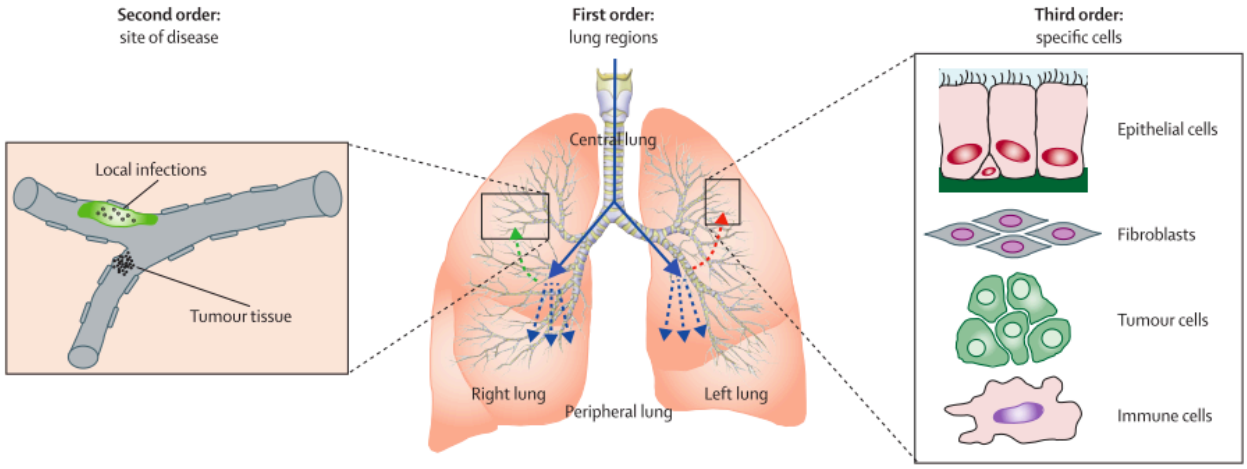

Figure 5.2 Levels of lung targeting. Different levels of dry powder aerosol deposition targeting within the lungs for pulmonary delivery. Reproduced with permission from Ruge et al.[20]

5.2.3 Therapeutic Applications of PRINT Protein Dry Powders

The generalizable formulation strategy developed in Chapter 2 was applied to develop dry powder formulations of deoxyribonuclease I (DNase) and butyrylcholinesterase (BuChE). The ability to rapidly develop new protein formulations with little formulation optimization is advantageous for both pre-clinical and clinical formulation development, where liquid formulations delivered by nebulizer are frequently preferred due to their rapid development time, regardless of their inconvenience to patients and poor delivery efficiency.[24]

Taking advantage of the limited physical forces imparted by the PRINT process, a dry powder formulation of DNase, which is known to be liable to physical denaturation, was developed. A dry powder formulation of DNase could be administered in a matter of seconds, whereas the current nebulized formulation takes about 30 minutes to administer and significantly increases the daily treatment burden for cystic fibrosis (CF) patients.[25] The decreased treatment burden enabled by dry powder formulations could also be applied to other nebulized formulations, including antibiotics. Importantly, the DNase dry powders exhibited excellent aerosol properties *in vitro*, even at a decreased flow rate that more closely represents the impaired lung function of CF patients. This suggests that PRINT protein dry powders can consistently achieve efficient and precise aerosol delivery, even when used by patients to treat respiratory conditions frequently characterized by impaired respiratory function. Formulation development of DNase dry powders should first be continued by measuring the DNase activity retained in the lyophilized formulation and performing an excipient screening study to maximize the stability of DNase in PRINT dry powders. Following confirmation of enzymatic activity, the application of DNase dry powders to *ex vivo* sputum from CF patients would support the therapeutic potential of PRINT DNase dry powders.

As PRINT allows for the rapid formulation of novel dry powders, a co-formulated particle containing both DNase and ciprofloxacin could be rapidly developed. A study by Yang et al.[26] demonstrated the ability of concomitant DNase to improve the efficacy of ciprofloxacin as an antibiotic in sputum samples due to increased exposure of ciprofloxacin to bacteria. A co-loaded formulation of DNase and ciprofloxacin with high-performance aerosol behavior could even further decrease the treatment burden for CF patients while improving the efficacy of intermittent antibiotic administration. Beyond this specific application, the general ability of PRINT to develop co-formulations could be applied to create high-performance therapies for additional respiratory conditions, including asthma and chronic obstructive pulmonary disease (COPD).

PRINT was also used to develop precisely engineered dry powder aerosols of BuChE to prophylactically protect against organophosphate exposure by inhalation. While the 48-hour residence time observed *in vivo* provides some protection, it would be desirable to further increase the residence time of BuChE in the lungs to maximize the time of protection offered by a single dose.

Prolonged residence time could potentially be achieved by controlling the release of BuChE from the particles. Currently, there are no marketed respirable controlled-release formulations, though there are significant efforts to develop one.[21] A controlled-release system for PRINT protein particles that releases unmodified proteins was previously developed in the DeSimone lab.[27] The system relies on a disulfide-based crosslinker to stabilize the particles in aqueous solution. Upon exposure to a reducing environment, such as the epithelial lining fluid (ELF) of human lungs, the disulfide bonds are reduced and protein is released from the particles in a controlled manner. Preliminary studies performed in C57BL/6 mice determined that a

sufficient concentration of glutathione is present in the ELF of the lungs to serve as an appropriate animal model and trigger the controlled release of proteins from crosslinked particles **(Table 5.1)**.

Table 5.1 ELF glutathione. Glutathione concentrations in the ELF of C57BL/6 mice (n=7).

Epithelial Lining Fluid (ELF)	
Component	**Concentration (μM)**
Total glutathione	74.4 ± 12.9
GSH	42.6 ± 10.0
GSSG	31.8 ± 3.5

To evaluate the protective effect of PRINT BuChE powders, organophosphate challenge studies should be performed. While it may be possible to perform these inhalation challenge studies in-house, it is advisable to initiate a collaboration with a government agency that is better equipped to safely carry out these studies.

5.3 Outlook

The work presented in this dissertation highlights the utility of PRINT as both a protein formulation and particle engineering platform. The ability to independently manipulate particle parameters, including size, shape, density, and composition, provides an unparalleled opportunity to systematically investigate the role of particle parameters in the performance of respirable dry powder formulations. Improved understanding of the impact of particle parameters can be applied to precisely engineer more safe and efficacious respirable formulations and to enable the development of the next generation of inhaled therapies.

REFERENCES

1. Garcia, A. *et al.* Microfabricated Engineered Particle Systems for Respiratory Drug Delivery and Other Pharmaceutical Applications. *J. Drug Deliv.* **2012,** 1–10 (2012).

2. Fromen, C. A. *et al.* Synthesis and Characterization of Monodisperse Uniformly Shaped Respirable Aerosols. *AIChE J.* **59,** 3184–3194 (2013).

3. Kelly, J. Y. & DeSimone, J. M. Shape-specific, monodisperse nano-molding of protein particles. *J. Am. Chem. Soc.* **130,** 5438–5439 (2008).

4. Claus, S., Weiler, C., Schiewe, J. & Friess, W. How can we bring high drug doses to the lung? *Eur. J. Pharm. Biopharm.* **86,** 1–6 (2014).

5. Timsina, M. P., Martin, G. P., Marriott, C., Ganderton, D. & Yianneskis, M. Drug delivery to the respiratory tract using dry powder inhalers. *Int. J. Pharm.* **101,** 1–13 (1994).

6. Rolland, J. P. *et al.* Direct fabrication and harvesting of monodisperse, shape-specific nanobiomaterials. *J. Am. Chem. Soc.* **127,** 10096–10100 (2005).

7. Gratton, S. E. a *et al.* Nanofabricated particles for engineered drug therapies: a preliminary biodistribution study of PRINT nanoparticles. *J. Control. Release* **121,** 10–8 (2007).

8. Chow, A. H. L., Tong, H. H. Y., Chattopadhyay, P. & Shekunov, B. Y. Particle engineering for pulmonary drug delivery. *Pharm. Res.* **24,** 411–437 (2007).

9. Lin, Y.-W., Wong, J., Qu, L., Chan, H. K. & Zhou, Q. T. Powder production and particle engineering for dry powder inhaler formulations. *Curr. Pharm. Des.* **21,** 3902–3916 (2015).

10. Yang, M. Y., Chan, J. G. Y. & Chan, H. K. Pulmonary drug delivery by powder aerosols. *J. Control. Release* **193,** 228–240 (2014).

11. Hassan, M. S. & Lau, R. W. M. Effect of particle shape on dry particle inhalation: study of flowability, aerosolization, and deposition properties. *AAPS PharmSciTech* **10,** 1252–1262 (2009).

12. Carstensen, J. T. & Chan, P. C. Relation between particle size and repose angles of powders. *Powder Technol.* **15,** 129–131 (1976).

13. Visser, J. Van der Waals and other cohesive forces affecting powder fluidization. *Powder Technol.* **58,** 1–10 (1989).

14. Heyder, J., Gebhart, J., Rudolf, G., Schiller, C. F. & Stahlhofen, W. Deposition of particles in the human respiratory tract in the size range 0.005-15 μm. *J. Aerosol Sci.* **17,** 811–825 (1986).

15. Edwards, D. A. *et al.* Large Porous Particles for Pulmonary Drug Delivery. *Science.* **276,** 1868–1871 (1997).

16. Vanbever, R. *et al.* Formulation and physical characterization of large porous particles for inhalation. *Pharmaceutical Research* **16,** 1735–1742 (1999).

17. Kleinstreuer, C., Zhang, Z. & Donohue, J. F. Targeted Drug-Aerosol Delivery in the Human Respiratory System. *Annu. Rev. Biomed. Eng.* **10,** 195–220 (2008).

18. Hickey, A. J. *et al.* Physical characterization of component particles included in dry powder inhalers. I. Strategy review and static characteristics. *J. Pharm. Sci.* **96,** 1282–1301 (2007).

19. Hickey, A. J. *et al.* Physical characterization of component particles included in dry powder inhalers. II. Dynamic characteristics. *J. Pharm. Sci.* **96,** 1302–1319 (2007).

20. Ruge, C. C., Kirch, J. & Lehr, C. M. Pulmonary drug delivery: From generating aerosols to overcoming biological barriers-therapeutic possibilities and technological challenges. *Lancet Respir. Med.* **1,** 402–413 (2013).

21. Weers, J. G. *et al.* Pulmonary Formulations: What Remains to be Done? *J. Aerosol Med. Pulm. Drug Deliv.* **23,** S-5-S-23 (2010).

22. Shen, T. W. *et al.* Distribution and Cellular Uptake of PEGylated Polymeric Particles in the Lung Towards Cell-Specific Targeted Delivery. *Pharm. Res.* **32,** 3248–3260 (2015).

23. Weers, J. G. & Miller, D. P. Formulation Design of Dry Powders for Inhalation. *J. Pharm. Sci.* **104,** 3259–3288 (2015).

24. Hertel, S. P., Winter, G. & Friess, W. Protein stability in pulmonary drug delivery via nebulization. *Adv. Drug Deliv. Rev.* **93,** 79–94 (2015).

25. Sawicki, G. S., Sellers, D. E. & Robinson, W. M. High treatment burden in adults with cystic fibrosis: Challenges to disease self-management. *J. Cyst. Fibros.* **8,** 91–96 (2009).

26. Yang, Y. *et al.* Inhalable antibiotic delivery using a dry powder co-delivering recombinant deoxyribonuclease and ciprofloxacin for treatment of cystic fibrosis. *Pharm. Res.* **27,** 151–160 (2010).

27. Xu, J. *et al.* Rendering protein-based particles transiently insoluble for therapeutic applications. *J. Am. Chem. Soc.* **134,** 8774–7 (2012).